Relicensing Study 3.3.19

Evaluate the Use of an Ultrasound Array to Facilitate Upstream Movement to Turners Falls Dam by Avoiding Cabot Station Tailrace

2018 Study Report

Northfield Mountain Pumped Storage Project (No. 2485) and Turners Falls Hydroelectric Project (No. 1889)

Prepared for:

FirstLight Power Resources

Prepared by:

Kleinschmidt

Gomez and Sullivan Engineers

MARCH 2019

TABLE OF CONTENTS

LIST OF TABLES

LIST OF FIGURES

LIST OF APPENDICES

LIST OF ABBREVIATIONS

AIC	Akaikes Information Criteria
Alden	Alden Research Laboratory
ANOVA	Analysis of Variance
cfs	cubic feet per second
kcfs	thousand cubic feet per second
CJS	Cormack Jolly Seber
CRC	Connecticut River Conservancy
COXPH	Cox Proportional Hazards Regression
CRWC	Connecticut River Watershed Council
dB	Decibel
DIDSON	Dual Frequency Identification Sonar
FERC	Federal Energy Regulatory Commission
FirstLight	FirstLight Hydro Generating Company
GLM	Generalized Linear Model
GOF	Goodness of fit
HG&E	Holyoke Gas and Electric
ILP	Integrated Licensing Process
kHz	kilohertz
MHz	Megahertz
NHFGD	New Hampshire Fish and Game Department
NMFS	National Marine Fisheries Service
PIT	Passive Integrated Transponder
QAQC	Quality Assurance and Quality Control
RM	River Miles
SNS	Shortnose Sturgeon
SPL	Sound Pressure Levels
SQL	MS Access Query
SSI	Scientific Solutions, Inc
TFD	Turners Falls Dam
TFI	Turners Falls Impoundment
USFWS	United States Fish and Wildlife Service
USGS	United States Geological Survey

EXECUTIVE SUMMARY

FirstLight Hydro Generating Company (FirstLight) is the current licensee of the Northfield Mountain Pumped Storage Project (Northfield Mountain Project, FERC No. 2485) and the Turners Falls Hydroelectric Project (Turners Falls Project, FERC No. 1889). FirstLight has initiated with the Federal Energy Regulatory Commission (FERC, the Commission) the process of relicensing the Northfield Mountain and Turners Falls Projects using the FERC's Integrated Licensing Process (ILP). The current licenses for the Northfield Mountain and Turners Falls Projects were issued on May 14, 1968 and May 5, 1980, respectively. This report documents the second year (2016 and 2018) of *Evaluating the Use of an Ultrasound Array to Facilitate Upstream Movement to Turners Falls Dam by Avoiding Cabot Station Tailrace.*

The purpose of this study was to build on knowledge gained from the 2016 ultrasound evaluation and to further investigate whether the use of ultrasound is an effective method to deter adult American Shad from the Cabot Station tailrace and facilitate movement up into the Turners Falls bypass reach toward the fish ladder at the Turners Falls Dam (TFD) spillway (Spillway Ladder). The configuration of the 2016 ultrasound array and its proximity to the Cabot Station discharge was affected by significant air entrainment, which likely increased the attenuation and scattering of sound propagating through the water, causing reduced effectiveness of the sound barrier unless American Shad were within the immediate vicinity of the array. Using the results from the 2016 study and additional sound measurements collected in November 2017, a new configuration of ultrasound transducers was designed to optimize signal strength, minimize air entrainment, and produce a continuous sound field spanning across the Cabot Station tailrace.

For the 2018 evaluation, 250 early migrating adult American Shad were radio tagged and released at the fish lift at Holyoke Dam for use in this study. Monitoring of tagged fish was achieved through the use of eleven (11) radio monitoring stations positioned between Montague and the Spillway Ladder. Telemetry data analysis revealed that 137 (~55%) of the 250 tagged fish successfully reached the Project area, defined as those fish detected by the monitoring station (T02) at Montague. Any fish that did not reach the Project area were removed from the analysis.

Of the 137 tagged fish arriving to the Project area in 2018, 112 fish were detected in the Cabot Station tailrace and 55 of those fish made 117 movements toward the Cabot Station fish ladder (Cabot Ladder). The fish that made these 117 movements in 2018 toward the Cabot Ladder were recaptured in other locations, with fish quickly moving back to the tailrace, bypass reach, or elsewhere downstream subsequent of their preliminary movement toward the ladder. While these movements are a sign that the ultrasound array was triggering a response in adult shad, the Cabot Ladder still provided attraction for fish even when the ultrasound array was on, and a significant amount of passage via the Cabot Ladder occurred with 24,031 fish counted during 2018. Historically, the Cabot fish ladder has passed more American Shad than the Spillway fish ladder. Interestingly, when bypass flow was manipulated for telemetry studies, the ratio of Spillway to Cabot count increased, and in 2018, the ratio was greater than 1, meaning more fish used Spillway Ladder than Cabot Ladder.

An analysis of movement within the Cabot tailrace revealed that fish are more likely to move into the bypass reach from the tailrace when short term variability at Cabot Station is high (i.e. operations change). Conversely, when fish are present in the Cabot tailrace, they are less likely to move into the bypass reach the higher Cabot Station is discharging. For every 1,000 cfs over baseline, fish are 0.87 times as likely to move.

In 2018, FirstLight assessed the arrival rate at the next upstream telemetry station within the bypass reach. Of the 85 fish that arrived at the entrance to the bypass (*Conte Discharge Radio Telemetry Station*), 36

(36/85 = 42%) were able to reach just downstream of the Station No.1 discharge, and 33 of those 36 fish (33/36 = 92%) continued upstream, while the remaining fish moved back downstream. During the study, approximately 1/3 of the total bypass flow was passed via Station No. 1 and the remaining 2/3 of the bypass flow was provided by the TFD spill and the Spillway Ladder fishway/attraction flow. Since 92% of the fish passed Station No. 1, the 1/3 and 2/3 flow split appeared to be successful at moving fish above Station No. 1.

Only 42% of the fish that entered the bypass reach continued moving upstream until just downstream of Station No.1, suggesting there could be a natural physical or velocity barrier near Rawson Island and Rock Dam, which is discussed later in this report. This was corroborated by the 2015 shad telemetry study, which showed that shad made several attempts to move upstream within either channel around Rawson Island, including toward Rock Dam, before eventually moving back downstream. These results may warrant further research within the area of Rawson Island to fully understand upstream movement in the area. Of the fish that made it to the vicinity of the spillway, 23 moved back downstream and did not enter the Spillway Ladder, suggesting that fish are having trouble finding the entrance to the Spillway Ladder, further corroborating the results of the 2015 telemetry study.

In 2015, 2016 and 2018, most of the fish that moved upstream within the bypass reach did so when flows were within the range of 3,000 to 6,000 cfs. However, there was an interaction effect with day of year and flow. Every day, the likelihood that a tagged fish is attracted to the spillway decreases (HR = 0.99). If we were to compare the likelihood of movement for two fish entering the bypass reach 30 days apart, the effect of flow decreases over this time, and is only 0.74 times as effective 30 days later. The aggregated bypass model also demonstrated that the likelihood of moving to the spillway decreases if bypass flow is unstable. The reach is generally wide, shallow, with complex channels and hydraulics, and is predominantly bedrock ledge in some areas. We hypothesize that small changes in flow while a fish is present can have effects on the localized zone of passage, meaning fish have to constantly adapt to a dynamic riverscape while in the bypass reach.

A detailed analysis of fallback fish was performed using information from American Shad telemetry studies in 2015, 2016, and 2018 (n = 1,258 tagged fish) to assess the factors that may influence a fish to "fall back" after being tagged. A series of generalized linear models were created to pinpoint the most significant variables (sex, fat content, descaling, river flow, and water temperature) that may cause any adverse effects after tagging. The best model describing fallback fish included fish tested with the fat meter (n=601), fish tested for descaling, sex and river flow, resulting in fish tested with the fat meter and river flow as significant covariates. Model results concluded that fish tested using the fat meter were 68% more likely to fall back after tagging. River flow was less significant but suggested that increased river flow as measured at the United States Geological Survey (USGS) gage[1] on the Connecticut River in Montague may increase the likelihood of fallback. We concluded that any activity that increases handling time of fish during the tagging process may increase the chances of fallback. Therefore, to get the best performance of fish after tagging, any metrics associated with increased handling time (recording: sex, length, descaling, fat content, etc.) may not be worth the effort due to the increased likelihood of fallback. Even 30 seconds of increased handling time could significantly decrease the proportion of tagged fish reaching the Project area.

[1] The USGS gage is located on the Connecticut River just below the confluence with the Deerfield River.

1 INTRODUCTION

Unlike most other fish species, it has been demonstrated that American Shad (*Alosa sapidissima*) are able to detect sound up to 180 kilohertz (kHz) (Higgs, 2004). Previously, it was proposed that ultrasound detection in shad involves swim bladder extensions; however, more recent work indicates that the utricle, an organ found in inner ear of some Clupeids, allows detection of ultrasonic stimulation (Higgs, 2004). Researchers theorized that Clupeids can detect the ultrasonic clicks of one of their major predators, echolocating cetaceans.

An evaluation of the use of an ultrasound array to deter adult shad from the Cabot Station tailrace and facilitate their upstream movement by Cabot and through the bypass reach to Turners Falls Dam (TFD) was requested by U.S. Fish and Wildlife Service (USFWS), New Hampshire Fish & Game Department (NHFGD) and Connecticut River Watershed Council (now the Connecticut River Conservancy or CRC). A potential alternative to the current configuration of fish ladders at the Turners Falls Project would be to operate a single fish passage facility further upstream near the TFD. For this alternative, minimizing[2] attraction to the Cabot Station Ladder (Cabot Ladder) could encourage more fish to enter the bypass reach and move further upstream toward the fish passage facility at the Spillway.

In the spring of 2016, an ultrasound study was conducted to deter adult shad from entering the Cabot Station tailrace and facilitate upstream movement into the bypass reach. Fish behavior was evaluated with a combination of radio telemetry and Passive Integrated Transponders (PIT) technologies, as well as a Dual Frequency Identification Sonar (DIDSON) camera installed at the entrance to Cabot Ladder, within the vicinity of the ultrasound array. Count data from the DIDSON camera revealed that there was no significant difference between median daily fish counts on days that the array was on and when it was off. However, when the count data from the DIDSON were further analyzed on an hourly scale, within the first two hours of activating the ultrasound system ("on"), there was a significant interaction effect between the system status (on or off) and shad counts at the Cabot Ladder. This suggested that the ultrasound array affected adult shad, but they may have been able to acclimate to the sound when the array was on for relatively long periods of time.

This study builds on knowledge gained in 2016 and furthers the investigation into whether the use of ultrasound technology is an effective method to minimize shad attraction to the Cabot Ladder, while moving shad up the bypass reach. In the 2016 study, the sound was emitted from three transducers with different horizontal orientations mounted to a pole located on the Cabot Ladder wall near the entrance and two transducers, with different horizontal orientations, mounted on a pole installed approximately at the midpoint on the back of the powerhouse (discharge location). Air entrainment from the Cabot Station turbine discharge and fish ladder flow significantly increased the attenuation and scattering of the sound field, effectively reducing sound pressure levels (SPLs) below thresholds that would elicit strong and prolonged avoidance reactions from adult shad unless fish were within the immediate vicinity of the transducers including at the fish ladder entrance. This is most likely why we observed a reaction near the Cabot ladder entrance for the two hours subsequent to reactivating the system in 2016. Using the new data from sound measurements collected on November 15, 2017 and from the results of sound modeling, transducer locations, numbers, and orientations for the 2018 study were selected to minimize interference from air entrainment and optimize signal strength in an attempt to produce a continuous sound field spanning across the edge of the tailrace and with SPLs greater than the 160 decibels (dB) (Figure 1-1).

FirstLight radio-tagged 250 early migrating adult shad for this study. Priority was given to those fish arriving early at the Holyoke fish lift, as it is believed that these fish are more motivated and more fit to

[2] What is considered effective at minimizing the attraction to the Cabot tailrace is discussed later in this document.

successfully traverse the 35 river miles from Holyoke to Cabot Station, when compared to those arriving later in the migration season at Holyoke.

These radio-tagged fish were monitored with a combination of Orion and Lotek receivers (n=14). The monitoring equipment was deployed and calibrated to inform on the effects of the ultrasound array on migration routes and behavior.

The location of the ultrasound array includes habitat known to be used by spawning Shortnose Sturgeon (SNS). For the purposes of this study, the array operated during the overlapping SNS spawning and upstream shad migration season. As SNS are not capable of hearing sounds in the frequency proposed for this study, they were not predicted to be disturbed by the operation of the ultrasound array. Staff from National Marine Fisheries Service (NMFS) Protected Resources Division agreed that the ultrasound array proposed for this study would not impact the SNS (Pers. Comm., J. Pruden, NMFS).

1.1 Background

Every spring, mature adult American Shad enter the Connecticut River to search for spawning and rearing habitat necessary for their anadromous life history. Shad migrate inland from marine waters and spawn in areas of suitable habitat as they move upstream. During the upstream migration, prior to entering Project waters, shad first encounter the Holyoke Dam in Holyoke, MA. The Holyoke Dam provides upstream passage via a fish lift and allows access to approximately 35 river miles of mainstem habitat in the Connecticut River. All fish used in this study were captured at the Holyoke Dam fish lift at the existing fish trapping facility.

The next manmade barrier encountered by upstream migrating fish is the TFD, located at approximately river mile 122 on the Connecticut River mainstem. Upstream migrating fish may pass the TFD via two potential routes. Just downstream of the TFD, fish may use the Cabot Ladder, located at approximately river mile 120, to enter the power canal. Adult shad moving up the power canal can pass through the Gatehouse Ladder which provides access to Turners Falls Impoundment (TFI). Fish that bypass the Cabot Ladder may continue to move upstream via the approximate 2.1-mile bypass reach toward the base of the TFD where they can find passage via the Spillway Ladder, from which they can pass directly into the Gatehouse Ladder and then into the TFI.

The purpose of this study was to evaluate the use of an ultrasound array to deflect shad away from the Cabot Station tailrace and facilitate upstream movement through the bypass reach toward the Spillway Ladder. A potential alternative to the current configuration of fishways at the Turners Falls Project would be to minimize attraction to the Cabot Ladder and operate a single fishway facility further upstream, closer to the TFD.

1.1.1 Ultrasound Array Studies

To date, there is no universal behavioral barrier that is effective for all species and lifestages of fish. The use of behavioral barriers or deterrents is considered experimental. Previous work has demonstrated that the alosine species (e.g., American Shad, Blueback Herring, and Alewife) can detect high-frequency sound, and studies that attempted to produce behavioral avoidance by adult shad suggests that ultrasound is an effective stimulus (Carlson and Popper, 1997). Clupeids are able to detect high-frequency sound due to their modified inner ear structure that differs from other fishes (Higgs, 2004). The inner ear of Clupeiformes is surrounded by gas-filled bubbles known as bullae that are connected to the swim bladder via a thin elastic-like thread (Blaxter and Hunter, 1982). As pressure waves intersect a shad, they cause vibrations in the swim bladder and the attached auditory bullae (Denton and Blaxton, 1979). This pressure transfer allows the fish to respond to high-frequency sound that other fish may miss due to the absence of this connected pathway (Higgs, 2004).

Recent studies have shown the effectiveness of high-frequency sound fish diversion, particularly for deterring fish in the family Clupeidae at hydroelectric generating facilities. A study at the Annapolis Tidal Generating Station in Nova Scotia, Canada assessed the effectiveness of high-frequency sound to reduce fish passage through the turbines. Researchers concluded the system was not effective for many of the fish species tested, but for members of the genus *Alosa* (specifically, American Shad and Alewife), rates of passage through the turbines decreased by 42% and 48%, respectively, when the system was activated (Gibson, Jamie and Myers, 2002).

High frequency sound used at the James A. Fitzpatrick nuclear power plant on Lake Ontario was found to reduce impingement of Alewife by more than 80%, and its use was approved by the regulatory agencies (Kynard and Taylor, 1984). Upstream migrants were guided well and were even stopped entirely by the ensonified field (Kynard and Taylor, 1984). Creating an ensonified field caused adult shad to leave their preferred location in the river upstream of trashracks at Holyoke Dam while the sound system was on.

Blueback Herring also avoided the ultrasound field and behaved like shad in the Holyoke Canal studies (Kynard and Taylor, 1984). Acoustic barriers have been used for migrating Blueback Herring on the Savannah River (Richard B. Russell Dam) and Santee River (St. Stephen fish lift) in South Carolina and emigrating Blueback Herring on the Mohawk River in New York (Crescent Project, FERC No. 4678; Vischer Ferry, FERC No. 4679). In a 2012 study at the Crescent Hydroelectric Project on the Mohawk River, NY, researchers assessed the use of an ultrasonic field to deter out-migrating adult and juvenile Blueback Herring from entering the intake channel to reduce turbine passage impacts. In an attempt to expose fish to an increasing gradient of sound, and to allow more time for avoidance, the sound field was redirected from a perpendicular to a 45-degree, upstream orientation in the main channel of the Mohawk River (Gurshin et al., 2014). Once the ultrasound array was redirected, a 76.5% increase in the proportion of herring migrating downstream via the main channel rather than the intake channel was observed (Gurshin et al., 2014).

Since 2006, Hydro-Québec has successfully used an ultrasound device in front of the water intakes of the Rivière-des-Prairies Hydroelectric Facility to guide downrunning spent adult shad away from the intakes (Guindon and Desrocher, 2016a). Based on the success of the ultrasound guidance system, Hydro-Québec is currently studying efforts using ultrasound to prevent adult shad from entering Rivière-des-Prairies and guide them to other outlets (Guindon and Desrocher, 2016b).

The use of high frequency sound as a deterrent for some fish species is becoming more popular but more research is needed to fully assess its effectiveness in field settings; each location is unique with regard to its configuration and the potential designs of an effective ultrasound array.

1.2 Goals and Objectives

In 2016, FirstLight evaluated the use of an ultrasound array to deter shad from the Cabot Station tailrace and facilitate upstream movement of American Shad toward the TFD as requested by the USFWS, NHFGD, and CRC. The goal was to determine if an ultrasound barrier could be used to repel adult shad from the Cabot Station tailrace and guide them into the bypass reach.

The goal of this 2018 study was to establish a high-frequency sound (ultrasound) array across the entire Cabot Station tailrace and determine the effect of the ensonified field on upstream migrating shad moving past Cabot Station. Specific objectives for this study included:

- to establish an ultrasound array extending to the edge of the Cabot Station tailrace;
- to determine if migrating adult shad that experience the ultrasound array continue migrating further upstream in the bypass reach (to be determined using radio telemetry); and
- to investigate if the magnitude of the bypass flow and magnitude of Cabot Station discharges affect how adult shad respond to the array and specifically whether they migrate further up the bypass reach.

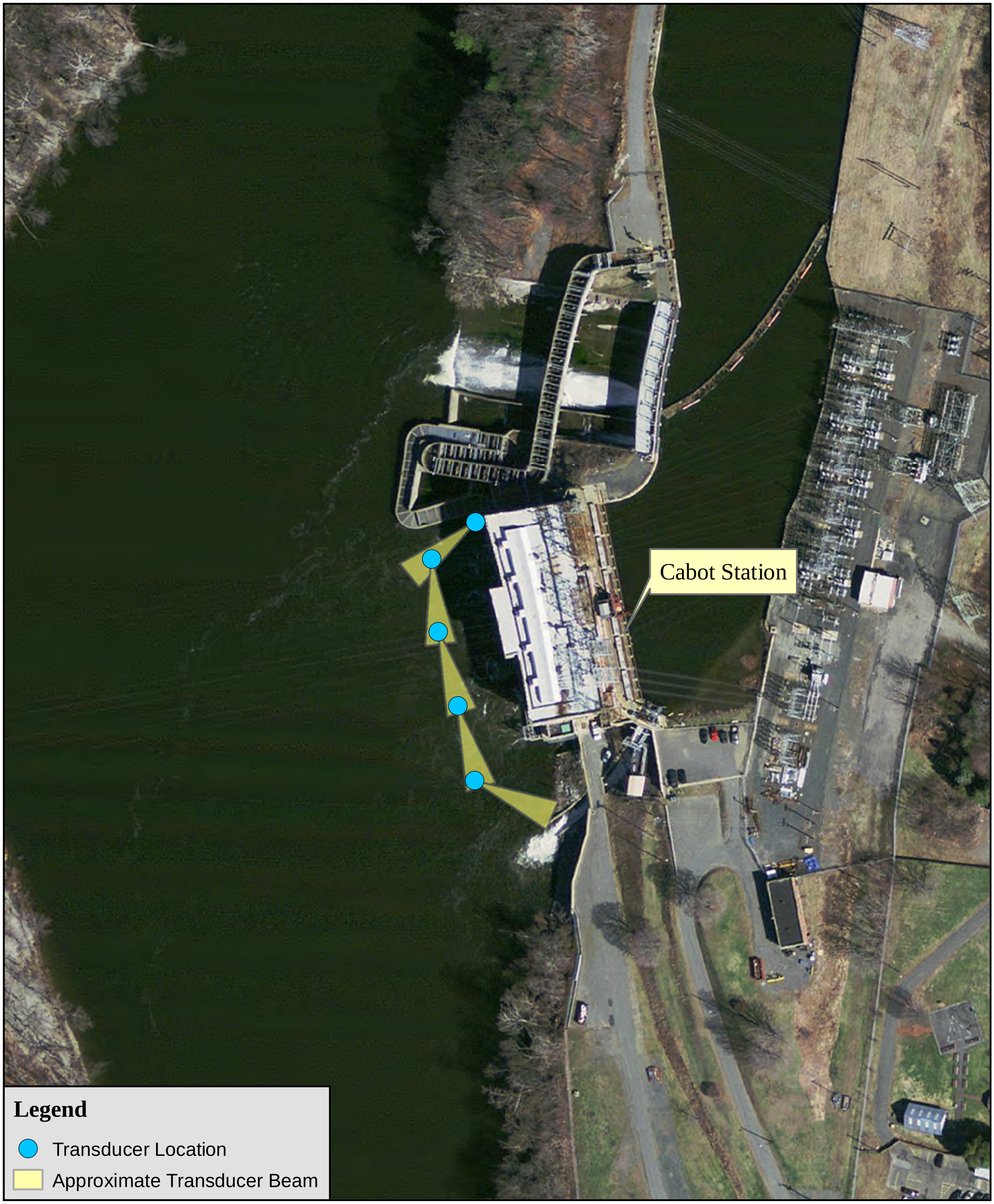

FirstLight Power Resources

N

0 75 150 300 Feet

Northfield Mountain Pumped Storage Project (No. 2485)
and Turners Falls Hydroelectric Project (No. 1889)

Relicensing Study 3.3.19

Figure 1-1: Transducer locations and approximate associated ultrasound coverage fields

© 2018 FirstLight Power Resources. All rights reserved.

Path: W:\gis\studies\3_3_19\maps\ReportFigure2018\Figure1-1.mxd

2 STUDY AREA

The study area generally consisted of the Connecticut River extending from the Holyoke Dam in Holyoke, MA to the TFD, in Turners Falls, MA (Figure 2-1). Fish were considered to enter the study area when they arrived at the Montague Wastewater Treatment Facility. Between the Montague Wastewater Treatment Facility and the Spillway at the TFD, fish encounter the following:

Cabot Station

Fish moving into and/or through the Cabot Station tailrace encounter flows from Project generation, the log sluice, and the Cabot Ladder. Depending on inflow, flows from Cabot Station generation can range from no flow up to Project capacity at 13,728 cfs. Continuous flows of approximately 200 cfs and 368 cfs are released from the log sluice and Cabot Ladder, respectively, during typical operations within the shad passage season.

The Cabot Ladder is a modified "ice harbor" design consisting of 66 pools. Each pool is situated approximately one foot higher than the previous pool. The entrance to the fishway is located adjacent to the Cabot Station tailrace and the exit deposits fish into the power canal. Approximately 2.1 miles upstream at the head of the canal, the Gatehouse Ladder permits access to the TFI.

Bypass Reach

Fish moving into the bypass reach encounter Smead Island across from Cabot Station (see Figure 2-2). Adult shad that move by Smead Island and beyond the Conte Lab encounter Rawson Island, which divides the river into two channels (see Figure 2-2). On river-left (looking downstream), fish would encounter Rock Dam, a natural rock falls having a steep vertical drop. On river-right (looking downstream), fish would have to negotiate through the river-right channel or a second smaller channel to continue upstream. As discussed later in this report, based on the telemetry findings it appears there is a natural velocity barrier on the river-right side of Rawson Island making it difficult for adult shad to negotiate. Also, on river-left, Rock Dam appears to be a natural vertical barrier to fish passage.

Fish moving beyond Rawson Island encounter the Station No. 1 discharge (if operating). As discussed later in this report, when the 2018 ultrasound study was conducted, FirstLight tried to maintain a flow split such that approximately 33% of the total bypass flow was from the Station No. 1 discharge and the remaining approximately 67% was provided from a combination of the TFD spill and the Spillway Ladder attraction/fishway flow.

Spillway Ladder

Fish swimming beyond the Station No. 1 discharge arrive at the TFD where they can find passage via the Spillway Ladder (modified ice harbor design with 42 pools), which moves fish into the Gatehouse's vertical slot fishway, where they rejoin fish that have used the fish ladder at Cabot Station to pass upstream through the power canal.

Northfield Mountain Pumped Storage Project (No. 2485)
and Turners Falls Hydroelectric Project (No. 1889)
Relicensing Study 3.3.19

N

0 2 4 8 Miles

Figure 2-1: Overview of the study area extending from the Turners Falls Impoundment to Holyoke, MA

Copyright © 2017 FirstLight Power Resources All rights reserved.

Path: W:\gis\studies\3_3_19\maps\ReportFigure2018\Figure2-1.mxd

FirstLight Power Resources

Northfield Mountain Pumped Storage Project (No. 2485)
and Turners Falls Hydroelectric Project (No. 1889)
Relicensing Study 3.3.19

Figure 2-2:
Lower Bypass Reach Features

N

0 0.125 0.25 0.5
Miles

Copyright © 2019 FirstLight Power Resources All rights reserved.

Path: W:\gis\studies\3_3_19\maps\ReportFigure2018\figure_2-2_bypass_features.mxd

3 METHODS

3.1 Study Design and Methods

Beginning in the first week of April 2018, FirstLight installed a series of active radio telemetry monitoring stations within the study area. Fixed monitoring stations were confined to the area between the Montague Wastewater Treatment Facility and the Spillway Ladder entrance just below the TFD (Figures 3.1-1 and 3.1-2). Fixed monitoring locations were sited to answer specific questions as defined in the study objectives.

3.2 Ultrasound Array

Alden Research Laboratory (Alden) and Scientific Solutions, Inc. (SSI) configured and installed the ultrasonic deterrent system as a method for repelling adult American Shad away from the Cabot tailrace and the adjacent fish ladder entrance during the 2018 upstream spawning migration (installation - April 28, 2018). Figure 1-1 depicts the configuration of the array within the Cabot Station tailrace.

The 2018 ultrasound configuration included additional transducers and power amplifiers, as improvements to the 2016 design. The intent for 2018 was to move the array outward, away from the powerhouse, to minimize the impact of entrained air and to achieve higher projector source levels with a more uniform sound pressure field at the outer perimeter of the Cabot Station tailrace. A full report detailing the methods of Alden and SSI's installation process and testing regarding the ultrasound system is provided in Appendix A.

3.3 Telemetry Network

FirstLight deployed 14 radio telemetry monitoring stations within the study area (Table 3.3-1and Figures 3.1-1 and 3.1-2). In some locations, receivers were grouped together into super stations to take advantage of receiver overlap, maximize coverage, and to understand the logical pathways that connect critical locations throughout the study reach. Super stations are denoted '*SXX*' and are generally numbered from downstream to upstream; whereas telemetry stations denoted with '*TXX'* can have random numbering in no apparent order as evidenced with the Deerfield station labeled as T01 and the Montague station labeled T02. Superstations are logical groupings of receivers; they were used in the background when developing models, were crucial to understanding and removing overlap between receiver detection areas, and are depicted in Figure 3.3-3.

Radio telemetry monitoring was achieved through the use of Orion receivers manufactured by Sigma Eight, and SRX 800 receivers manufactured by Lotek. Orion and Lotek receivers were deployed to maximize the effectiveness of monitoring stations. The Orion receiver is a broadband receiver capable of monitoring multiple frequencies simultaneously within a 1-megahertz (MHz) band. These receivers are particularly well-suited for monitoring tagged fish in areas where movement through a monitoring zone can occur quickly, such as intakes or bypasses. Lotek receivers are narrowband receivers that have longer detection ranges than Orion receivers. However, narrowband receivers can only monitor a single frequency at once and require frequency switching, which can result in less detection reliability in areas where fish move quickly. The telemetry receivers were powered by 12-volt deep-cycle batteries, which were maintained via alternating current or solar powered chargers.

The radio telemetry monitoring network was designed to monitor tagged shad as they migrated within the study area. Prior to initiating the study, all monitoring locations were tested for calibration to ensure that the desired detection zones were achieved. The results of the calibration efforts are detailed in Appendix B.

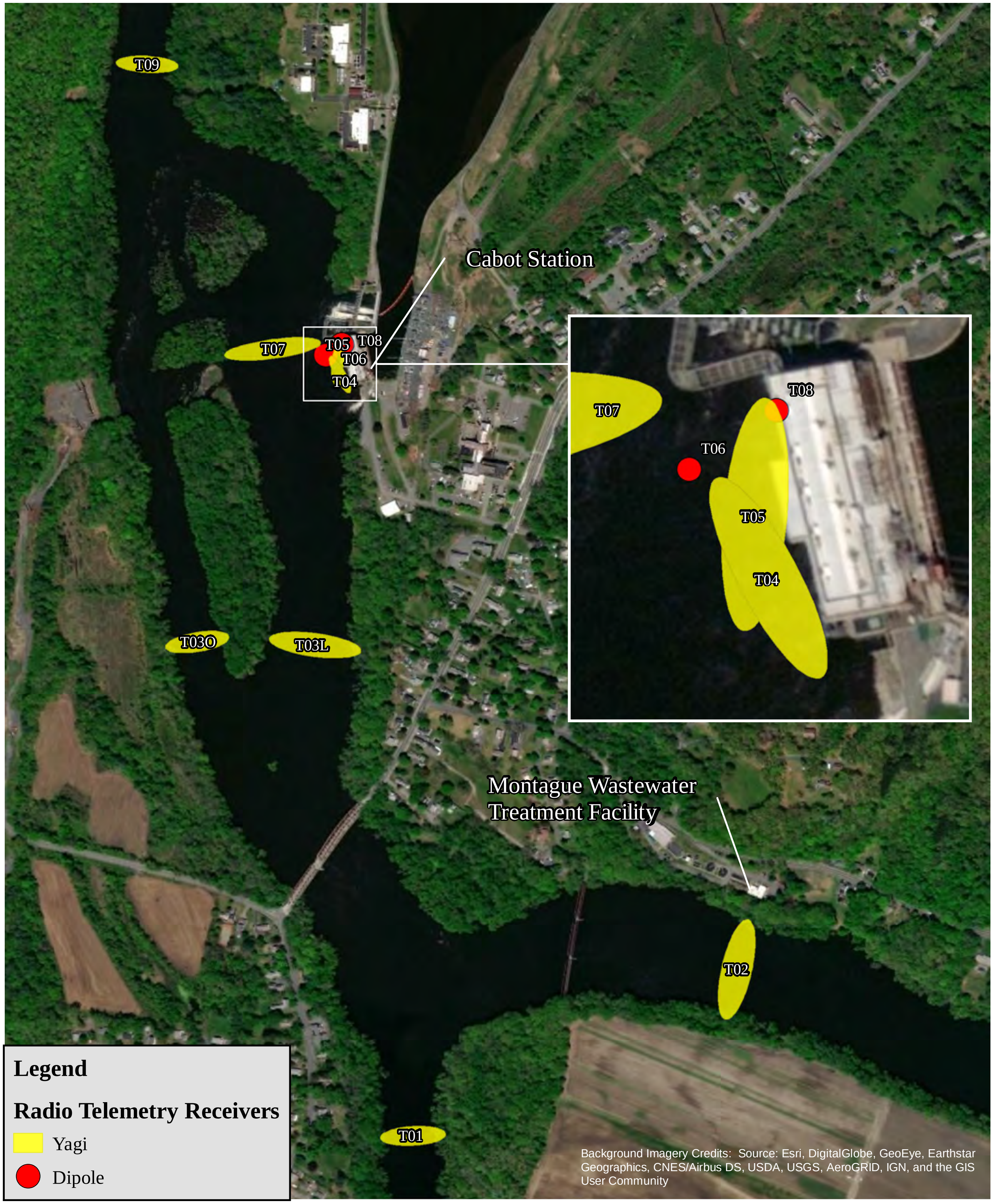

Northfield Mountain Pumped Storage Project (No. 2485)
and Turners Falls Hydroelectric Project (No. 1889)

Relicensing Study 3.3.19

Figure 3.1-1: Radio Telemetry Sites for Ultrasound Array Study

© 2018 FirstLight Power Resources. All rights reserved.

Path: W:\gis\studies\3_3_19\maps\ReportFigure2018\Figure3.1-1.mxd

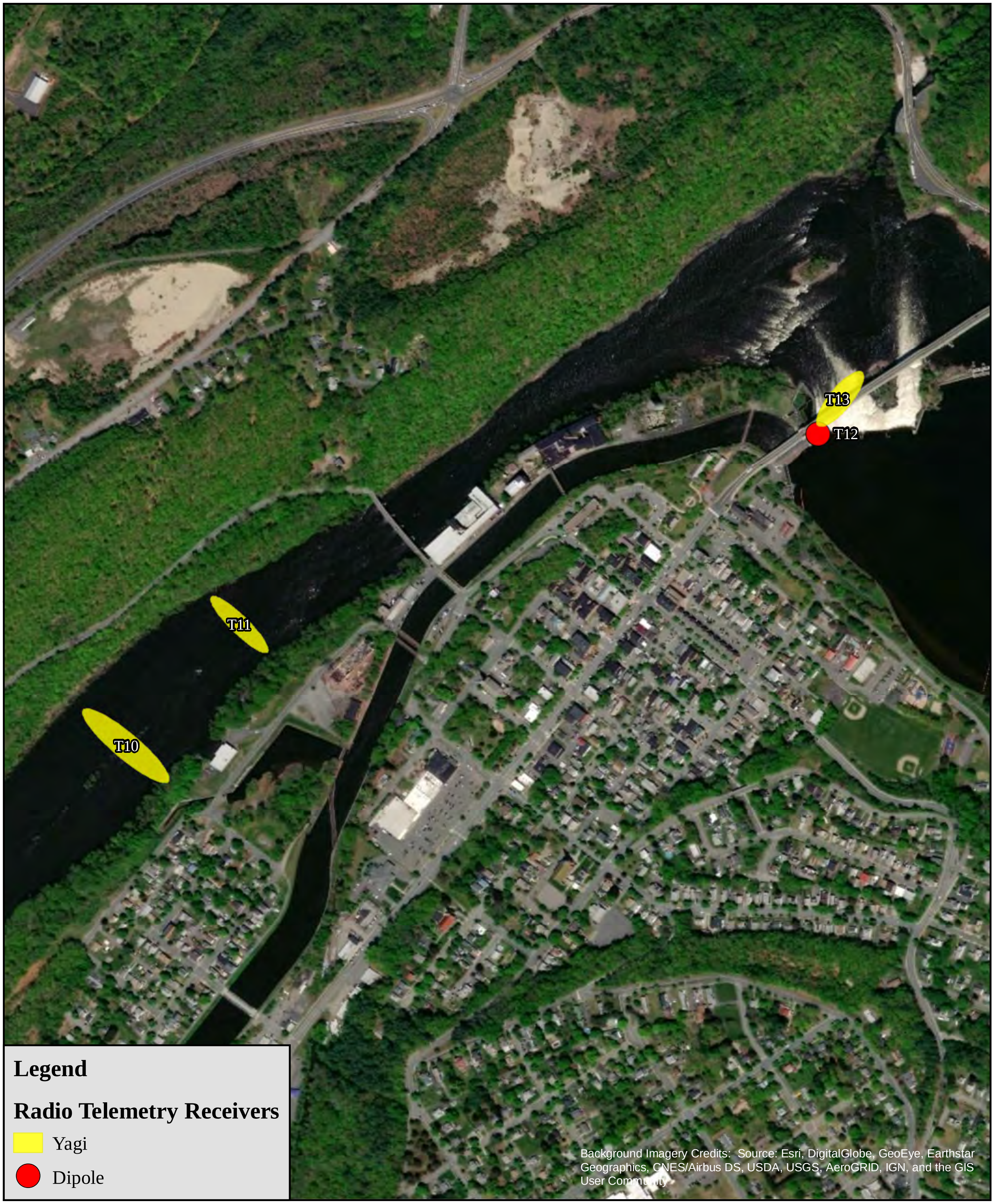

Northfield Mountain Pumped Storage Project (No. 2485)
and Turners Falls Hydroelectric Project (No. 1889)

Relicensing Study 3.3.19

N

0 375 750 1,500
Feet

Figure 3.1-2: Radio Telemetry Sites for Ultrasound Array Study

© 2018 FirstLight Power Resources. All rights reserved.

Path: W:\gis\studies\3_3_19\maps\ReportFigure2018\Figure3.1-2.mxd

Table 3.3-1: Shad monitoring locations and equipment used in the 2018 ultrasound evaluation

Station Location	Telemetry Receiver	Station ID	RM	Receiver Station
Montague Wastewater Treatment Facility	T02	S01	118.3	A Lotek SRX receiver with Yagi antenna monitored the full width of the river
Deerfield River	T01	S02	118.8	An Orion receiver with Yagi antenna
Smead Island West	T03O	S03	119.0	A Lotek SRX receiver with Yagi antenna
Smead Island East	T03L	S04	119.0	An Orion receiver with Yagi antenna
Cabot Tailwater (farfield)	T07	S05	119.3	A Lotek SRX receiver with Yagi antenna monitored the Cabot tailrace
Right Side of Cabot Tailrace	T05	S06	119.3	An Orion receiver with Yagi antenna monitored the Cabot tailrace
Left Side of Cabot Tailrace	T04	S06	119.3	An Orion receiver with Yagi antenna monitored the Cabot tailrace
Cabot Tailrace (nearfield)	T06	S07	119.3	An Orion receiver with stripped coaxial antenna array
Cabot Ladder Entrance	T08	S08	119.3	An Orion receiver with dipole antenna
Conte Discharge Area	T09	S09	119.7	An Orion receiver with Yagi antenna
Bypassed Reach, Downstream of Station No. 1	T10	S10	121.1	A Lotek SRX receiver with Yagi antenna
Bypassed Reach, Upstream of Station No. 1	T11	S11	121.2	A Lotek SRX receiver with Yagi antenna
Spillway Ladder Entrance	T12	S13	122.2	An Orion receiver with dipole antenna
Spillway Ladder Vicinity	T13	S12	122.2	A Lotek SRX receiver with Yagi antenna

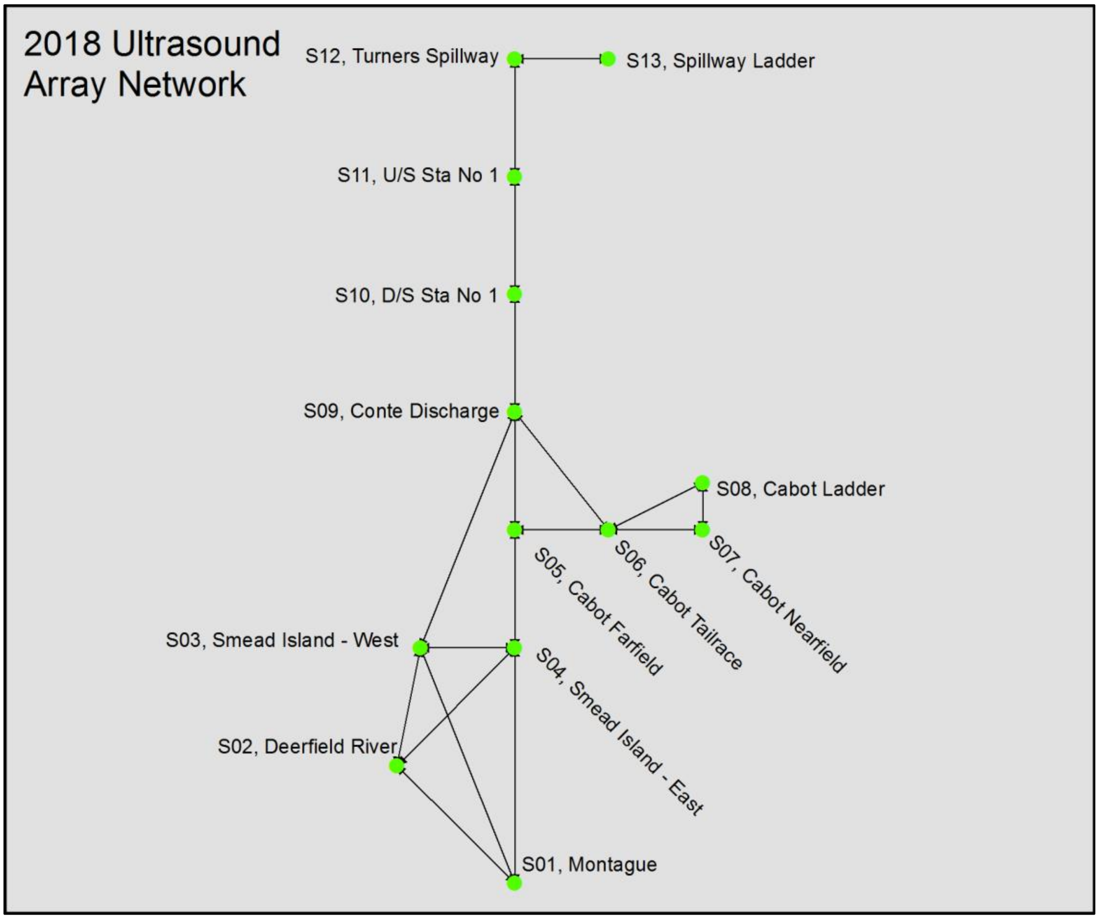

Figure 3.3-3: Radio telemetry network for 2018 ultrasound evaluation

3.4 Adult Shad Collection and Tagging

Test fish were collected and tagged at the fish trapping facility at the Holyoke Dam. Multiple cohorts were tagged and immediately released upstream of the Holyoke Dam via the fish lift exit flume. Tagging priority was given to the first groups of shad arriving at Holyoke based on previous telemetry study results indicating that shad arriving first are more motivated and more biologically fit to successfully make the upstream journey from Holyoke to Turners Falls, MA as compared to the fish arriving later in the migratory season. A full description of results and comparisons of tagging early and late in the season are discussed in the 2018 Study Plan for this Ultrasound Study.

Tagging consisted of esophageal implantation of radio tags. Data were recorded on field data sheets and included sex, total length, condition, and tag identification number for each tagged shad. Shad were selected at random, but only those that exhibited vigor and minimal scale loss (less than 10%, evaluated subjectively in the field) were tagged. Shad were tagged with TX-PSC-I-80-M Pisces transmitters manufactured by Sigma Eight. The tags measured 10 mm by 28 mm and operated on two frequencies, 150.500 and 150.560 MHz. They were programed with a two-second burst and a mortality function, which defaulted to an eleven-second burst upon activation. Activation of mortality was based on relative motionlessness for a period of six hours. The expected tag life was approximately 80 days.

3.5 Project Operations

A series of test flows were proposed for release into the bypass reach during the 2018 study, including 3,500 cfs, 4,400 cfs, and 6,500 cfs, and would be dependent on ambient river flow conditions. The configuration of flows was such that in May, specific test flows would each be released into the bypassed reach over a 3-day period. In June, flows to the bypass reach remained at about 2,100 cfs until the end of the study period on June 12, 2018 due to low river flow (Figure 3.5-1).

The bypass reach was separated into three smaller reaches (Figure 3.5-2) as defined in Study 3.3.1 *Instream Flow Habitat Assessments in the Bypass Reach and below Cabot Station* and described below:

- Reach 1: TFD Spillway to Station No.1
- Reach 2: Station No.1 to the upstream end of Rawson Island / Rock Dam
- Reach 3: The upstream end of Rawson Island / Rock Dam to Montague, includes inflow from Cabot Station and the Deerfield River.

Flow to Reach 1 during the study included releases from Bascule Gates 1 and 4, flows from the Spillway Ladder and associated attraction flow (about 318 cfs), and estimated inflow from the Fall River[3] (Figure 3.5-3).

Flows in Reach 2 included inflow from Reach 1 and generation flow or leakage flow from Station No.1 (Figure 3.5-4). The total bypass flow in this study references the flow in Reach 2.

Flows in Reach 3 included inflow from Reach 2, Cabot Ladder fishway/attraction flow, downstream fish bypass sluice flow (about 568 cfs), Cabot generation flow (0 to about 13,728 cfs), and Deerfield River[4] flow (varied between about 340 to 2,070 cfs) (Figure 3.5-5).

As part of Relicensing Study 3.3.1 Instream Flow Study, in Reach 1 and the upper part of Reach 2, water levels and habitat suitability were modeled at different flows. A two-dimensional (2-D) hydraulic model was developed for the upstream end of the Rawson Island complex downstream to just below the Deerfield River confluence. This includes the lower part of Reach 2 and all of Reach 3. A 2-D approach best represents hydraulics in this area due to the relatively wide and shallow river channel with complex multiple-channel characteristics and hydraulics. The 2-D hydraulic modeling was performed using River2D modeling software, which is described in Steffler and Blackburn (2002). River2D is a depth-averaged two-dimensional (lateral-longitudinal), finite-element hydraulic and habitat model. Output from the River2D provides depths and velocities on a fine scale throughout the 2D modeled area, including near Rawson Island. As noted earlier and discussed later in this document, it appears there could be a velocity barrier on the river-right side of Rawson Island. The hydraulic model, which produces depth and velocity data, was used as part of this assessment.

[3] As described in detail in the report for Study No. 3.3.1 (IFIM) on page 3-2, 15-minute interval flows from the Fall River were estimated by use of proration of the nearby USGS Gage No. 01170100 Green River near Colrain, MA.
[4] Inflow from the Deerfield which enters the downstream portion of Reach 3 was estimated by prorating the total drainage area of the Deerfield River (665 mi^2) divided by the drainage area at USGS Gage No. 01170000 Deerfield River near West Deerfield, MA (557 mi^2).

May						
S	M	T	W	T	F	S
		1	2	3	4	5
6	7	8	9	10	11	12
13	14	15	16	17	18	19
20	21	22	23	24	25	26
27	28	29	30	31		

June						
S	M	T	W	T	F	S
					1	2
3	4	5	6	7	8	9
10	11	12	13	14	15	16
17	18	19	20	21	22	23
24	25	26	27	28	29	30

ramp day
6,500 cfs
4,400 cfs
3,500 cfs
2,100 cfs

Figure 3.5-1: Flow calendar for the 2018 ultrasound evaluation

Note that the flows above include only flows from Bascule Gates 1 and 4 and Station No.1 and not flows from the Fall River and the TFD Spillway Ladder and associated attraction flow.

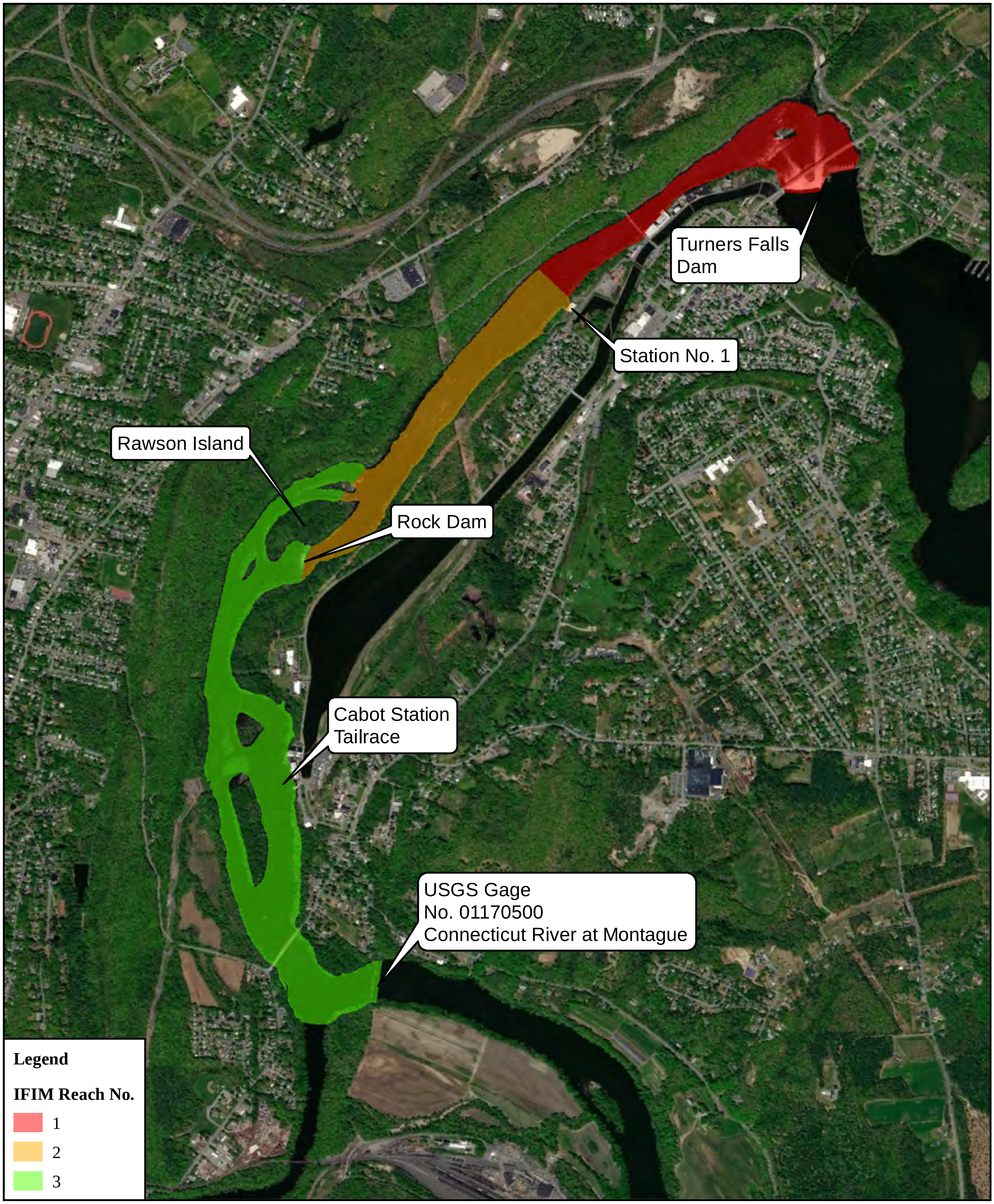

FirstLight Power Resources

Northfield Mountain Pumped Storage Project (No. 2485)
and Turners Falls Hydroelectric Project (No. 1889)

Relicensing Study 3.3.19

Figure 3.5-2: Reaches 1 to 3 from Relicensing Study 3.3.1

N

0 1,000 2,000 4,000 Feet

© 2018 FirstLight Power Resources. All rights reserved.

Path: W:\gis\studies\3_3_19\maps\ReportFigure2018\Figure3.5-2.mxd

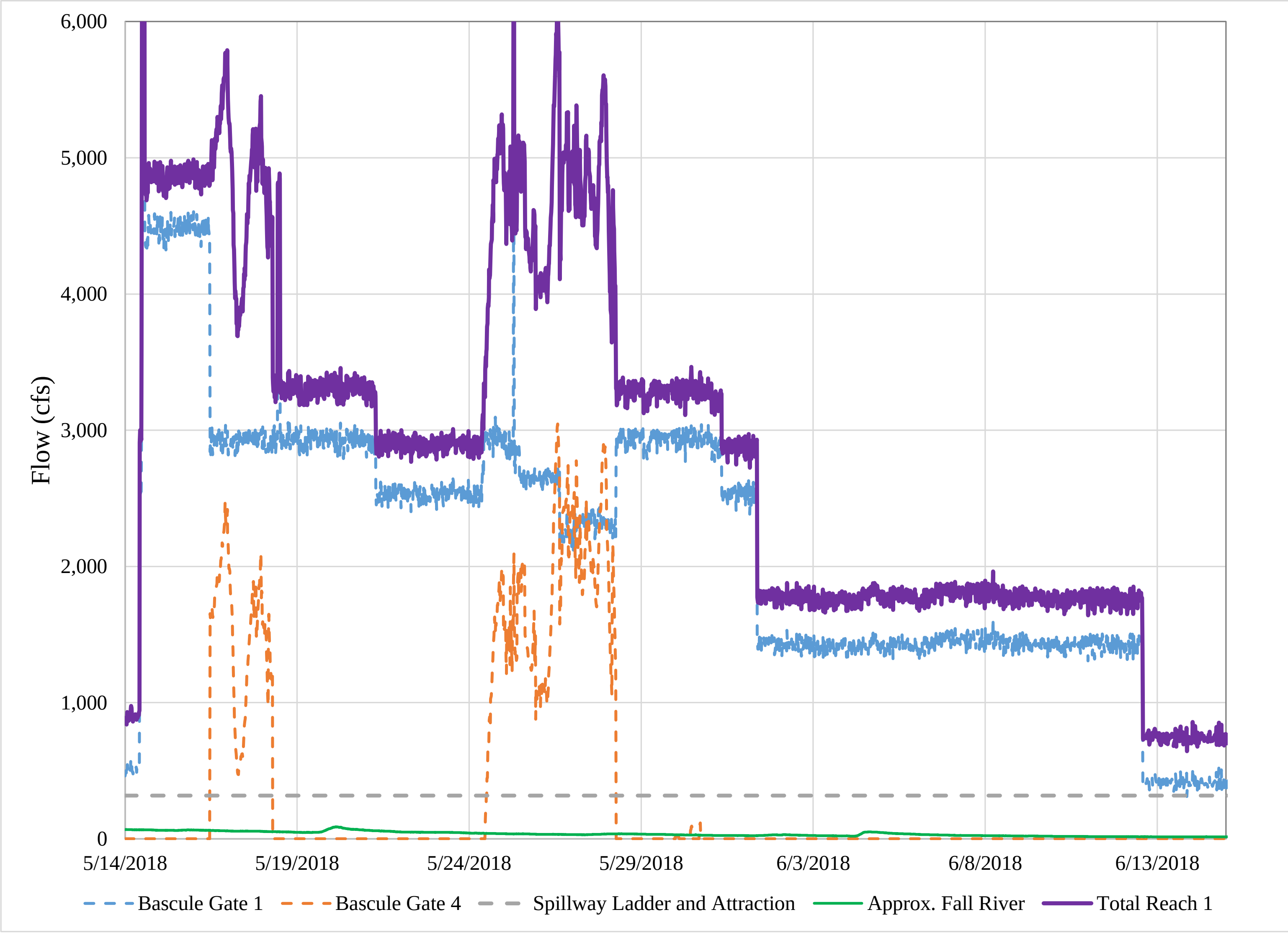

Figure 3.5-3: Reach 1 flow during the 2018 ultrasound evaluation

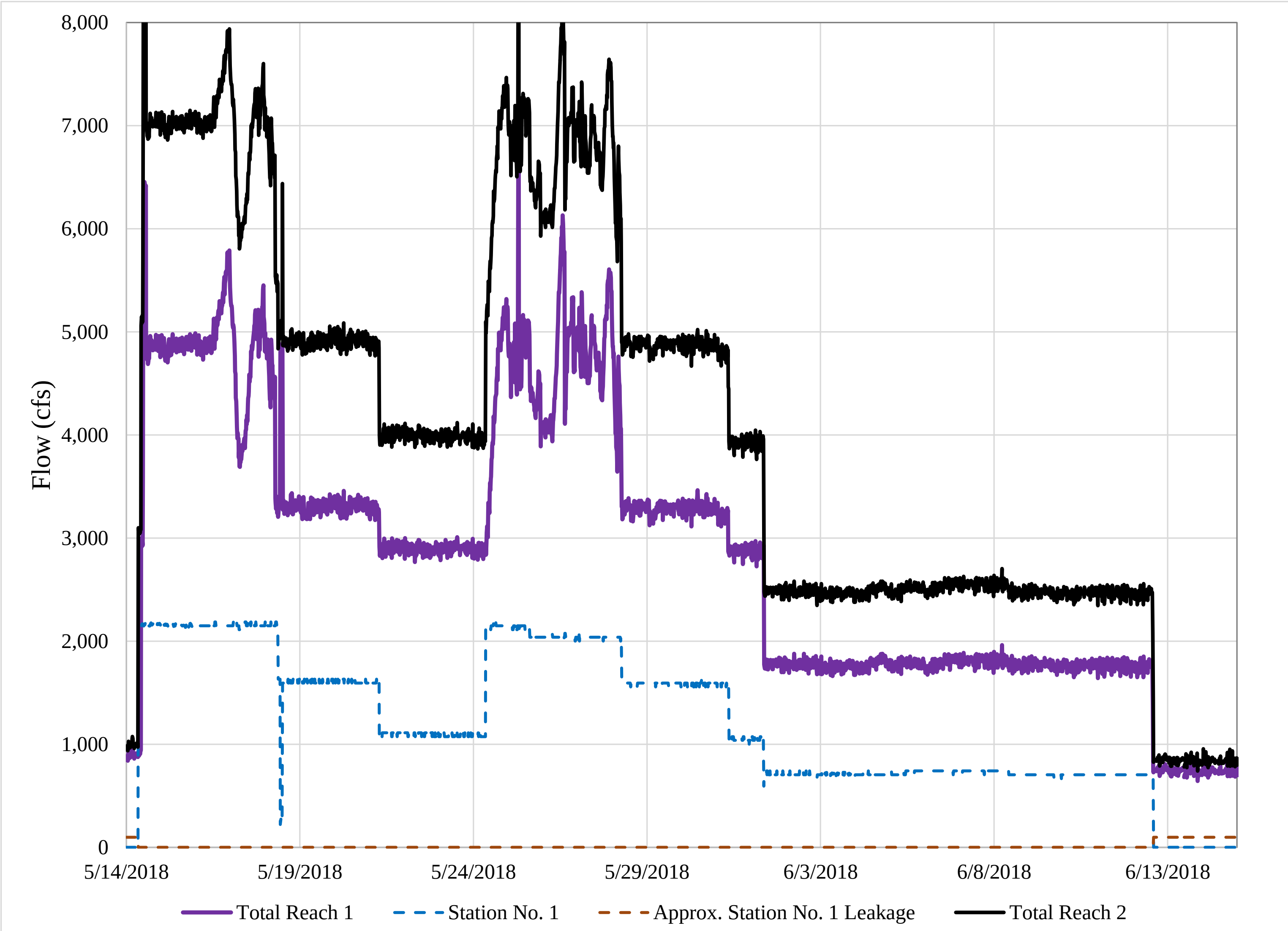

Figure 3.5-4: Reach 2 flow during the 2018 ultrasound evaluation

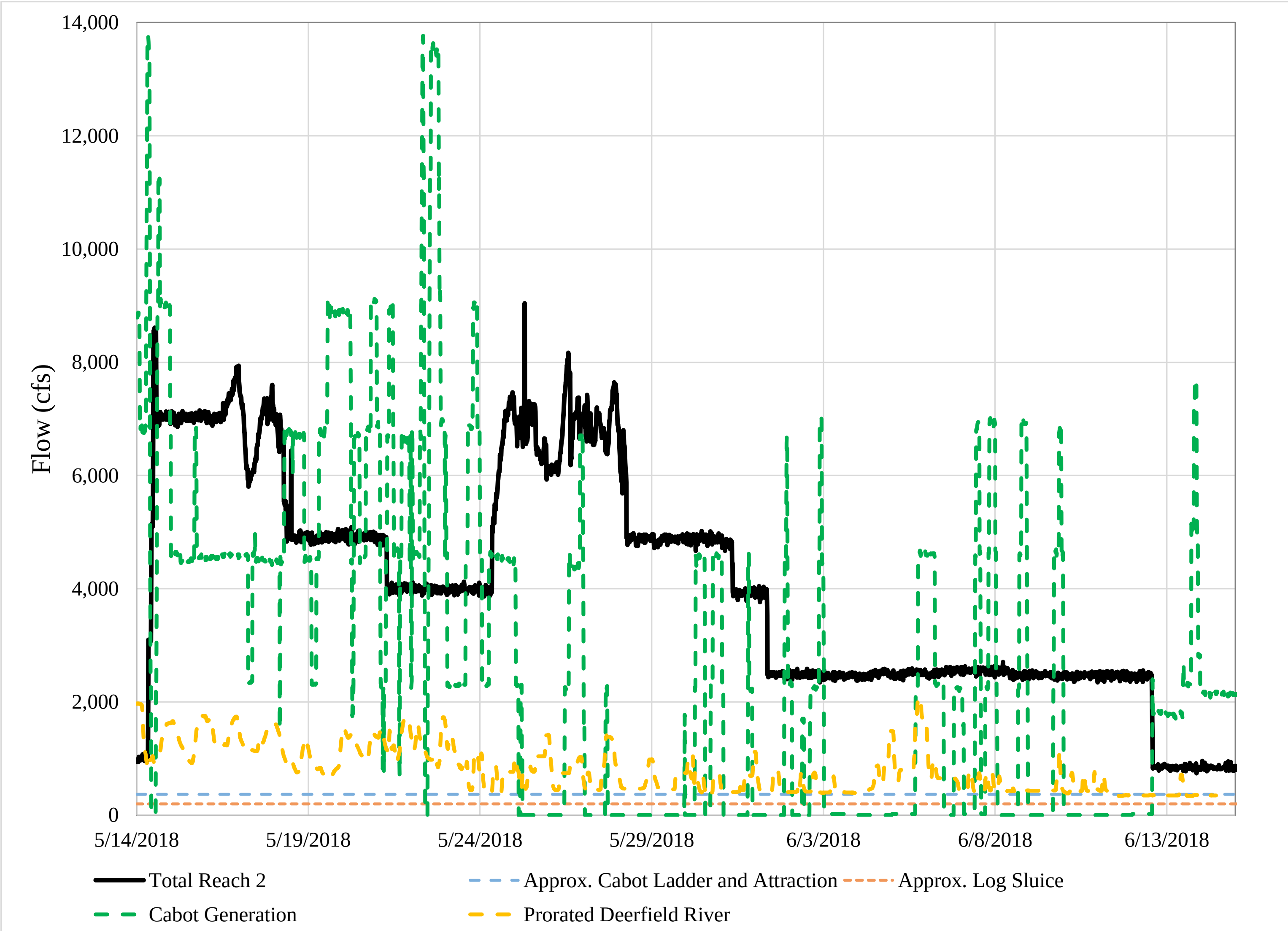

Figure 3.5-5: Flow contributions to Reach 3 during the 2018 ultrasound evaluation

3.6 Data Analysis

Large-scale, multi-objective passage studies that assess movement of anadromous fish through telemetered river-reaches are complex in nature. Further, analysis is made difficult because of the presence of false positive signals and receivers with overlapping detection zones. Considerable data cleaning is required before an assessment of movement can occur. FirstLight implemented the following protocol to analyze radio telemetry data collected for the ultrasound evaluation:

1. Identify and remove false positive detections with a Naïve Bayes Classifier,
2. Reduce overlap between detection zones,
3. Assess upstream arrival with an open population mark recapture model,
4. Assess movement with time-to-event analysis using a competing risks framework,
5. Assess the likelihood of fallback with a logistic regression.

A complete synopsis of the data reduction and statistical methods applied, as well assumptions, is provided in Appendix C.

In addition, FirstLight developed competing risks models to describe movement through the project area. Competing risk models assessed movement within the Cabot Station tailrace area and bypassed reach using movement data from 2015, 2016, and 2018. For the purposes of this report, movement occurs between two telemetered reaches. Competing risk models always assume movement from an initial location or spoke. The initial state for the tailrace model was considered as the Cabot Station tailrace (T06/T07), while the initial state for the bypass movement model was the Conte Discharge (T09). The counting process style data were arranged so that the first detection for every fish was always in the initial state. However, assumptions were relaxed on absorbing states, and we allowed movement back into the initial state to be enumerated as well. These secondary movements were queried out of the initial competing risks assessment using methods of Therneau, Crowson, and Atkinson (2016 and 2017) and with data frame filtering in R. The bypass movement model was also bolstered with data from the 2015 and 2016 telemetry studies, which themselves suffered from low sample sizes and poor statistical power in the bypass reach. Random effects associated with the tagging year were controlled with a covariate (*tag year*). We felt it appropriate to combine datasets and bolster statistical power for this assessment and to provide before/after comparisons of movement with and without the ultrasound array present. Because an analysis of the bypass reach was not an objective of this study, we felt it appropriate to include those sections in an appendix of supplemental results.

4 RESULTS

4.1 Shad Tagging

In total, 250 American Shad were collected, tagged, and released upstream via the fish lift exit flume at Holyoke Dam. Tagging and release dates occurred in three batches: May 14 (n=100), May 15 (n=75), and May 18, 2018 (n=75) (Table 4.1-1). The average total length for all tagged shad was 497 mm, with a minimum of 401 mm and a maximum of 576 mm (Figure 4.1-1). There was a 50-percent split between males (n=125) and females (n=125) tagged for this study. The average total length for females was 524 mm, with a range of 428 to 576 mm. The average total length for males was 470 mm, with a range of 401 to 557 mm.

Table 4.1-1: Summary of American Shad tagged for use in the 2018 ultrasound evaluation

Date	Number of Shad Tagged	Tag Frequency
5/14/2018	100	150.500 (n=50) 150.560 (n=50)
5/15/2018	75	150.500
5/18/2018	75	150.500 (n=10) 150.560 (n=65)

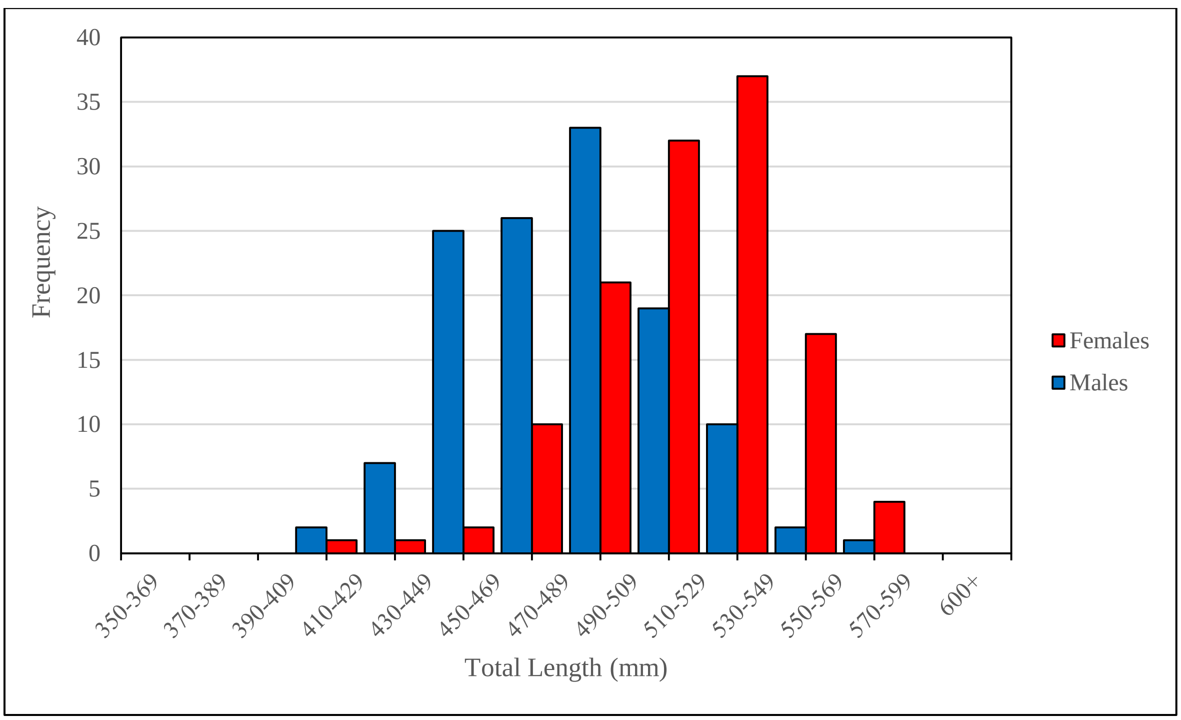

Figure 4.1-1: Length frequency of the 250 shad tagged for use in the 2018 ultrasound evaluation

4.2 Telemetry Analysis: Data Reduction

Results of FirstLight's data reduction efforts are provided in Appendix D (Data Reduction). In general, false positive removal was successful and retained 71% of the detections at Orion receivers and 91.7% of the detections at Lotek receivers. Following false positive removal, the Russian-doll algorithm removed another 421,090 overlapping detections. The resultant recapture data used for modeling contained 4,311,962 detections from 213 unique fish (some of which were only recaptured at Holyoke) at 20 receivers (some of which were at Holyoke and not part of the movement analysis at Turners Falls).

4.3 Telemetry Analysis: Recaptures and Movement Analysis

The results of the telemetry study presented below begin with the number of recaptures at each telemetry station, followed by an assessment of the probability of arrival at the TFD Spillway and an analysis of movement within the Cabot Station tailrace. FirstLight has also aggregated three years of movement data and conducted a detailed analysis of movement in the bypass reach, which is provided in Appendix E (Bypass Movement Analysis). Appendix E discusses potential barriers to fish passage around two natural features in the bypass—Rawson Island and Rock Dam.

4.3.1 Study Statistics and Raw Recaptures by Numbers

Table 4.3.1-1 contains the number of fish recaptured by node in the 2018 telemetry network. Note that 135 fish were detected at the Montague Wastewater Treatment Facility[5], while 112 were recaptured within the Cabot Station tailrace area. Of those fish that were attracted to the tailrace, 85 made it into the bypass reach, while only 33 were recaptured at the TFD Spillway. Also note that the Orion receivers at Holyoke were not part of this project; however, they were used to identify fallback.

Table 4.3.1-1: Number and proportion of fish recaptured by telemetry network node.

Node	Receivers	Reach	Fish Per Node
S01	T02	Montague	135
S02	T01	Deerfield River	23
S03	T03O	Smead Island - West	15
S04	T03L	Smead Island - East	112
S05	T06	Cabot Farfield	115
S06	T04, T05	Cabot Tailrace (partially ensonified)	112
S07	T07	Nearfield (ensonified)	41
S08	T08	Cabot Ladder (ensonified)	55
S09	T09	Conte Discharge	85
S10	T10	D/S Station No. 1	36
S11	T11	U/S Station No. 1	18
S12	T13	Turners Spillway	33
S13	T12	Spillway Ladder	2
S00	T02Hol	Hadley Intake	74
S00	T03Hol	Gatehouse	81
S00	T04Hol	Surface Bypass	35
S00	T08Hol	Plunge Pool	115

[5] While 137 tagged fish were confirmed to enter the project area, only 135 tagged fish were detected by the receiver at the Montague Wastewater Treatment Facility (i.e., two tagged fish escaped detection at receiver T02, but were detected further upstream in the telemetry network).

Node	Receivers	Reach	Fish Per Node
S00	T09Hol	Fish Lift Entrance	5
S00	T10Hol	South Hadley	1

4.3.2 Probability of Arrival at TFD Spillway

A Cormack Jolly Seber (CJS) mark-recapture model assessed the probability that a tagged fish recaptured at the entrance of the project (Montague) will arrive in the TFD Spillway. Fallback fish were not included in the analysis as only those fish recaptured at Montague were included. Therefore, the release location for the mark-recapture model was Montague (T02). Recapture locations included below Cabot tailrace (downstream end of Smead Island (T03O and T03L)), at the Cabot tailrace (T04, T05, T06, T07, and T08), bypass reach entrance (Conte discharge (T09)), Station No. 1 tailrace (T10 and T11), and TFD Spillway (T13). The recapture histories for every fish in the upstream CJS model are provided in Appendix F. The model met goodness of fit ($\mathrm{X}^2 = 0.18, p = 0.67$). Model selection criteria was simple; the model with the lowest Akaike's Information Criteria (AIC) was best, which was the fully saturated model (Table 4.3.2-1).

Tables 4.3.2-2 and 4.3.2-3 summarize the arrival and recapture estimates of the $\varphi(t)\rho(t)$ model (lowest AIC). The cumulative rate of arrival for tagged fish at the TFD Spillway was 25% (range of 12-39%). There is a clear bottleneck between the bypass reach entrance and the Spillway as 61% (range of 48-72%) of the tagged non-fallback fish in 2018 that arrived at Montague entered the bypass reach, but only 25% (range of 12-39%) are expected to arrive at the Station No. 1 tailrace[6]. While the CJS cannot differentiate between mortality and non-recapture at the last station, we have high confidence in the estimate of arrival at the Spillway because of the 36 fish recaptured at Station No. 1, 33 were also recaptured within the Spillway.

[6] As noted earlier and later in this document it is suspected that the bottleneck is where river bifurcates around Rawson Island where one channel includes a natural rock falls- Rock dam, and the other side has potential velocity barriers to fish passage.

Table 4.3.2-1: Model selection results for the reduced upstream arrival model (Holyoke – TFD Spillway)

Model Type	Specification	AIC	Delta AIC	No. Parameters
Independent survival, independent recapture rates	$\varphi(t)\rho(t)$	475.76	0.0	7
Independent survival, singular recapture rate	$\varphi(t)\rho(.)$	483.80	8.05	5
Singular survival, independent recapture rates	$\varphi(.)\rho(t)$	564.83	89.07	6
Singular survival, singular recapture rate	$\varphi(.)\rho(.)$	580.24	104.49	2

Table 4.3.2-2: Arrival rate (φ) results for the CJS model of arrival at the TFD Spillway

Parameter	Estimate	SE	Lower	Upper
(φ1) Montague > D/S Tailrace	0.87	0.03	0.81	0.92
(φ2) D/S Tailrace > Tailrace	0.98	0.01	0.95	0.99
(φ3) Tailrace > Bypass	0.72	0.04	0.63	0.79
(φ4) Bypass > Station No. 1	0.43	0.05	0.33	0.54
(φ5) Station No. 1 > Spillway	0.94	28.69	0.75	1.00

Table 4.3.2-3: Recapture rate (p) results for the CJS model of arrival at the TFD Spillway

Parameter	Estimate	SE	Lower	Upper
(p1) DS Tailrace	0.94	0.02	0.89	0.97
(p2) Tailrace	1.0	<0.001	0.99	1.00
(p3) Bypass (Cabot discharge)	1.0	<0.001	0.99	1.00
(p4) Station No.1 tailrace	0.97	0.03	0.87	0.99
(p5) Spillway	0.94	28.69	0.75	1.00

4.3.3 Cabot Tailrace Movement

We assessed movement within the Cabot Station tailrace using the competing risks framework of Therneau, Crowson, and Atkinson (2016). The intent of the study was to assess the ability of an ultrasound array at impeding movement towards or repelling American Shad from the Cabot Ladder. In 2015, fish could travel from the Cabot Station tailrace (consisting of the farfield and tailrace antennas) towards the Cabot Ladder unimpeded by ultrasound arrays, while in 2018 fish had to travel through two ensonified reaches (Figure 1-1). The states for the competing risks assessment included the tailrace (1), Cabot Ladder (2), bypassed reach (3), and anywhere downstream (4). In 2018, the Cabot tailrace consisted of the farfield (T07) and nearfield (T06) antenna arrays, while in 2015 it was just farfield (T06) and tailrace antenna (T05). In both years, the second state was recapture anywhere within Cabot Ladder, the third state was recapture anywhere within the bypassed reach, and the fourth state was recapture anywhere downstream.

FirstLight compared tailrace movement in 2015 (without the ultrasound array) to tailrace movement in 2018 (with the ultrasound array). However, we restricted the 2015 data to require all initial movements from the tailrace. Without this, the 2015 dataset was not comparable to 2018 movement data. Therefore, the number of fish and movements into the Cabot Ladder is less than previously reported. We removed antennas T04 and T05 (left and right side of Cabot powerhouse; node S06) from the 2018 movement data because they completely overlapped the Cabot Ladder state. We found that if we included these antennas in the analysis, transitions from the ladder to the tailrace were instantaneous and biased results. Further, if a fish left the entrance and was no longer recaptured by T08 (Cabot Ladder entrance), it could not be determined if the fish remained in the tailrace (T04/T05) or traveled further in the ladder. We could not resolve ambiguity in a fish's position, which is required for movement. Therefore, these antennas were removed from analysis, so we were ensured movement occurred from the tailrace and into the ladder, or from the ladder and into the tailrace. With receivers T04/T05 removed, the number of fish reported in the tailrace is different from the number of fish reported in the CJS model, as some fish went undetected at the farfield and nearfield antennas. With these data restrictions and caveats in mind, we constructed models and enumerated movement in the tailrace.

In 2015, 23 fish (23/66 = 35%) made 87 movements from the tailrace into the Cabot Ladder (Table 4.3.3-1), while 53 fish (53/112 = 47%) made 117 movements in 2018 (Table 4.3.3-2). The total number of movements into Cabot Ladder was higher in 2018 than in 2015, but the median number per fish was lower, meaning that although more fish attempted the ladder in 2018, there were fewer attempts per fish. While it appears that tagged fish attracted to the Cabot Ladder in 2018 eventually moved elsewhere, non-tagged fish were recorded using the Cabot Ladder during routine fishway video monitoring that occurs annually. From all routes, entrance into the Cabot Ladder was attempted 129 times by tagged fish in 2018, and there were 129 subsequent movements from the ladder to the tailrace, bypass reach, or anywhere downstream. In 2015, 30 fish (30/66 = 45%) made 40 movements towards the bypassed reach (Table 4.3.3-1), while 72 fish (72/112 = 64%) made 135 movements in 2018 (Table 4.3.3-2).

Nelson-Aalen cumulative incidence plots for 2015 (Figure 4.3.3-1) and 2018 (Figure 4.3.3-2) were limited to 10 hours to show detail when a majority of the movement occurs. The 2015 cumulative incidence function showed approximately 40 – 50% of the movements were towards the Cabot Ladder after 6 hours of being in the tailrace (Figure 4.3.3-1), in 2018 only 30 – 40% of the movements were towards the ladder after this time (Figure 4.3.3-2). Overall, a higher proportion of movements from the tailrace were directed towards the ladder in 2015, while in 2018 the proportion of movements directed towards the ladder was approximately the same as the proportion of movements directed towards the bypass reach. In 2018, an interesting phenomenon occurred when a majority of the to-bypass movement occurred between 1.5 and 2 hours of being in the tailrace. The median time until movement into the Cabot Ladder was only 1.2 hours in 2015, while in 2018 this increased to 1.37 hours (Table 4.3.3-3). However, given the widths of the confidence intervals around the Nelson-Aalen functions for movement toward the Cabot Ladder, there is likely no statistical difference between these rates (FirstLight did not conduct a format test of significant difference).

The model that best described movement from the tailrace into the ladder incorporated the ultrasound array (Table 4.3.3-4). The test of proportionality was significant, and the effect of the array on the likelihood of movement towards the Cabot Ladder decreases with time. Likewise, movement from the ladder into the tailrace was also affected by the ultrasound array. The test of proportionality was significant; therefore, time was incorporated into the model to account for the fact that the effect of the ultrasound array reduces with the duration of exposure. The CoxPH model found that fish were 3.13 times more likely to move towards the tailrace from the ladder when the ultrasound array was operational. However, for every hour a fish was exposed to the array, it was 0.62 times as likely to move. In other words, the effect of the array at repelling fish decreases with time.

The model that best describes movement into the bypass reach from Cabot tailrace (Table 4.3.3-5) incorporated short term volatility (1 hour) and the cumulative average discharge from Cabot Station while present as additive variables. As the cumulative average Cabot Station discharge increased by 1,000 cfs as compared to the baseline, fish were 0.87 times as likely to move. In other words, the higher Cabot Station discharge was while a fish was present, the less likely it was to move into the bypass reach. Flow was modeled as a continuous variable in units of 1,000 cfs; however, note that Cabot Station operates with units either all the way on or off, and each unit is rated to approximately 2,288 cfs. There may be ramping flows at rates smaller than 2,288 cfs, but the units are not operated at those flows for long durations. The model also indicated that a change in operations at Cabot Station may spur movement into the bypass reach. The hazard ratio associated with an increase in the short-term volatility (or variance) at Cabot indicates that fish are 1.2 times more likely to move. In other words, changing operations, whether a unit is coming on or off, will spur movement.

Table 4.3.3-1: Tailrace movement in 2015 enumerating the number of fish (n) making (m) movements from a row towards a column

	Tailrace	Cabot Ladder	Bypass Reach	Downstream
Tailrace	n = 66	n = 23 m = 87 min = 1 med = 3 max = 13	n = 30 m = 40 min = 1 med = 1 max =4	n = 19 m = 31 min = 1 med = 1 max = 5
Cabot Ladder	n = 22 m = 86 min = 1 med = 3 max = 13	n = 23	n = 0 m = 0 min = 0 med = 0 max =0	n = 0 m = 0 min = 0 med = 0 max =0
Bypass Reach	n = 30 m = 14 min = 1 med = 1 max = 3	n = 1 m = 1 min = 1 med = 1 max = 1	n = 30	n = 3 m = 4 min = 1 med = 1 max = 2
Downstream	n = 15 m = 26 min = 1 med = 1 max = 5	n = 0 m = 0 min = 0 med = 0 max = 0	n = 2 m = 3 min = 1 med = 1.5 max = 2	n = 20

Table 4.3.3-2: Tailrace movement in 2018 enumerating the number (n) of fish making (m) movements from a row towards a column

	Tailrace	Cabot Ladder	Bypass Reach	Downstream
Tailrace	n = 112	n = 53 m = 117 min = 1 med = 2 max = 7	n = 72 m = 135 min = 1 med = 1 max = 6	n = 73 m = 94 min = 1 med = 1 max = 5
Cabot Ladder	n = 52 m = 114 min = 1 med = 2 max = 7	n = 55	n = 3 m = 3 min = 1 med = 1 max = 1	n = 11 m = 12 min = 1 med = 1 max = 2
Bypass Reach	n = 53 m = 89 min = 1 med = 1 max = 4	n = 3 m = 3 min =1 med = 1 max = 1	n = 80	n = 38 m = 51 min = 1 med = 1 max = 3
Downstream	n = 29 m = 40 min = 1 med = 1 max = 5	n = 7 m = 9 min = 1 med = 1 max = 3	n = 29 m = 37 min = 1 med = 1 max = 3	n = 92

Table 4.3.3-3: Comparison of time (hours) spent within tailrace until movement to a state

	2015			2018		
Movement	**Min**	**Median**	**Max**	**Min**	**Median**	**Max**
Tailrace to Cabot Ladder	0.17	1.20	44.90	0.06	1.37	325.0
Tailrace to Bypass	0.38	1.23	69.20	<0 .01	1.56	131.0
Tailrace to Downstream	0.37	4.60	322.0	<0.01	1.18	260.0

Table 4.3.3-4: CoxPH regression for Farfield to Cabot Ladder movement data

Model Number	Covariates	AIC	Robust LR Test	Hazard Ratio	SE	p	(+/-)	Proportional Hazard Assumption
1	Array Operational	1822.44	0.002	1.98	0.20	<0.001	(1.36,2.91)	<0.001
1a	**Array Operational**	**1722.66**	**<0.001**	**0.80**	**0.26**	**0.37**	**(0.48,1.32)**	**0.88**
	Time			**0.91**	**0.26**	**<0.001**	**(0.86,0.96)**	**0.11**
	Array Operational * Time			**1.07**	**0.03**	**<0.007**	**(1.02,1.13)**	**0.39**
2	Cabot kcfs	2305.94	0.77	1.01	0.03	0.77	(0.96,1.06)	0.38
3	Bypass kcfs	2305.95	0.72	0.98	0.05	0.72	(0.88,1.09)	0.16
4	Cabot: Bypass Flow Ratio	2306.01	0.80	1.02	0.26	0.79	(0.90,1.14)	0.80
5	1 hour rolling Cabot discharge average	2305.90	0.75	1.01	0.03	0.75	(0.96,1.06)	0.32
6	1 hour Cabot discharge volatility	2304.23	0.21	1.09	1.57	0.12	(0.98,1.22)	0.38
7	2 hour rolling Cabot discharge average	2305.81	0.72	1.01	0.03	0.72	(0.96,1.07)	0.36
8	2 hour Cabot discharge volatility	2303.38	0.20	1.05	0.03	0.08	(0.99,1.11)	0.08
9	5 hour rolling Cabot discharge average	2305.65	0.67	1.01	0.03	0.66	(0.96,1.07)	0.57
10	5 hour Cabot discharge volatility	2304.07	0.38	1.02	0.02	0.30	(0.98,1.07)	0.04
11	24 hour rolling Cabot discharge average	2306.15	0.92	0.99	0.03	0.92	(0.93,1.07)	0.49
12	24 hour Cabot discharge volatility	2304.67	0.45	1.01	0.02	0.43	(0.98,1.05)	0.28
13	Cumulative average Cabot discharge while present	2306.01	0.82	0.99	0.03	0.83	(0.93,1.06)	0.02
14	1 hour rolling Bypass discharge average	2305.98	0.73	0.98	0.05	0.74	(0.88,1.10)	0.16
15	1 hour Bypass discharge volatility	2301.20	0.002	0.02	2.45	0.10	(0.00,2.05)	0.58
16	2 hour rolling Bypass discharge average	2306.00	0.75	0.98	0.05	0.75	(0.88,1.09)	0.15
17	2 hour Bypass discharge volatility	2300.30	0.002	0.04	1.45	0.03	(0.002,0.76)	0.67
18	5 hour rolling Bypass discharge average	2305.98	0.74	0.98	0.05	0.74	(0.88,1.10)	0.14
19	5 hour Bypass discharge volatility	2305.06	0.25	0.66	0.44	0.34	(0.28,1.55)	0.69
20	24 hour rolling Bypass discharge average	2305.98	0.73	0.98	0.06	0.73	(0.88,1.10)	0.15
21	24 hour Bypass discharge volatility	1841.91	0.30	0.96	0.05	0.42	(0.96,1.07)	0.23
22	Cumulative average Bypass discharge while present	1842.26	0.62	0.97	0.07	0.62	(0.84,1.11)	0.75
23	Change in Cabot discharge while present (dQ/dt)	1842.60	0.53	0.99	0.0003	0.55	(0.99,1.00)	0.99
24	Change in Bypass discharge while present (dQ/dt)	1842.64	0.41	0.99	0.01	0.45	(0.97,1.01)	0.99

Table 4.3.3-5: CoxPH regression for Cabot tailrace to bypass (Conte Discharge) movement data

Model Number	Covariates	AIC	Robust LR Test	Hazard Ratio	Robust SE	p	(+/-)	Proportional Hazard Assumption
1	Cabot (kcfs)	1430.86	<0.001	0.92	0.02	<0.001	(0.88,0.96)	0.18
2	Bypass (kcfs)	1443.97	0.03	1.09	0.04	0.03	(1.01,1.17)	0.07
3	Cabot: Bypass flow ratio	1430.98	<0.001	0.79	0.06	<0.001	(0.70,0.90)	0.20
4	1 hour rolling Cabot discharge average	1430.99	<0.001	0.92	0.02	<0.001	(0.88,0.96)	0.16
5	1 hour Cabot discharge volatility	1442.19	0.03	1.17	0.06	0.01	(1.03,1.32)	0.16
6	2 hour rolling Cabot discharge average	1429.97	<0.001	0.91	0.02	<0.001	(0.87,0.95)	0.17
7	2 hour Cabot discharge volatility	1446.42	0.12	1.06	0.03	0.08	(0.99,1.13)	0.66
8	5 hour rolling Cabot discharge average	1428.91	<0.001	0.91	0.02	<0.001	(0.87,0.95)	0.22
9	5 hour Cabot discharge volatility	1448.46	0.76	1.01	0.03	0.74	(0.96,1.06)	0.08
10	24 hour rolling Cabot discharge average	1430.62	<0.001	0.90	0.03	<0.001	(0.85,0.95)	0.99
11	24 hour Cabot discharge volatility	1438.67	0.002	0.95	0.02	0.003	(0.92,0.98)	0.72
12	Cumulative Avg Cabot discharge while present	1415.59	<0.001	0.88	0.03	<0.001	(0.83,0.92)	0.20
13	Total Change in Cabot discharge while present (dQ)	1442.05	0.03	1.06	0.03	0.03	(1.01,1.12)	0.37
14	1 hour rolling Bypass discharge average	1444.15	0.03	1.08	0.04	0.03	(1.01,1.17)	0.08
15	1 hour Bypass discharge volatility	1448.58	0.89	0.87	0.98	0.89	(0.13,5.94)	0.94
16	2 hour rolling Bypass discharge average	1444.29	0.03	1.08	0.04	0.03	(1.01,1.16)	0.08
17	2 hour Bypass discharge volatility	1448.05	0.50	0.62	0.70	0.5	(0.16,2.46)	0.78
18	5 hour rolling Bypass discharge average	1444.16	0.03	1.08	0.04	0.03	(1.01,1.17)	0.08
19	5 hour Bypass discharge volatility	1448.10	0.51	0.80	0.34	0.51	(0.41,1.55)	0.61
20	24 hour rolling Bypass discharge average	1444.03	0.03	1.09	0.04	0.03	(1.01,1.19)	0.11
21	24 hour Bypass discharge volatility	1445.33	0.13	0.90	0.07	0.16	(0.78,1.04)	0.44
22	Cumulative Avg Bypass discharge while present	1438.53	0.001	1.18	0.05	0.002	(1.07,1.31)	0.82
23	Total Change in Bypass discharge while present (dQ)	1447.82	0.36	1.04	0.04	0.36	(0.96,1.13)	0.89
24	Change in Bypass discharge with time while present (dQ/dt)	1448.58	0.87	0.92	0.55	0.87	(0.31,2.71)	0.22
25	**Cumulative Avg Cabot discharge while present**	**1409.55**	**<0.001**	**0.87**	**0.02**	**<0.001**	**(0.83,0.91)**	**0.23**
	1 hour Cabot discharge volatility			**1.20**	**0.05**	**<0.001**	**(1.08,1.32)**	**0.25**
26	Total Change in Cabot discharge while present (dQ)	1436.70	0.01	1.07	0.03	0.02	(1.01,1.13)	0.53
	1 hour Cabot discharge volatility			1.19	0.06	0.002	(1.06,1.34)	0.32

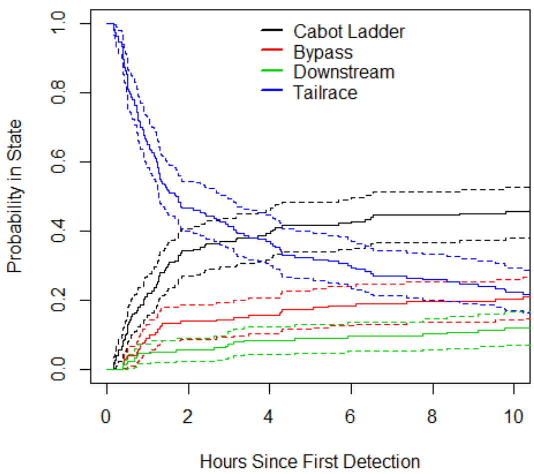

Figure 4.3.3-1: Nelson-Aalen cumulative incidence functions for probability in state at time during the 2015 season

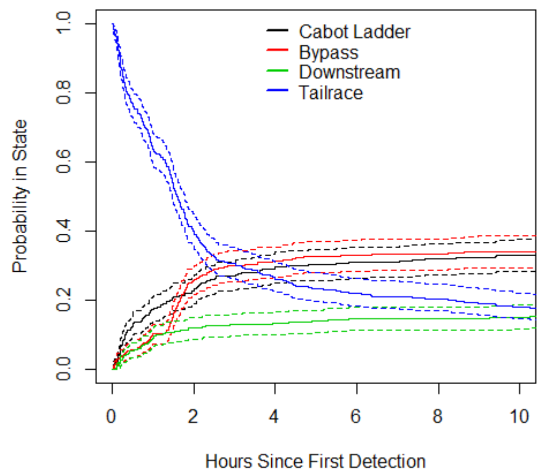

Figure 4.3.3-2: Nelson-Aalen cumulative incidence functions for probability in state at time during the 2018 season

5 DISCUSSION

The purpose of this study was to build off previous knowledge gained from the 2016 ultrasound study and to further investigate whether the use of ultrasound technology is an effective method to minimize shad attraction to the Cabot Ladder in an effort to move shad up the bypass channel toward the TFD. In the 2016 study, the effectiveness of the three transducers were limited by their placement (one located on the fish ladder wall near the entrance and two located on the midpoint of the back of the powerhouse) leading to excessive air entrainment from Cabot Station turbine discharge and fish ladder attraction flow. This air entrainment likely caused increased attenuation and scattering of the sound field. As a result, sound pressure levels were reduced and did not elicit strong and prolonged avoidance reactions from shad unless fish were within the immediate vicinity of the transducers. To mitigate these shortcomings, the design and configuration of the ensonified field was modified to minimize interference of air entrainment and optimize signal strength in an attempt to produce a continuous sound field spanning the entirety of the Cabot Station tailrace with SPLs greater than 160 dB. New data from sound field monitoring collected on November 15, 2017 allowed for improved placement of more transducers. Another benefit of a second year of the ultrasound study was the ability to compare data collected from both the 2016 ultrasound study and the 2015 shad telemetry studies for use in this analysis.

The 2018 configuration of the transducers allowed for a more robust sound array when compared to the array used in 2016. The 2018 design included the use of additional transducers as well as power amplifiers to achieve higher projector source levels and a more uniform sound pressure field around the outer perimeter of the Cabot Station tailrace. To minimize the air entrainment issue, the configuration of the transducers was moved outward, away from the Cabot Station powerhouse. In practice, the ultrasound array did not act like a fence, rather it was permeable as evidenced by the Cabot Ladder fish counts. There were issues keeping all the transducers activated and aligned throughout the entire study. Even with the array operational, fish were still attracted toward the Cabot Ladder because attraction flow was still provided. Further, the ability of the array to push fish away reduced with time. This confirms the 2016 conclusion that the effect of the array reduces with time, as fish that encounter the array become acclimated to the ultrasound. Even though the array failed in its primary objective of deterring fish from entering the Cabot Ladder, a higher proportion of movements from the tailrace were directed towards the bypass reach in 2018 as compared to 2015. At this time, it is unknown if bypass flow manipulation or the ultrasound array may have led to this finding. FirstLight will address this research objective in 2019. Historically, the Cabot fish ladder has passed more American Shad than the Spillway fish ladder. Between 2008 and 2018, the Spillway fish ladder passed as little as 4% of the Shad passed at the Cabot fish ladder (Table 5-1). Several studies were conducted in 2015, 2016, and 2018, during which time bypass flows were manipulated. In 2016 and 2018 an ultrasound array was deployed in the Cabot tailrace to deter Shad from the Cabot tailrace and facilitate upstream movement to the Spillway fish ladder. In 2015, 2016, and 2018 the percentage of Shad passing at the Spillway fish ladder to Cabot fish ladder increased to 88%, 56%, and 136% respectively (Table 5-1). Interestingly, in 2017, when bypass flows were not manipulated, nor was the ultrasound array deployed, the number of Shad that passed Spillway dropped to 39% of the passage at Cabot fish ladder.

Table 5-1 Spillway and Cabot Ladder Count by Year.

Year	Spillway	Cabot	Ratio
2008	627	15,809	0.04
2009	928	13,360	0.07
2010	2,735	30,232	0.09
2011	1,966	27,077	0.07

Year	Spillway	Cabot	Ratio
2012	10,608	51,901	0.20
2013	10,571	46,886	0.23
2014	24,262	40,666	0.56
2015*	41,836	47,588	0.88
2016**	19,337	34,709	0.56
2017	16,741	43,269	0.39
2018**	32,593	24,031	1.36

*Bypass flow manipulated
**Bypass flow manipulated with Ultrasound Array at Cabot Tailrace

Movement of fish within the Project area was assessed with time-to-event analysis using a competing risks framework. Once fish reach the tailrace, they may attempt to pass via the Cabot Ladder, remain in or near the tailrace due to attraction of the flows from Cabot Station, or continue upstream to the bypass reach. The best model for movement into the bypass reach suggested fish are more likely to move if operations at Cabot Station change (1-hour volatility). In other words, if a unit comes on or off, fish are more likely to move out of the Cabot Station tailrace and into the bypass reach. However, fish are 13% less likely to move into the bypass reach for every 1,000 cfs increase over baseline. Please note that the flow statistic is cumulative average discharge over the entire time a fish is present in the tailrace. A fish may be present in the tailrace for 15 minutes or 15 hours. During this time, they will experience a range of flows as units are turned on or off. Flow is modeled as a continuous variable in 1,000 cfs increments. Thus 1.1 kcfs is 1,100 cfs, and 0.9 kcfs is 900 cfs. However, as Cabot Station operates with units either on or off, there will be discrepancy between a cumulative average discharge and what Cabot Station releases through the turbines, which are typically operated near their hydraulic capacity of 2,288 cfs/unit. Once fish move into the bypass reach, movement analysis suggests that fish prefer flows in the 3,000 to 6,000 cfs range. However, there was an interaction effect with the day of year, and discharge is subject to diminishing returns. For every day in the bypass reach, fish are 0.99 times as likely to move upstream. Therefore, flow will not be as effective in moving fish later in the season. Fish also prefer stable flows within the bypass reach. We believe American Shad respond negatively to flow variability in the bypass reach due to the complexity of the reach's topography and its bedrock substrate. Small changes in flow can have large effects on local zones of passage. What was once a clear route at 2,000 cfs could become impassable at 4,000 cfs, and vice versa. Rapidly changing passage routes and flow conditions (water depth and velocity) would prohibit efficient movement upstream as the fish must adapt to the ever-changing riverscape.

Rawson Island Complex

The 2018 CJS model depicted a bottleneck within the bypass reach (Table 4.3.2-2). Only 43% (33-54%) of the American Shad recaptured at the Conte discharge are predicted to arrive at the Station No. 1 tailrace. Between the Conte discharge and the Station No. 1 tailrace lies the Rawson Island complex, a relatively wide and shallow river channel with complex multi-channel characteristics and hydraulics. Flow paths around Rawson Island include a river-right channel, middle channel and river-left channel as shown in Figure 5-1. On river-left channel flow passes over a natural rock falls, Rock Dam, which includes a steep vertical drop making it inaccessible for shad to navigate over the falls. The alternative route is the river-right channel that bifurcates to include a middle channel (see Figure 5-1). Based on the radio telemetry studies it appears both the river-right channel and the middle channel are natural velocity barriers to shad passage. The Rawson Island complex was part of the River2D hydraulic modeled developed for Reach 3. A series of color-coded velocity maps is included in Appendix E to represent various magnitudes of bypass flow and different magnitudes of Cabot discharge. Shown in Figure 5-2, is one example of the velocity maps for a bypass flow of 4,000 cfs and a Cabot Station discharge of 7,000 cfs. As Figure 5-2 shows, velocities along the river-right channel exceed 6 feet per second and the Middle Channel lack sufficient flow. As bypass flow increases, the high velocity zone within the River-Right Channel elongates, and a migrating shad will have to endure a prolonged bout of high energetic swimming to successfully navigate past this area. Research published by Castro-Santos (2004, 2005, and 2006) found that a fish will deplete energy reserves during bouts of prolonged and sprint swimming while traversing velocity barriers. A fish will fatigue within 20 to 200 seconds during prolonged bouts and in as little as 20 seconds during sprint swimming (Castro-Santos 2006). Based on this research, for a given set of starting locations, it would be possible to model least-cost pathways (migratory zones of passage) and determine the expected maximum migratory distance a migrating shad will attain. It would be possible to verify this model with future tagging studies. With a verified model, FirstLight may simulate shad migrating through the bypass reach to understand how their maximum migratory extent is affected by velocity barriers that are created as flow is routed through the Project area.

Summary

Overall results of the 2018 study indicated that of the 112 adult American Shad that arrived at the Cabot tailrace, 85 fish (76%) moved upstream into the bypass reach entrance before encountering a velocity and physical barrier around Rawson Island. These findings indicate that the Ultrasound Array may be keeping a proportion of the migrating shad out of the Cabot Station tailrace. However, since two elements (additional flow in the bypass reach and the ultrasound array) were both added as part of the previous Ultrasound Array studies in 2016 and 2018, it is not possible to ascertain which contributed to the increased number of fish that moved upstream and entered the bypass reach. To determine if increased flow or the Ultrasound Array contributed to 76% of the tagged fish moving upstream to the bypass reach, it is proposed to conduct a movement study in 2019 with test flows in the bypass reach but without an Ultrasound Array.

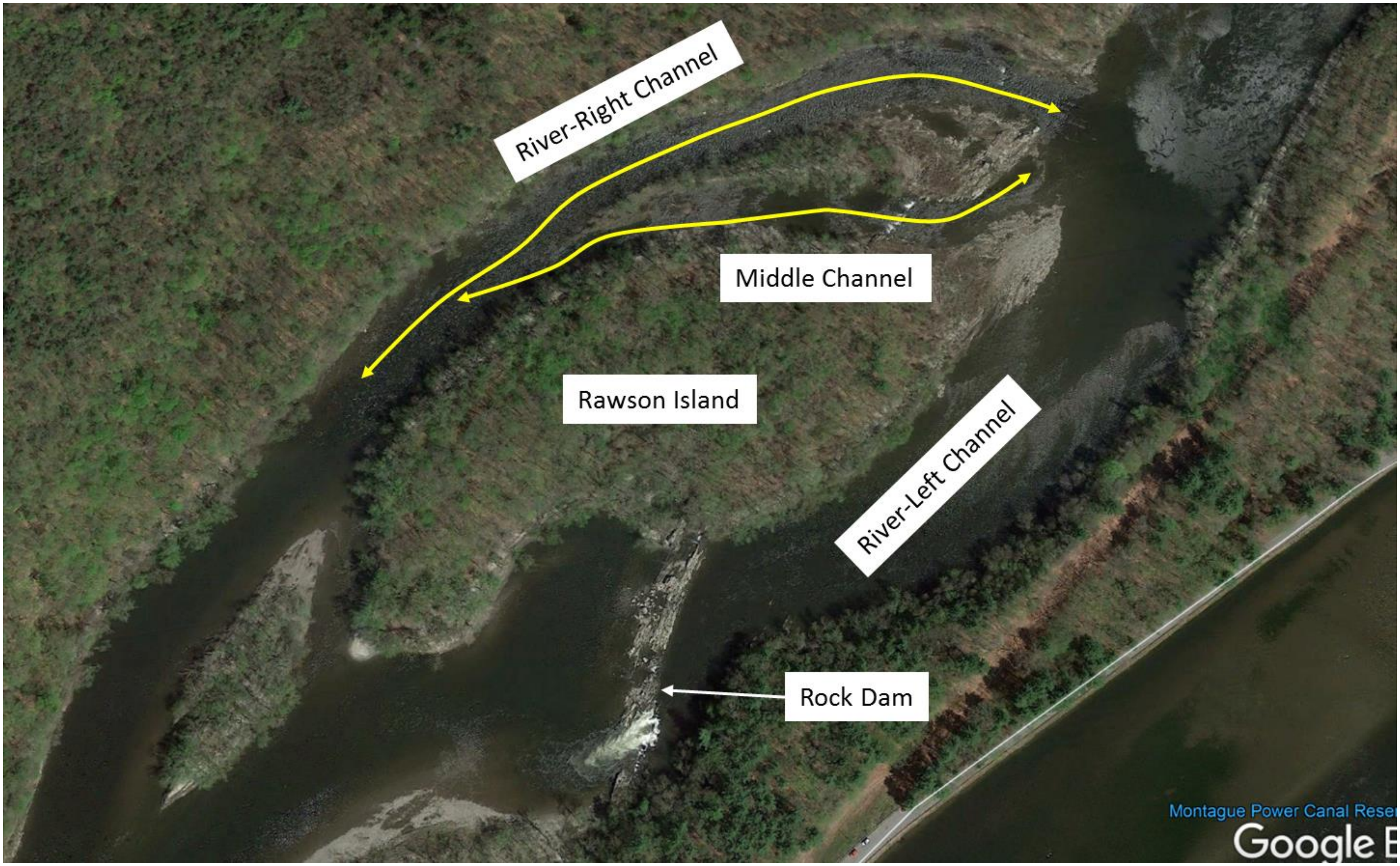

Figure 5-1: Plan view of Rawson Island complex

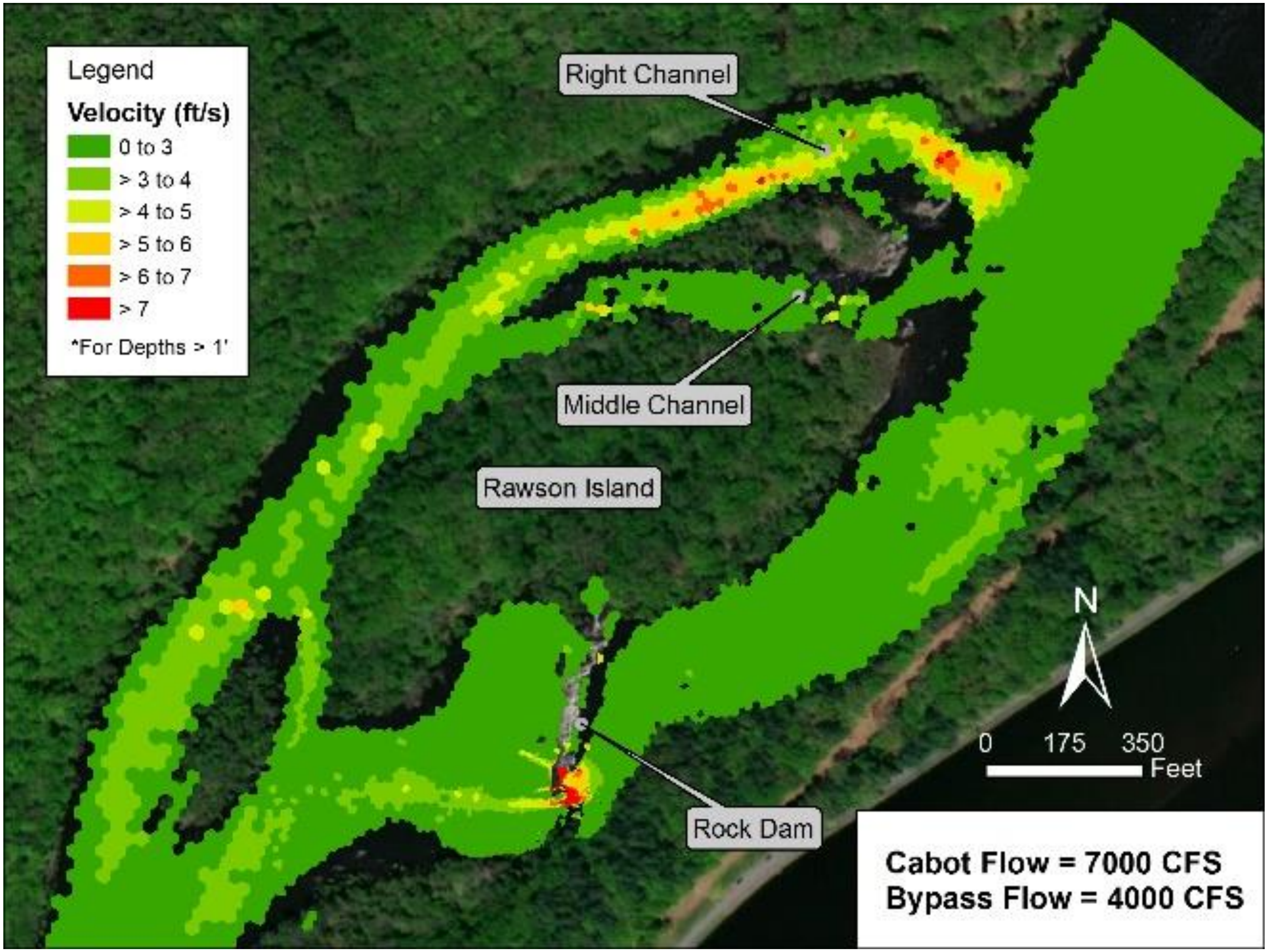

Figure 5-2: Rawson Island velocity with Cabot Station at 7,000 cfs and Bypass Flow of 4,000 cfs

6 LITERATURE CITED

Amstrup, S.C., McDonald, T.L., and Manly, F.J. (2005). Handbook of Capture – Recapture Analysis. Princeton University Press, Princeton and Oxford.

Beeman, J. W., & Perry, R. W. (2012). Telemetry Techniques: A User Guide for Fisheries Research. In N. Adams, J. Beeman, & J. Eiler (Eds.). American Fisheries Society.

Beyersmann, J., Allignol, A., & Schumacher, M. (2011). Competing Risks and Multistate Models with R. New, York, NY: Springer.

Blaxter, J.H.S., and Hunter, J.R. (1982). The biology of the Clupeid fishes. *Advances in Marine Biology Advances in Marine Biology Volume*, 20:1-223.

Carlson, T. J. & Popper, A. N. (editors) (1997). Using sound to modify fish behavior at power-production and water-control facilities. A workshop held December 12-13, 1995, Portland, Oregon. Published by Bonneville Power Administration, Portland Oregon, 362 pp.

Castro-Santos, T. (2004). Quantifying the combined effects of attempt rate and swimming capacity on passage through velocity barriers. *Canadian Journal of Fisheries and Aquatic Sciences, 61*, 1602-1615.

Castro-Santos, T. (2005). Optimal swim speeds for traversing velocity barriers: an analysis of volitional high-speed swimming behavior of migratory fishes. *Journal of Experimental Biology, 208*, 421-432.

Castro-Santos, T. (2006). Modeling the effect of varying swim speeds on fish passage through velocity barriers. *Transactions of the American Fisheries Society, 135*, 1230-1237.

Cooch, E., & White, G. (2006). Program MARK: A Gentle Introduction. Available in. pdf format for free download at http://www. phidot. org/software/mark/docs/book.

Denton, E. J., and Blaxter, J. H. S. (1976). The mechanical relationships between the Clupeid swimbladder, inner ear and lateral line. *Journal of the Marine Biological Association of the United Kingdom*, 56(3):787-807.

Frank, H.J., Mather, M.E., Smith, J.M., Muth, R.M., Finn, J.T. and McCormick, S.D. (2009) What is "fallback"?: metrics needed to assess telemetry tag effects on anadromous fish behavior. *Hydrobiologia* 635, 237–249.

Gibson, A., Jamie, F., and Myers, R.A. (2002). Effectiveness of a high-frequency-sound fish diversion system at the Annapolis Tidal Hydroelectric Generating Station, Nova Scotia. *North American Journal of Fisheries Management* 22(3):770-84.

Gurshin, C.W. D., Balge, M.P., Taylor, M., and Lenz, B. (2014). Importance of ultrasonic field direction for guiding juvenile blueback herring past hydroelectric turbines. *North American Journal of Fisheries Management* 34(6):1242-1258.

Guindon, A. and D. Desrochers. (2016a). Rivière des Prairies generating station – Monitoring downstream migration shad -2016 and evaluation of a guidance system, by MEDIUM Inc. for Environment, Asset Management and Regulatory Compliance Unit, Hydro-Québec and annexes.

Guindon, A. and D. Desrochers. (2016b). ESSAI DE GUIDAGE DE L'ALOSE SAVOUREUSE DANS LA RÉGION DE MONTRÉAL, by MEDIUM Inc. for Environment, Asset Management and Regulatory Compliance Unit, Hydro-Québec Production, 52 p.Higgs, D. M. (2004). Development of ultrasound detection in American Shad (*Alosa Sapidissima*). *Journal of Experimental Biology* 207(1):155-163.

Higgs, D. M, D. T. T. Plachta, A. K. Rollo, M. Singheiser, M. C. Hasting and A. N. Popper. (2004). Development of ultrasound detection in American shad (*Alosa sapidissima*). The Journal of Experimental Biology 207, 155-163.

Kynard, B., and Taylor, R. (1984). Studies of downrunning adult alosids in the Holyoke Dam Canal System. Final Report. Northeast Utilities. 29 pp.

Lebreton, J.-D., Burnham, K. P., Clobert, J., & Anderson, D. R. (1992). Modeling Survival and Testing Biological Hypotheses Using Marked Animals: A Unified Approach with Case Studies. Ecological Monographs, 62(1): 67-118.

Marsland, S. (2009). Machine Learning: An Algorithmic Perspective. Boca Raton, Florida: CRC Press, Taylor and Francis Group.

Richert, W., & Pedro-Coelho, L. (2013). Building Machine-Learning Systems with Python. Birmingham, UK: Packt Publishing.

Sibly, R., H. Nott. and D. Fletcher. (1990). Splitting behavior into bouts. Anim. Behavior 39: 63-69.

Steffler, P. & Blackburn, J. (2002). River2D: Two-dimensional depth-averaged model of river hydrodynamics and fish habitats. University of Alberta, Edmonton, Canada.

Stone, J. V. (2013). Bayes' Rule: A Tutorial Introduction to Bayesian Analysis. Lexington, KY: Sebtel Press.

Therneau, T., Crowson, C., & Atkinson, E. (2016). Multi-state models and competing risks. From https://cran.r-project.org/web/packages/survival/vignettes/compete.pdf

Therneau, T., Crowson, C., & Atkinson, E. (2017). Using Time Dependent Covariates and Time Dependent Coefficients in the Cox Model.

APPENDIX A – CABOT SOUND SYSTEM DESCRIPTION

This purpose of this document is to report on sound field modeling, sound system installation, and sound field measurements undertaken to support the study of ultrasound as a deterrent approach to repel American Shad from the tailrace and fish ladder regions of the Cabot Station in Turners Falls, Massachusetts as executed during spring 2018.

High Frequency Sound System Description

Overview

SSI was tasked to configure, test and install a high-frequency sound system for the ultrasound evaluation at Cabot Station. The system developed and deployed for this study was an expansion of the system deployed for a similar study in 2016 adding both additional transducers and power amplifiers in order to achieve higher projector source levels and a more uniform sound pressure field at the outer perimeter of the Cabot Station tailrace. Due to the high air entrainment in the turbine discharge and the associated adverse impact on sound propagation, several transducers were moved outboard away from the powerhouse in order to deploy these transducers in locations where air entrainment was minimized. These outboard transducers were AIRMAR Model B150M deployed from vertical poles mounted on moored floats. A cluster of inboard transducers consisting of three International Transducer Corporation Model ITC-3406 transducers were mounted on the fish ladder wall just outboard of the corner where the fish ladder wall meets the powerhouse wall. This group of transducers was arranged in a fan pattern duplicating the arrangement deployed at this location in the 2016 study, in which all transducers were driven in parallel from a single power amplifier. For the 2018 study, each transducer was paired with an individual power amplifier, significantly increasing the drive capability. The power amplifiers used were a custom SSI design developed in 2006 for a U.S. Navy high-frequency sonar application.

Hardware

The topology of the hardware system is presented schematically in Figure 1 and Figure 2. A photograph of the topside hardware is shown in Figure 14.. A 150 kHz low pass filter, custom built by SSI, is inserted between the PCI-6713 output and the L6 Amplifier input to remove high frequency signal content associated with the digital-to-analog conversion process.

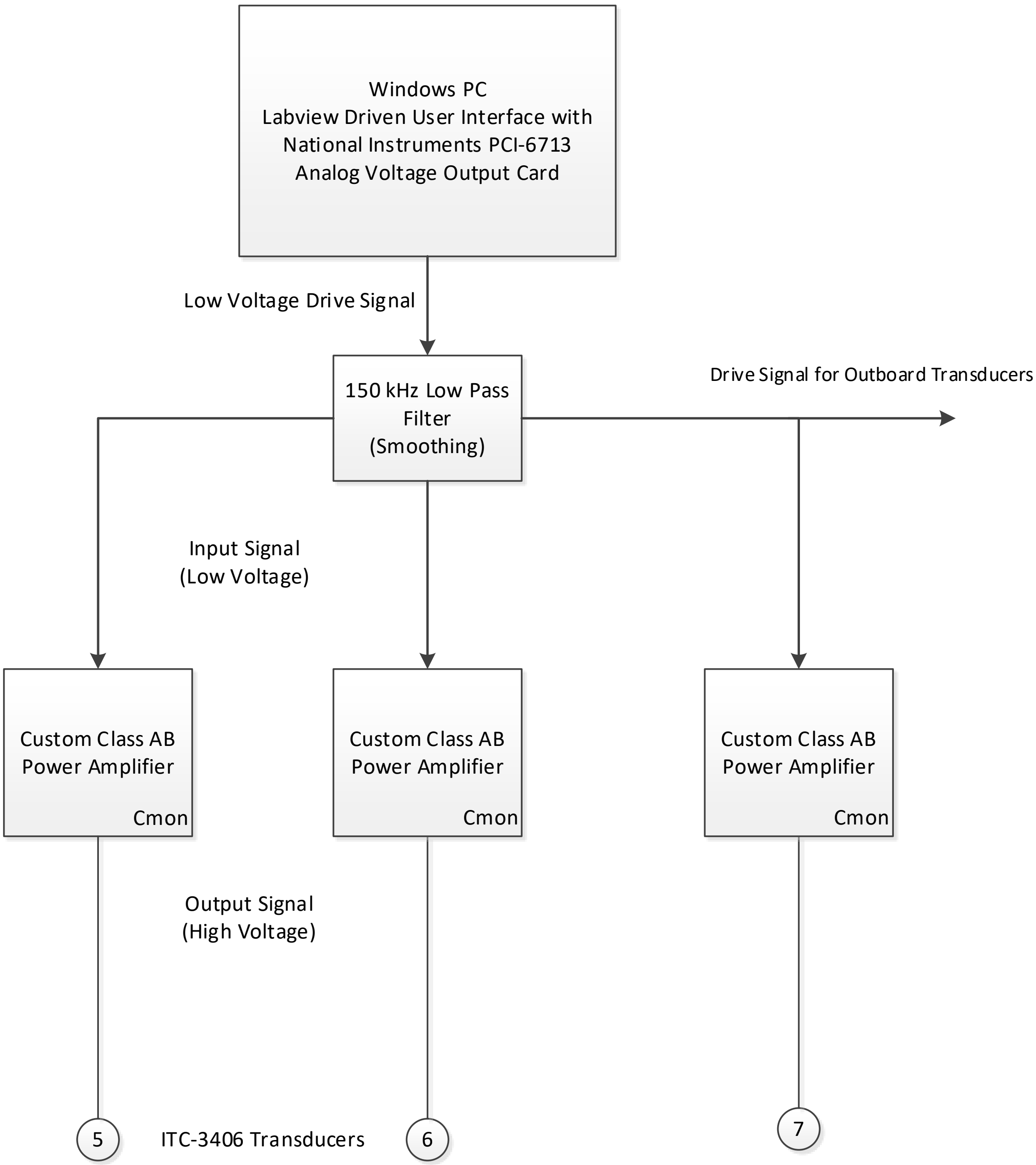

Figure 1 – High Frequency Sound System Schematic, Inboard Transducers

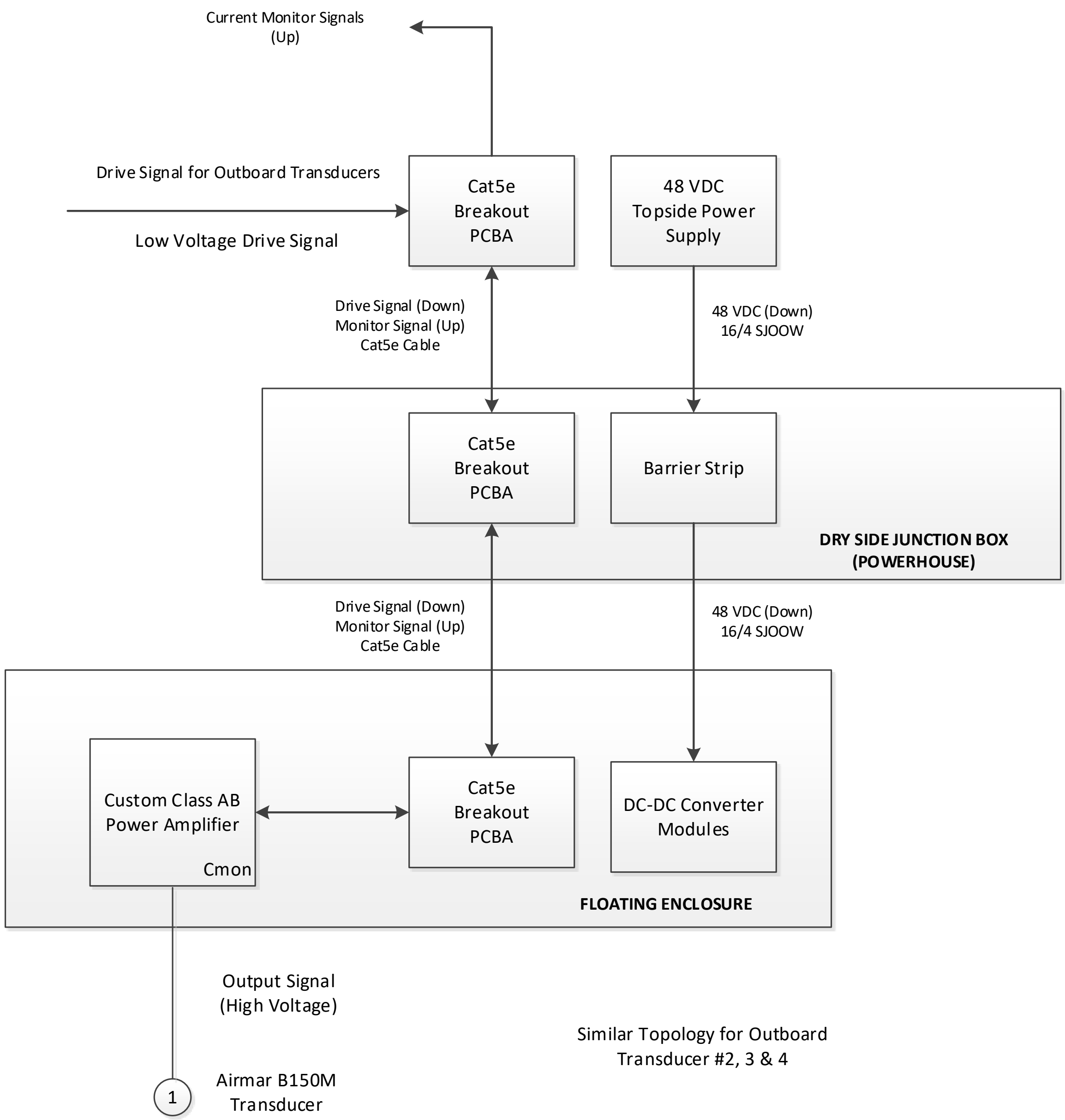

Figure 2 – High Frequency Sound System Schematic, Outboard Transducers

Transducers

The transducers used to generate the high frequency sound signals in the water were a combination of International Transducer model ITC-3406 and AIRMAR B150M (Figure 3). The ITC-3406 is a custom built circular piston type transducer with a radiating face diameter of approximately 1.12 inches. It produces a conical beam that is approximately 30 degrees wide (to the half power points in the beam radiation pattern) at 125 kHz. The Airmar B150M transducer is a commercial "fish-finder" transducer that is also a piston type transducer with a radiating face diameter that is approximately 1.75 inches. It will produce a conical beam that is approximately 20 degrees wide at 125 kHz.

Figure 3 - Transducers. ITC-3406 (Right) and Airmar B150M (Left)

The inboard cluster of ITC-3406 transducers (shown in Figure 4) was deployed on a pole mount near the corner of the tailrace where the fish ladder wall meets the powerhouse wall. The transducer mounting pole was free to move up and down (driven by a float on the moving section) on an I-beam mounted to the fish ladder wall.

Figure 4 - Inboard Transducer Cluster, ITC-3406 Transducers

The Airmar transducers were mounted at a depth of six feet on a pole supported by a discus buoy (float) that was deployed outboard in the Cabot Station tailrace. An outboard transducer float is shown in Figure 5). The four floats, with a single transducer deployed from each float, were tethered together in the upstream/downstream direction and were also tethered with mooring lines back to the powerhouse wall and to anchors deployed on the outboard side (toward the mid-river). The geometry of the four outboard transducer floats is shown in Figure 6. The location of the inboard transducer cluster in relation to outboard transducer float #1 is shown in Figure 7. The mooring line arrangement used to secure the outboard transducer floats are shown in Figure 8. Electrical cables were run along the tether line securing the transducer floats to the powerhouse wall using a cableway formed by passing the cables and mooring lines through a flexible “Chinese-finger” style fabric sheath (the red covering in the figure). On the inboard side, the signal and power cables were terminated within an electrical junction box secured to the railing at the powerhouse wall, as shown in Figure 9. The shore-side cables exited the junction box and were routed up the side of the powerhouse, through an open window and back down to the topside equipment/operator station on the main floor of the powerhouse. The transducer drive cables for the inboard transducer cluster were laid across the deck on the walkway and then up the side of the powerhouse through the open window and then down to the operator station inside the powerhouse.

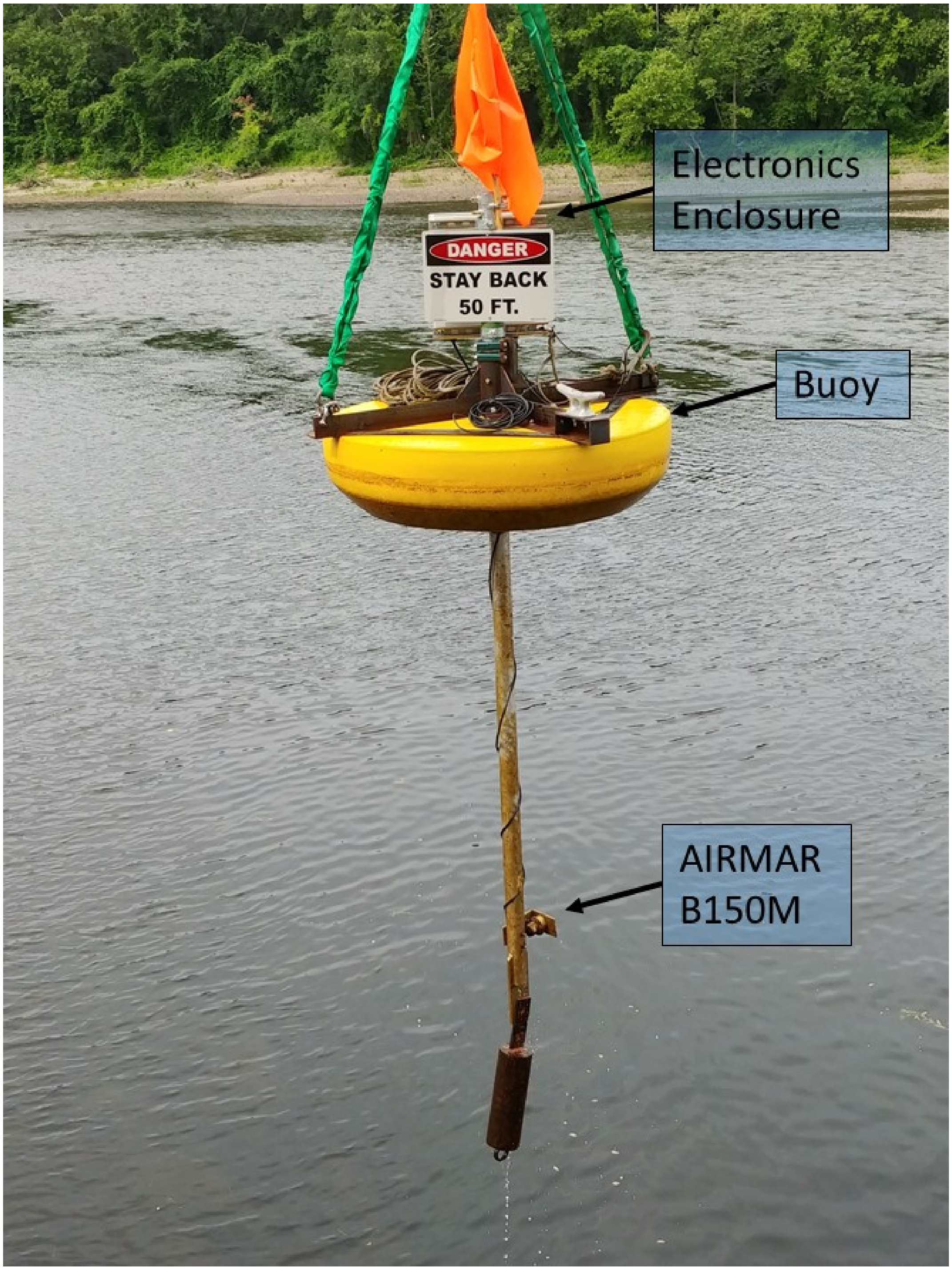

Figure 5 - Outboard Transducer Platform

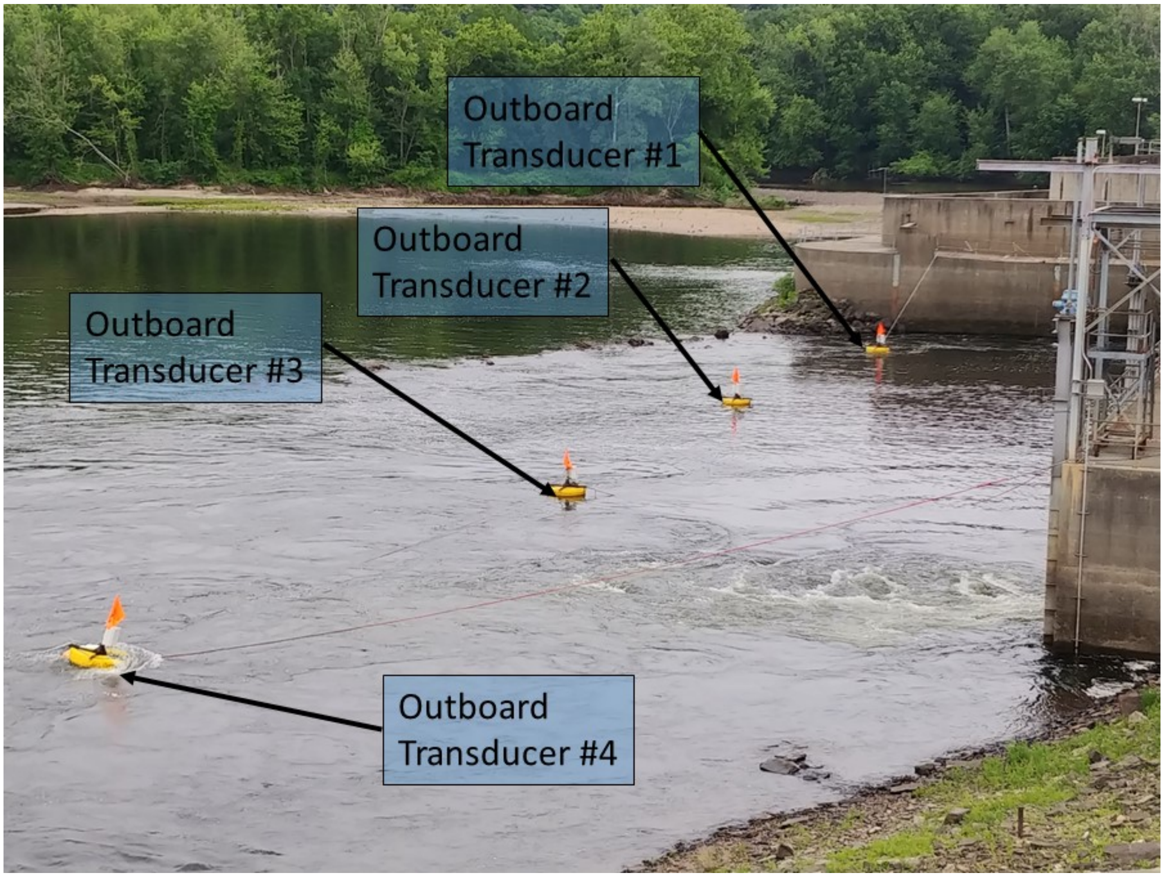

Figure 6 - Outboard Transducer Arrangement

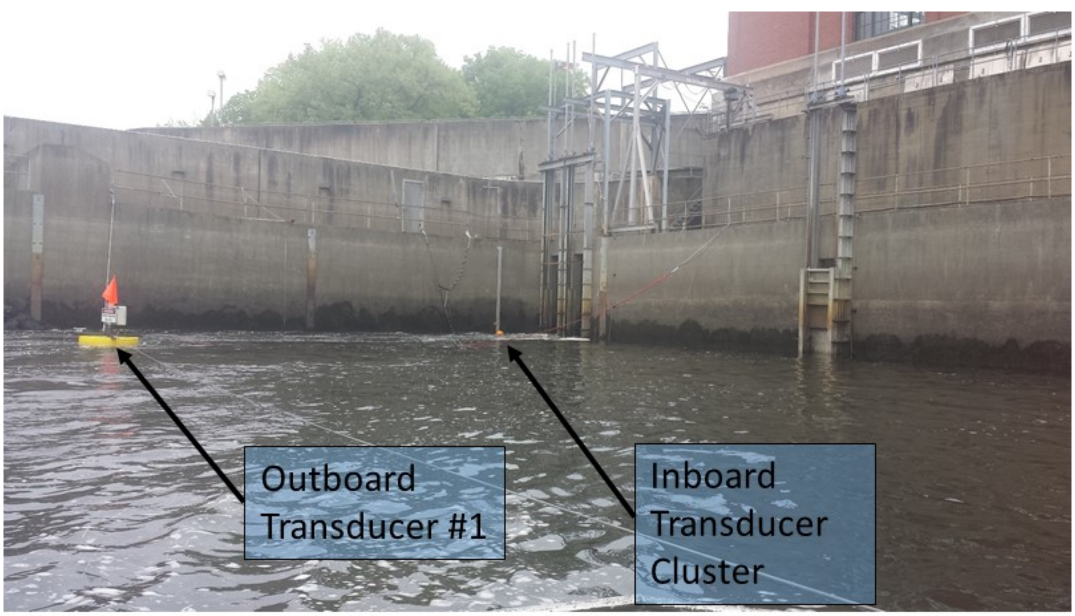

Figure 7 - Transducer Deployment shown Outboard Transducer #1 and Inboard Transducer Cluster

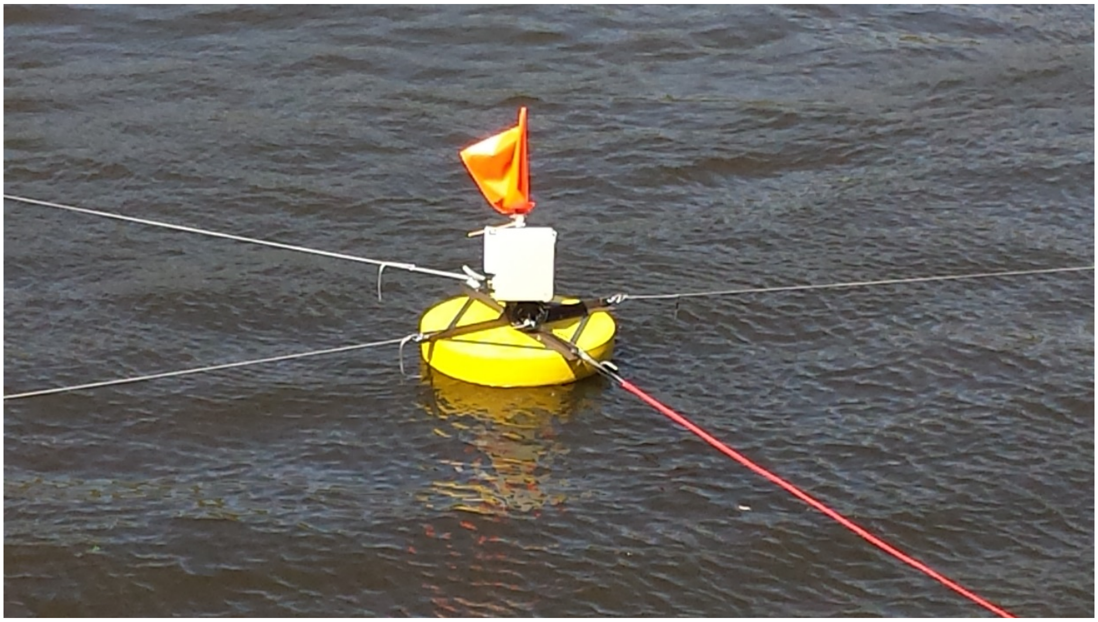

Figure 8 - Outboard Transducer Float Mooring Lines

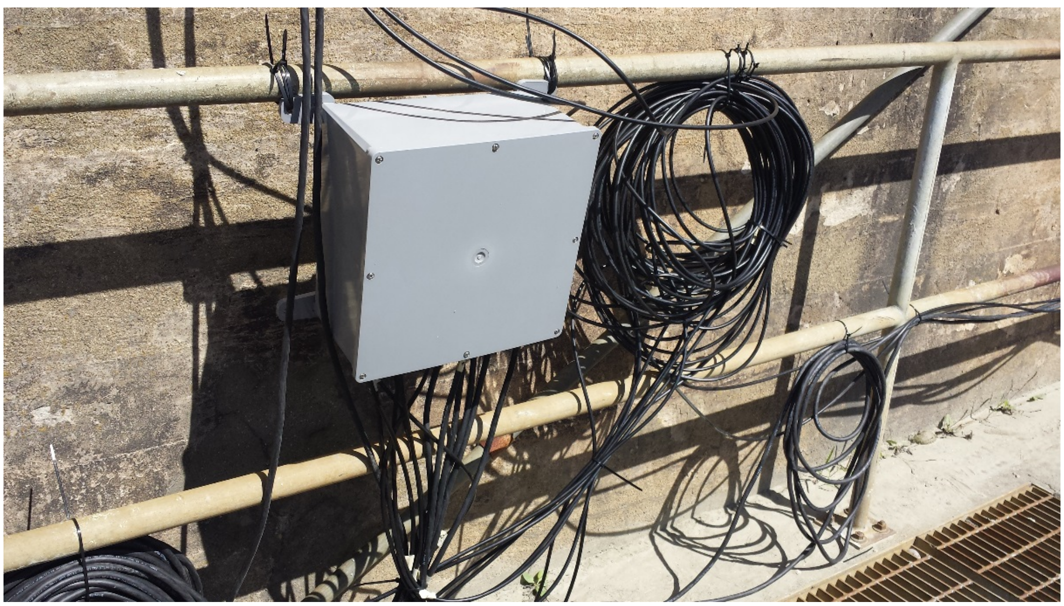

Figure 9 - Topside Junction Box

The internal electronics of the outboard transducer electronics enclosure are shown in Figure 10, Figure 11 and Figure 12. The electronics package included a Power Amplifier PCBA, a Cat5e Breakout PCBA, several DC-DC Converter PCBA, and an air circulation fan. A thermostatic switch was mounted on the Power Amplifier mounting bracket. The switch was intended to interrupt the 48 VDC power input to the enclosure if an over-temperature condition was reached. A thermistor was mounted on the Cat5e Breakout PCBA. The thermistor resistance could be measured at the topside operator station and from that resistance measurement the air temperature inside the enclosure could be derived.

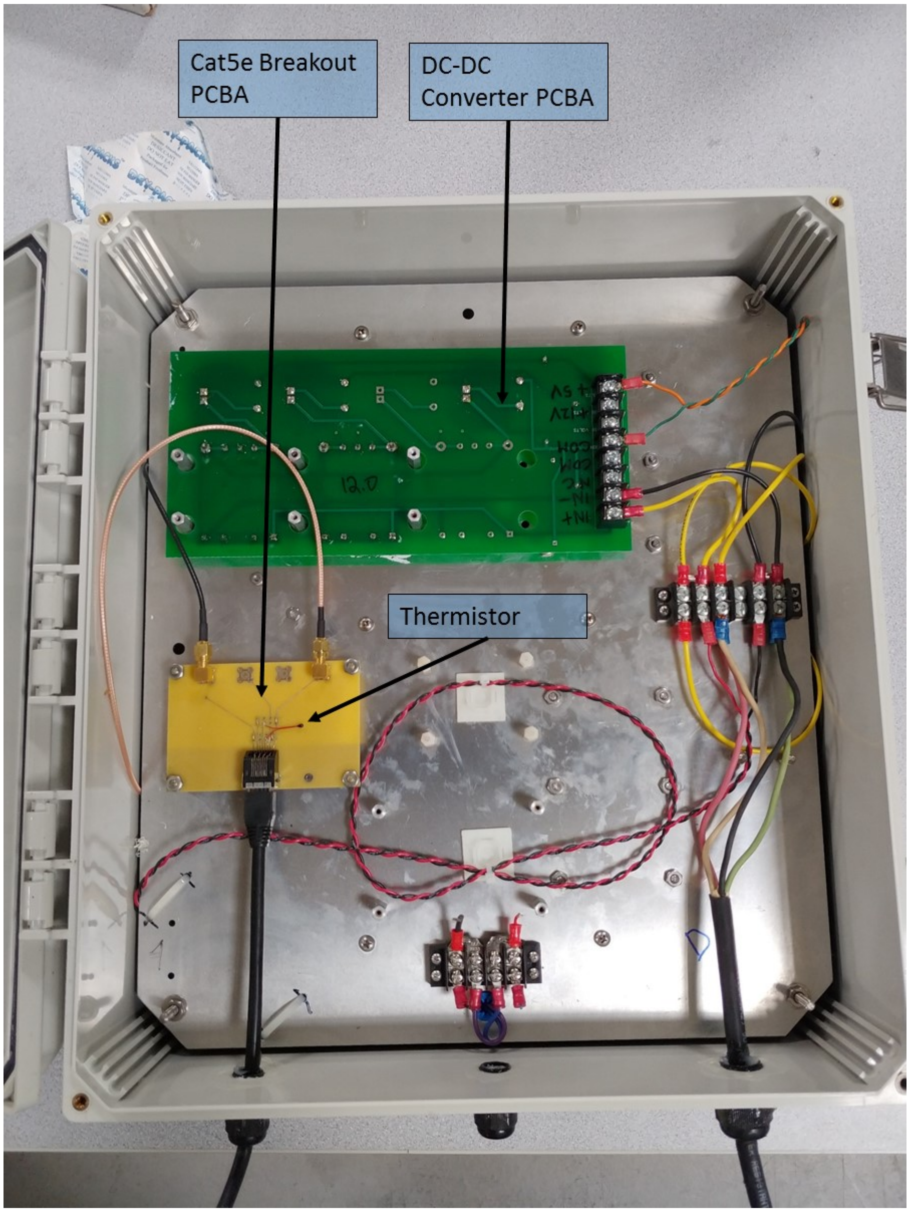

Figure 10 - Outboard Transducer Electronics Enclosure (Top View)

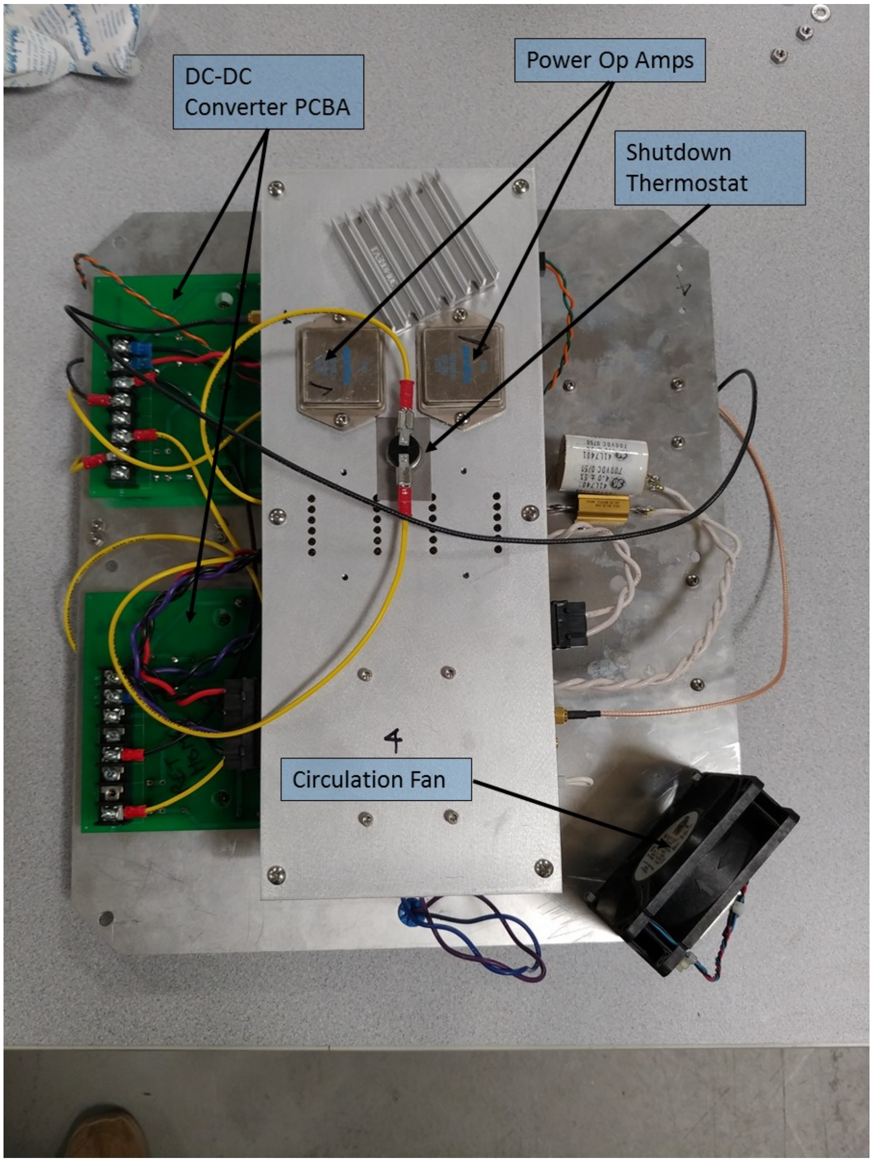

Figure 11 - Outboard Transducer Electronics Enclosure (Rear View)

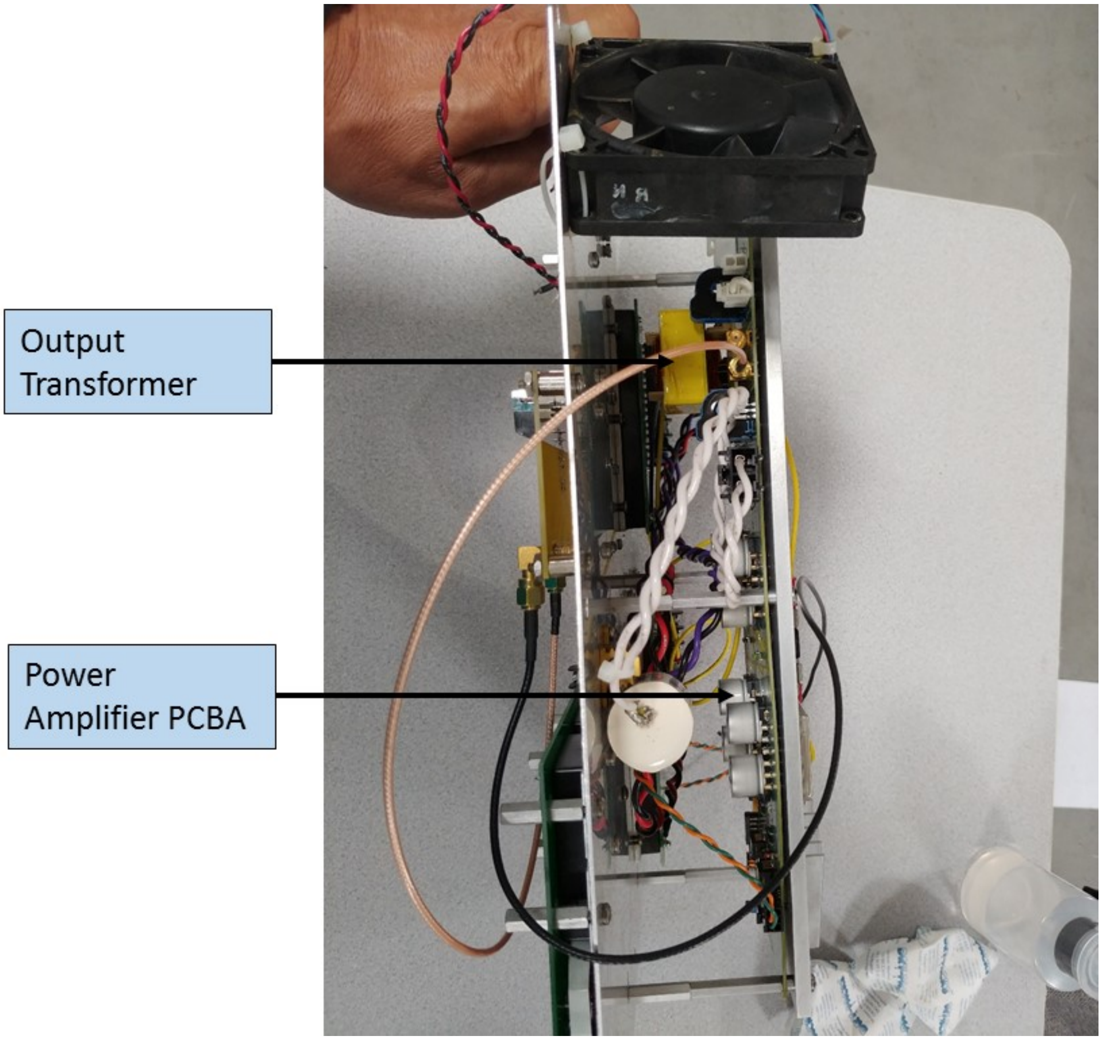

Figure 12 - Outboard Transducer Electronics Enclosure (Side View)

The equipment layout at the topside operator station is shown in Figure 13 and Figure 14. The sound system PC and the power amplifier equipment for driving the inboard transducer cluster were mounted in a rack. A fan unit mounted below the power amplifier assembly in the rack circulated air vertically to provide cooling to the power amplifiers. The 48 VDC power supplies and the Waveform Monitor PC, along with the power and signal interface hardware for the outboard transducer systems were located on a tabletop adjacent to the rack. Mid-way through the study, a 2nd desktop/tower PC was brought in as an alternate/replacement to the rack-mounted industrial PC to be used to drive the sound system following an inadvertent shutdown of the original rackmount system.

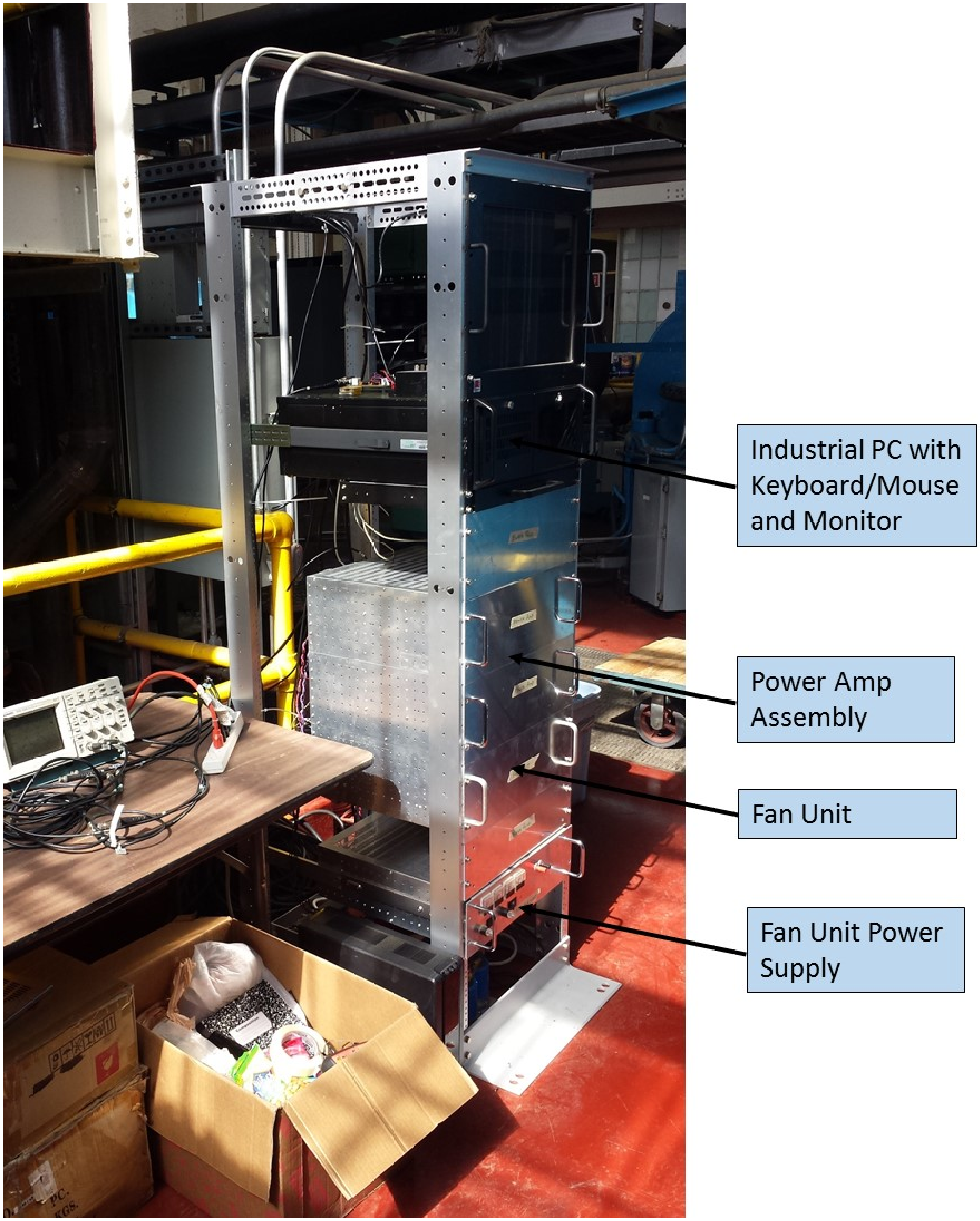

Figure 13 - Operator Station Equipment Rack

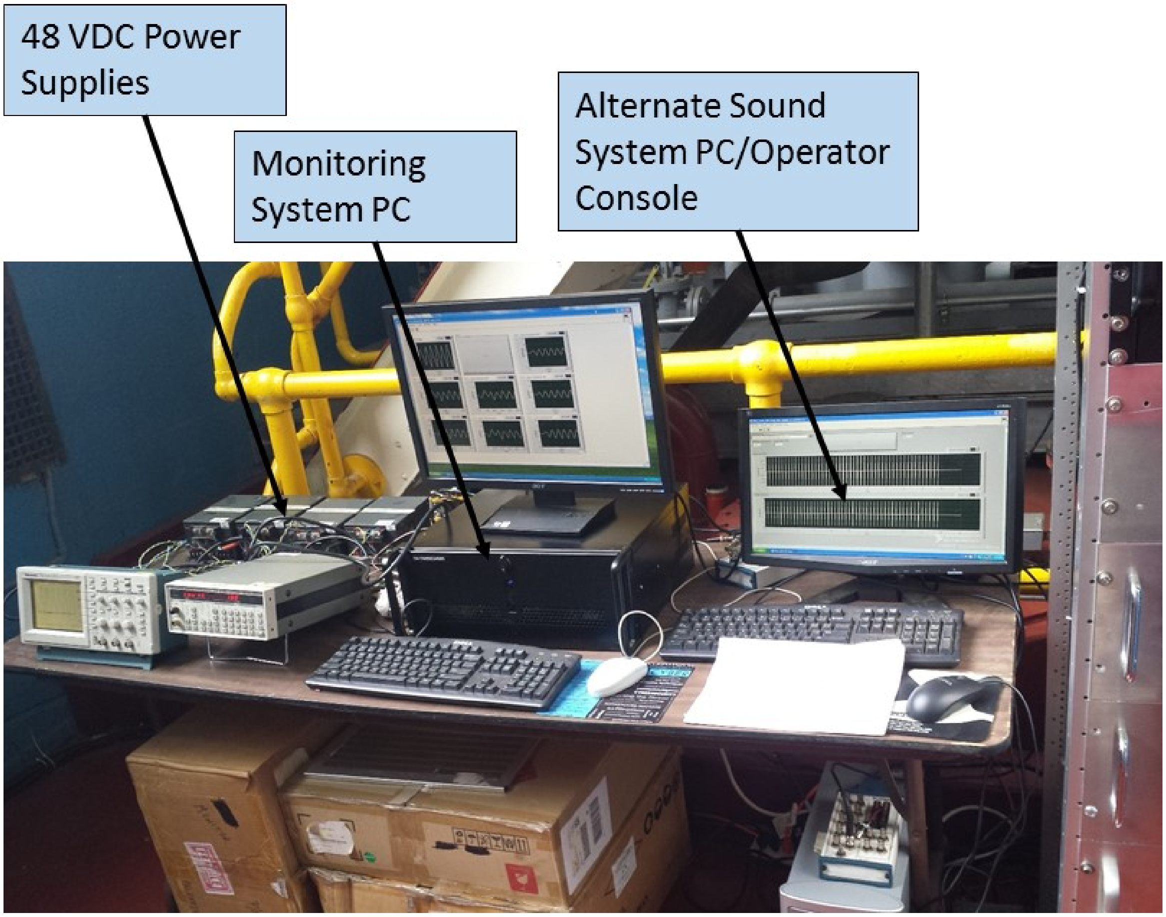

Figure 14 - Topside Equipment

Test Signal and Waveform Player

The attributes of the test signal/stimulus were defined by Alden Research Laboratory and implemented by SSI using the signal generation features of National Instruments Labview. A signal waveform was generated by a signal generation virtual instrument (VI) and stored as a Labview waveform file on the local PC hard disk drive. The signal used for the study was a repeating pattern of 1.5 millisecond long 125 kHz tone-burst. Within the stored waveform file, the 1.5 ms pulse is repeated every 200 milliseconds for 10 seconds followed by a 1 second rest period (sound off). The test signal waveform is shown graphically on the HMI display screen in Figure 15.

A waveform player VI was written to support the testing protocols for the study. The waveform player VI, which was a slight modification of the player used in 2016, allows the user to specify a waveform (from a stored waveform file on the local hard disk), to adjust the amplitude of the waveform by specifying a scale factor, to specify the repetition rate of the waveform, and to specify the total runtime of the test period.

Figure 15 - Test Signal Waveform

Waveform Monitor

A PC-based monitoring system was developed to provide continuous health assessment of the sound system. Current transducers integral to the power amplifier PCBA provided a voltage signal that was proportional to the current delivered to the attached transducer. The current monitor signals from the outboard transducers were routed to the topside equipment through a twisted pair cable within the Cat5e signal cables. The monitor signals for the inboard transducer cluster were available on BNC jacks located on the rear panel of the rack-mount power amplifier assembly. The current waveforms were monitored using another Labview application that captures the individual current monitor signals from each transducer power amplifier current monitor in sequence. The current waveforms were presented graphically on the PC Monitor as shown in Figure 17. The upper right-hand waveform graph in the waveform monitor display is the transducer drive signal. The waveform monitor system was periodically checked (visually) by the staff at Cabot Station to confirm proper operation of the sound system.

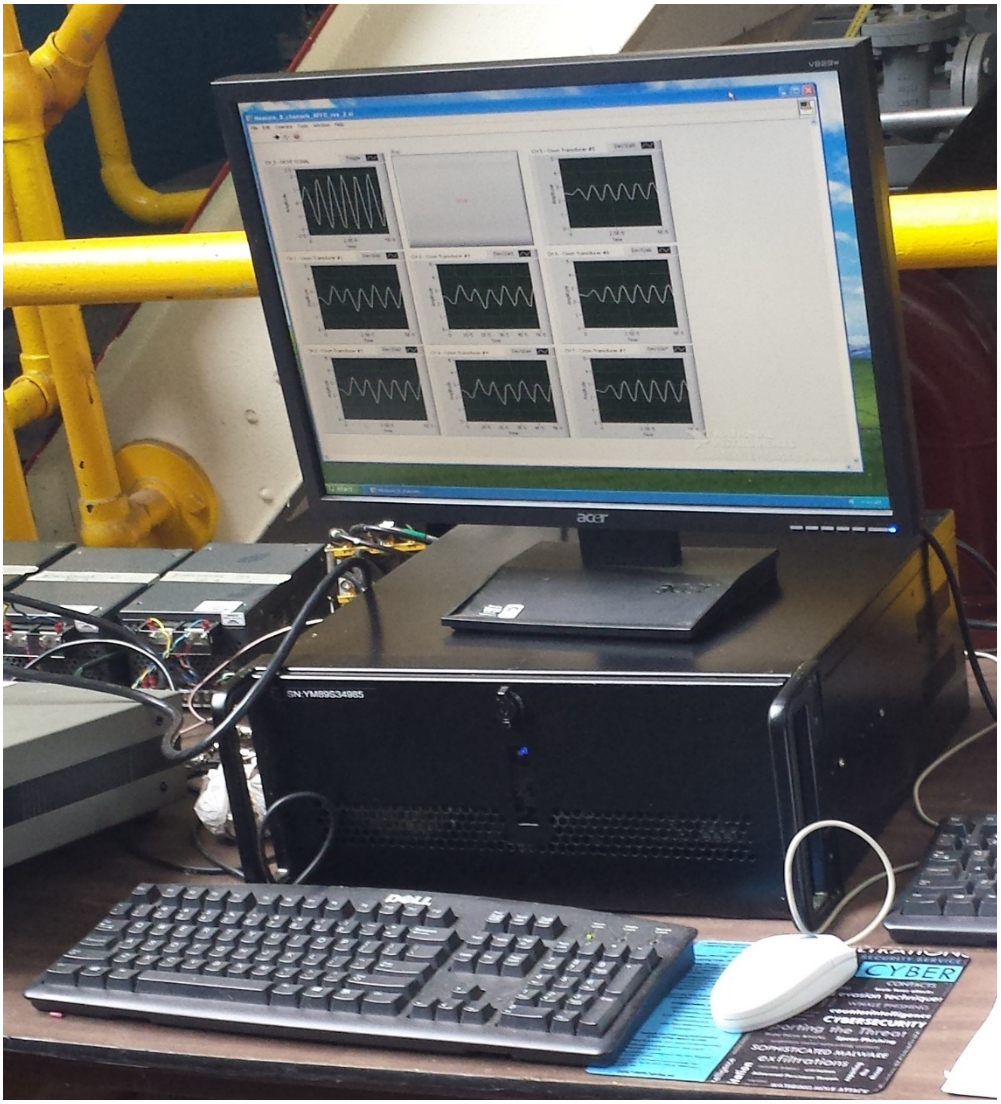

Figure 16 - Monitoring System

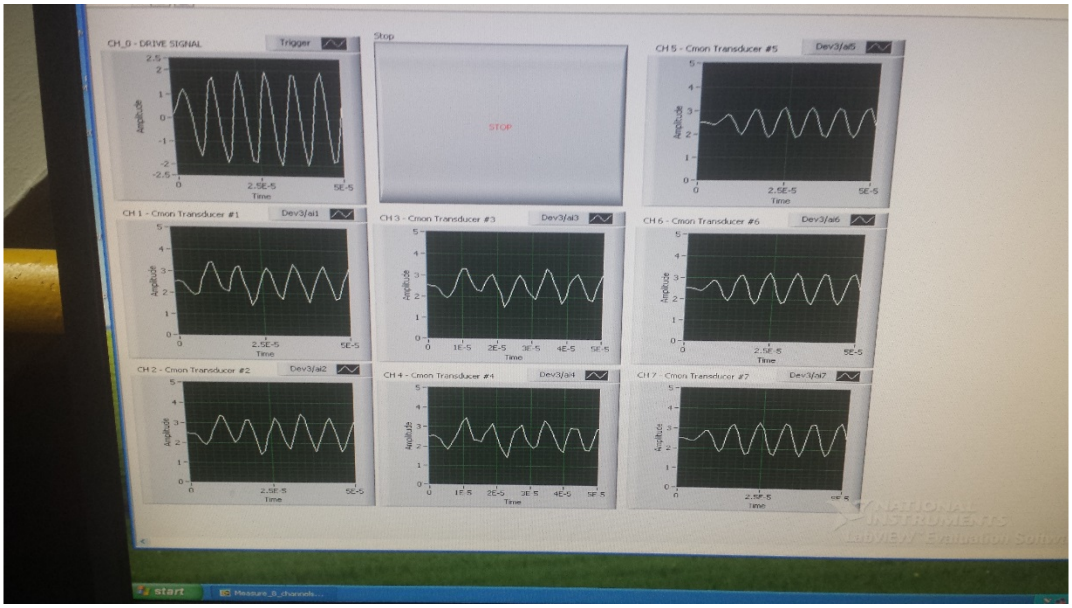

Figure 17 - Waveform Monitor Display

APPENDIX B – TELEMETRY STATION CALIBRATION RESULTS

APPENDIX B: Telemetry Network Calibration and Equipment Effectiveness

Radio Telemetry Calibration

Each telemetry station was calibrated with a transponder (or radio tag) prior to release of test fish to ensure adequate power readings, range, and proper calibration of equipment. One tag, programed with code 13, was used as a '*test tag*' during the calibration period. This code was not repeated for any tags inserted into test fish used for this study. The test tag was attached to fishing line and deployed to a water depth of approximately 4 to 5 feet to mimic the swimming depth of adult American Shad. One member of the field crew remained on land monitoring the receiver output signals and two field staff used a boat to test the targeted detection zone at each telemetry station. Communication via handheld two-way radios allowed transfer of power signals at different locations that were recorded on a map for calibration purposes.

A list of the receivers used for this study is provided in Table 4.1.2-1 of the main report. Orion receivers output an average power number for each detection, which is recorded in decibel levels (db). These numbers are negative, with less negative numbers being higher in signal strength. Lotek receivers output an average power level for each detection, with higher numbers indicating a stronger signal.

All figures of the telemetry stations below show the position of the 'test tag' and the average power levels associated within the detection zones recorded during testing (noted in white). Several test detections were recorded at each location.

Station: Entrance to the Deerfield River

Figure 1: The red star marks the approximate location of the Yagi antenna and the Orion receiver used to detect fish moving across the width of the Deerfield River at RM 119.5. The radio test tag produced power levels ranging from -80s to -100s db with highest powers located near the bank and attenuating slightly toward the far bank of the river.

Station: Montague Wastewater

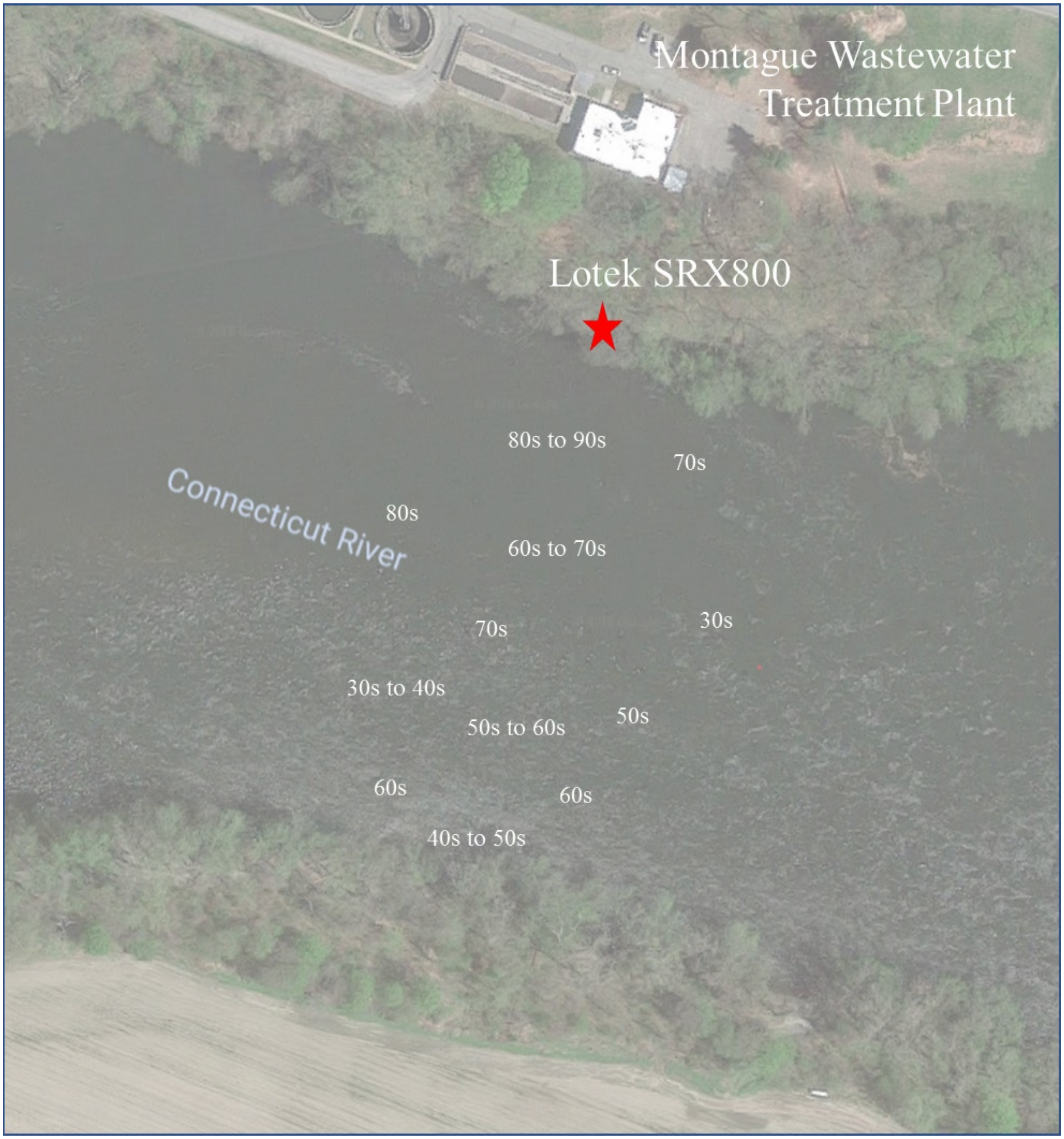

Figure 2: The red star marks the approximate placement of the Yagi antenna and the Lotek receiver used to detect fish moving across the width of the river at RM 119.5. The radio test tag produced power levels ranging from 40s to high 90s with highest powers located near the bank of the river closest to the Yagi antenna and attenuating slightly toward the far bank.

Station: Downstream Smead Island East Channel

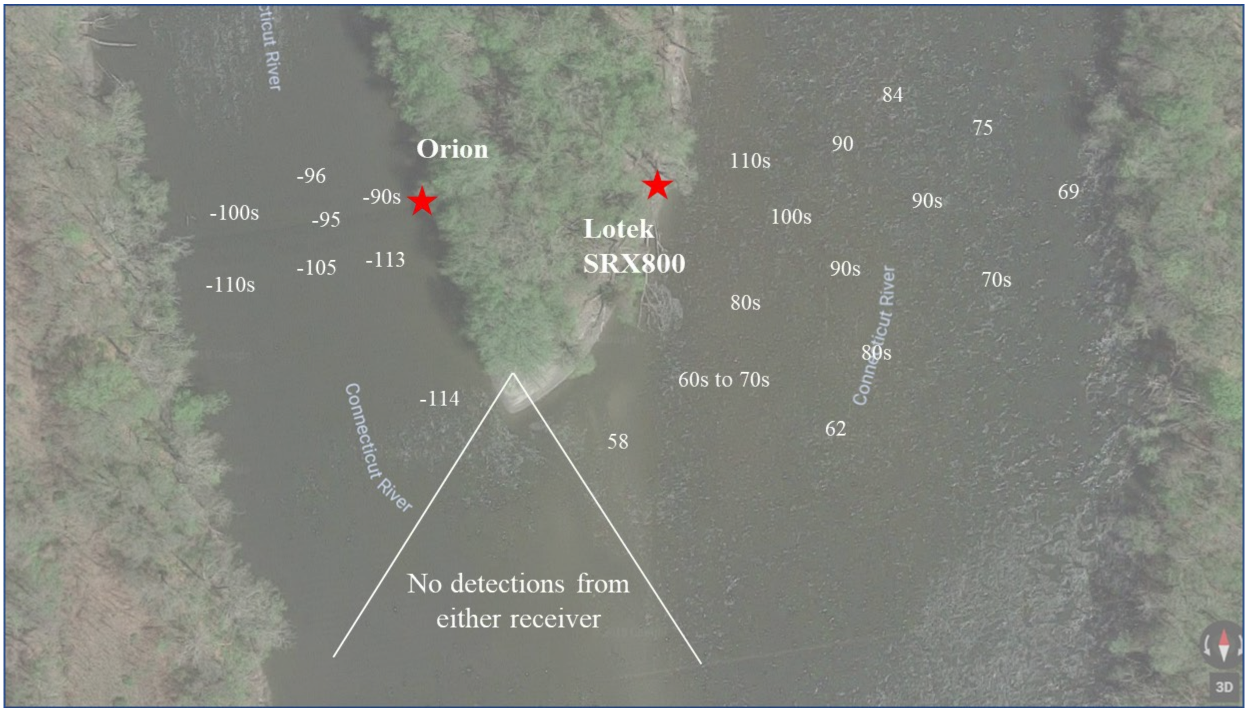

Figure 3: The red stars mark the approximate placement of the Yagi antennas and receivers used to detect fish moving across the width of the river at RM 120. An Orion receiver was used to monitor the western channel, and a Lotek receiver was used to monitor the eastern channel. The radio test tag produced power levels ranging from 70s to 110s at the Lotek receiver, with highest powers located near the bank of the river on the east channel of Smead Island closest to the Yagi antenna and attenuating slightly toward the far bank. The radio test tag produced power levels ranging from -90 to -110 db at the Orion receiver, with highest power levels read near the island bank, closer to the Yagi antenna, and attenuating toward the western bank. The test tag was not detected downstream of the island's point.

Station**:** Cabot Tailrace Right

Figure 4: The yellow star marks the approximate placement of the Yagi antenna and the Orion receiver used to detect fish moving into the right side of the Cabot Station tailrace at RM 120. The radio test tag produced power levels ranging from -70s to -100s db at both locations with highest powers located closest to the Yagi antennas and attenuating slightly toward the opposite bank. The approximate outer boundary of the detection zone is indicated by the blue arch. The red stars mark the approximate locations of the Cabot Station tailrace droppers. These sites were tested to confirm tag detections within the vicinity of each dropper. Due to unsafe conditions, a full, detailed calibration was not conducted.

<u>Station:</u> Cabot Tailrace Left

Figure 5: The red star marks the approximate placement of the Yagi antenna and the Orion receiver used to detect fish moving into the left side of the Cabot Station tailrace at RM 120. The radio test tag produced power levels ranging from -80s to -100s db at both locations with highest powers located closest to the Yagi antennas and attenuating slightly toward the opposite bank. The approximate outer boundary of the detection zone is indicated by the blue arch.

<u>Station:</u> Cabot Ladder Entrance Dipole

Figure 6: The red star marks the approximate placement of the dipole antenna and the Orion receiver used to detect fish moving to the Cabot Station ladder entrance at RM 120. The test tag produced power levels ranging from -57 to -89 db with highest powers located near Cabot Station ladder entrance and attenuating slightly farther out.

<u>Station</u>: Upstream end of Smead Island

Figure 7: The red star marks the approximate placement of the Yagi antenna and the Lotek receiver used to detect fish moving passed the upstream end of Smead Island at RM 120. The radio test tag produced power levels ranging from high 40s to mid-130s with highest powers located near the Yagi antenna and attenuating toward the bank of Smead Island.

<u>Station</u>: Bypass Reach- Conte Discharge

Figure 8: The red star marks the approximate placement of the Yagi antenna and the Orion receiver used to detect fish moving upstream through to the Bypass Reach at RM 120, near the Conte Discharge. The test tag produced power levels ranging from -70s to -110s db.

Station: Bypass Reach- Station No. 1

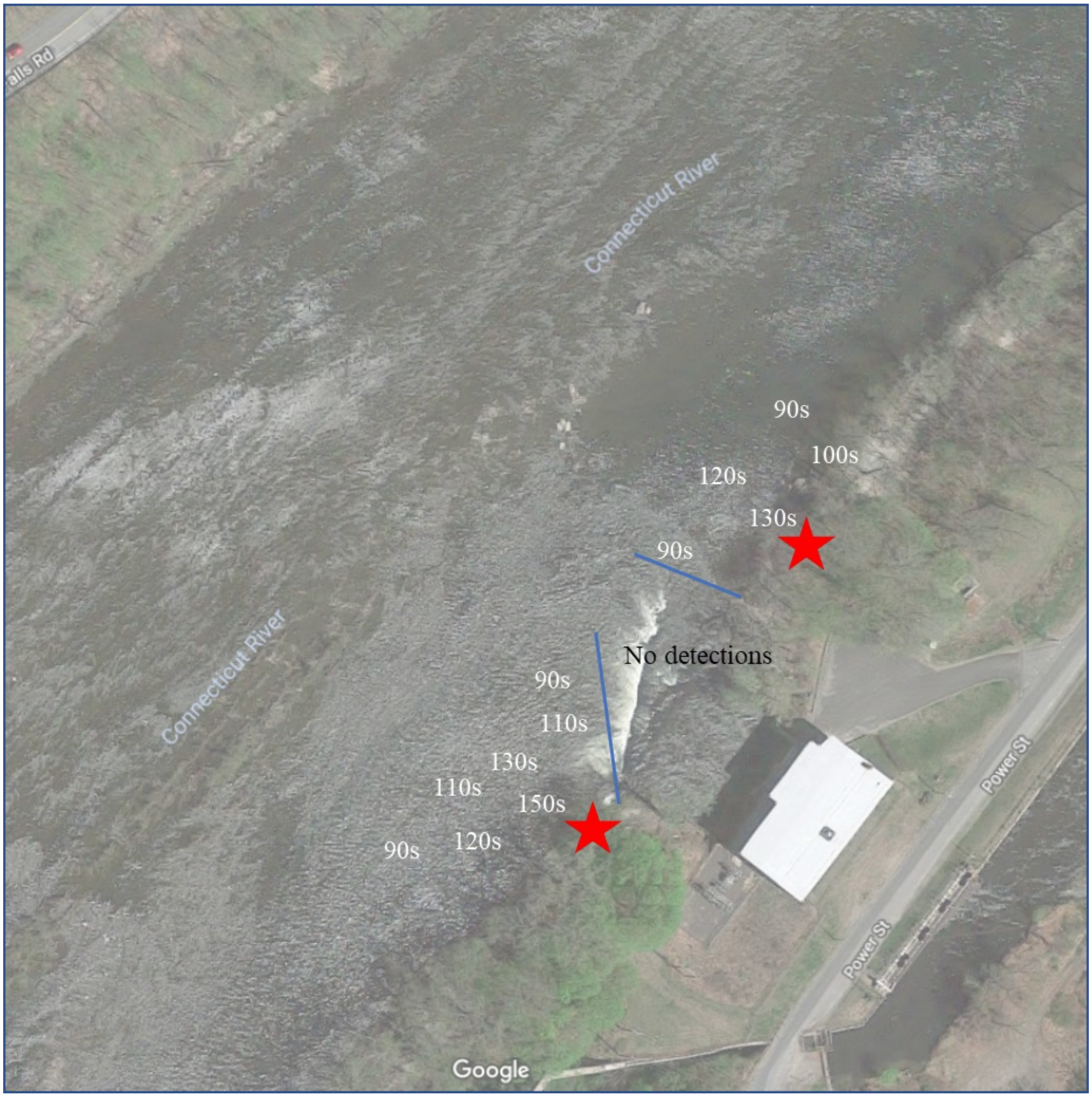

Figure 9: The red stars mark the approximate placement of the Yagi antennas and the Lotek receivers used to detect fish moving upstream through to the Bypass Reach, up to and past Station No. 1. The radio test tag produced power levels ranging from 90s to 150s with highest powers located near the Yagi antennas. The tag was not detected in the immediate area of the Station No. 1 discharge.

Station: Spillway Ladder Entrance Dipole

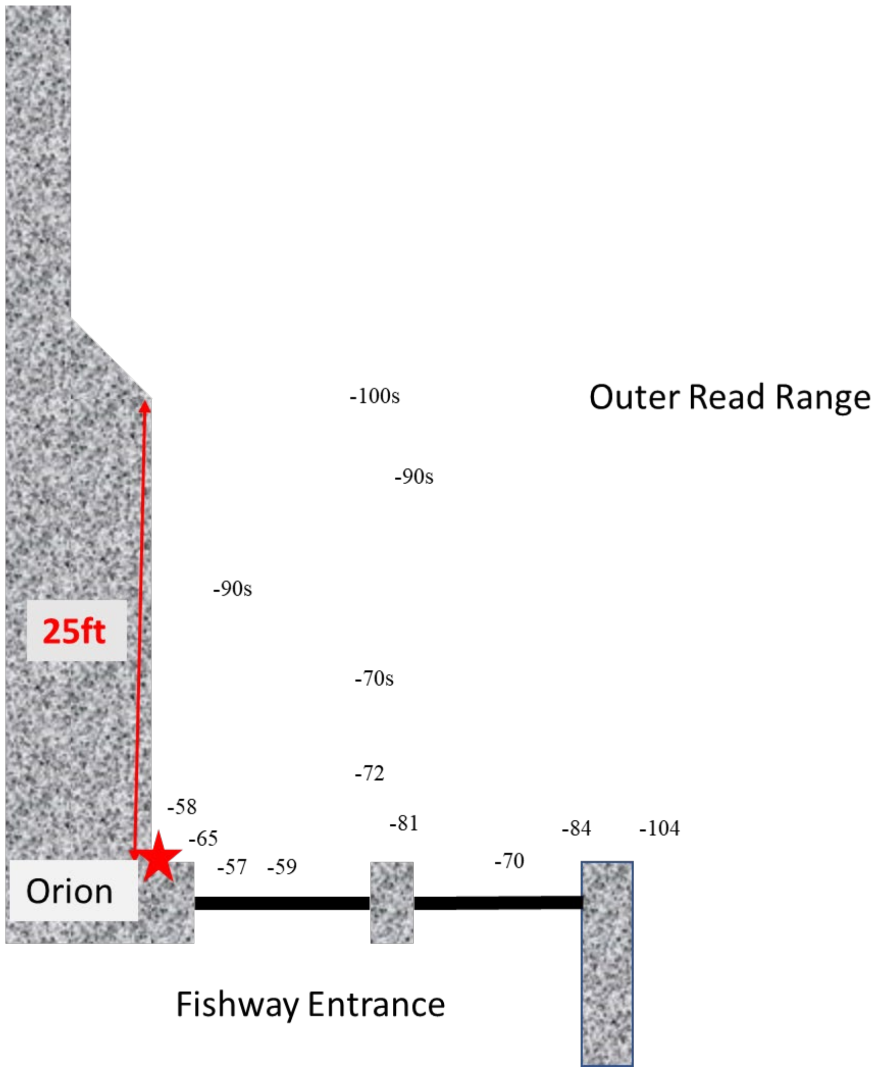

Figure 10: The red star marks the approximate placement of the dipole antenna and the Orion receiver used to detect fish moving to the TFD spillway ladder entrance at RM 122. The test tag produced power levels ranging from -50s to -100s db with highest powers located near the ladder entrance and attenuating farther out.

Station: Spillway Ladder Vicinity

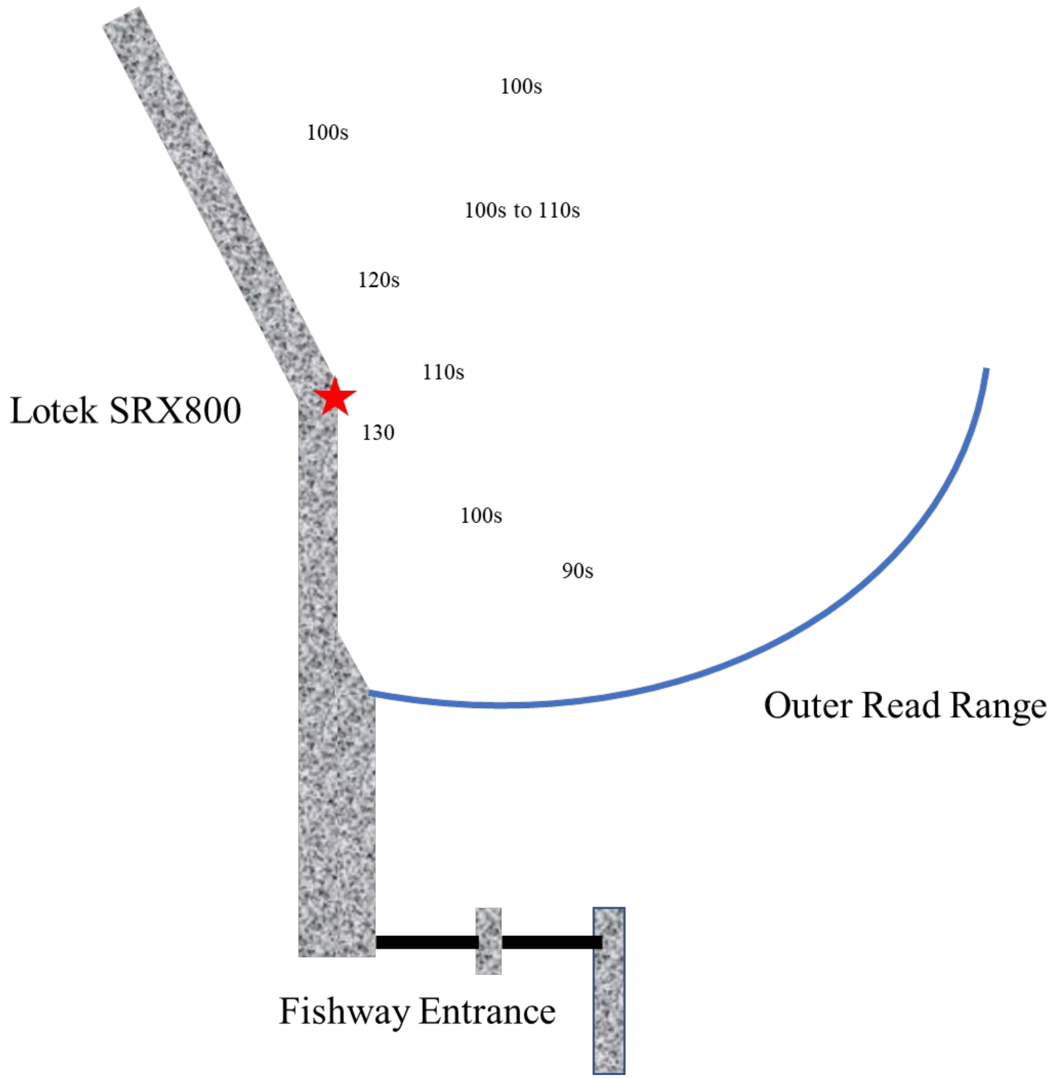

Figure 11: The red star marks the approximate placement of the Yagi antenna and the Lotek receiver used to detect fish moving in the vicinity of the TFD spillway ladder at RM 122. The test tag produced power levels ranging from 90s to 130 with highest powers located near TFD spillway ladder entrance and attenuating farther out.

APPENDIX C – STATISTICAL METHODS

APPENDIX C STATISTICAL METHODS

TABLE OF CONTENTS

LIST OF TABLES

LIST OF FIGURES

C. STATISTICAL METHODS INTRODUCTION

This appendix contains the unabridged statistical methods used to assess movement of radio-tagged American Shad at the Turners Falls Project. Statistical assessments of movement with radio telemetry are complex due to the amount of data produced, inclusion of false positives and significant overlap between receiver detection zones. Prior to analyzing movement within a competing risks or mark recapture framework, we implemented an algorithm that identifies and removes false positive detections while not being so strict as to introduce false negatives into the dataset, then we implemented an overlap reduction algorithm that reduced ambiguity in a fish's position. Both of these steps are necessary as they reduce bias and ambiguity that have traditionally plagued assessments of movement with radio telemetry.

C.1 False Positive Data Reduction

Radio telemetry receivers record four types of detections based upon their binary nature; true positives, true negatives, false positives and false negatives (Beeman and Perry, 2012). True positives and true negatives are valid data points that indicate the presence or absence of a tagged fish. A false positive is a detection of a fish's presence when it is not there, while a false negative is a non-detection of a fish that is there. False negatives arise from a variety of causes including insufficient detection areas, collisions between transmitters, interference from ambient noise, or weak signals (Beeman & Perry, 2012). Inclusion of false negatives may negatively bias statistics as there is no way to know if a fish's absence from a receiver was because it truly wasn't there or if it was not recaptured by the receiver. While the probability of false negatives can be quantified from sample data as the probability of detection, quantifying the rate of false positives (type I error) is more problematic (Beeman & Perry, 2012). Inclusion of false positives in a dataset can bias study results in two ways: they can favor survivability through a project by including fish that weren't there, or increase measures of delay when a fish has already passed. There are no statistical approaches that can reduce bias associated with false positives, therefore they must be identified and removed *a priori*. For the purposes of this study, false positive reduction methods relied upon a Naïve Bayes classifier and an overlap reduction algorithm inspired by nested Russian dolls.

C.2 Probabilistic Data Reduction – Weight of Evidence

Bayes Rule is a rigorous method for interpreting evidence in the context of previous experience or knowledge (Stone, 2013). Bayes Rule cannot guarantee the correct answer, but rather provides the probability that each alternative answer (either true or false positive) is correct. Bayes theorem updates conditional probabilities (probability of a record being true positive given some data) and is particularly useful when evaluating diagnostic tests (false positives and false negatives).

Specifically, Bayes Rule calculates the posterior probability, or the probability of a hypothesis occurring given some information about its present state, and is written with $P(\theta_i|x_j)$; where θ_i is the hypothesis (true or false positive) and x_j is observed data. Formally, Bayes Rule is expressed as:

$$P(\theta_i|x_j) = \frac{P(x_j|\theta_i)P(\theta_i)}{P(x_j)}$$

Equation 1

Where $(x_j|\theta_i)$ is referred to as the likelihood of the j^{th} data occurring given the hypothesis (θ_i); $P(\theta_i)$ is the prior probability of the i^{th} hypothesis (θ); and $P(x_j)$ is the marginal likelihood or evidence. In most applications, including this one, the marginal likelihood is ignored as it has no effect on the relative magnitudes of the posterior probability (Stone, 2013). Therefore, there is no need to waste computational effort by calculating the joint probability. We can state that the posterior probability is approximately equal to the prior probability times the likelihood or:

$$posterior \propto prior * likelihood \qquad \text{Equation 2}$$

The prior probability is estimated by looking at how often each class (true or false positive) occurs in the training dataset, while the likelihood is estimated from the histogram of the values of each predictor (observed data) in the training dataset given each hypothesis (true or false positive) (Marsland, 2009). A kernel density function was fit for continuous predictors while qualitative predictors replied upon a multinomial probability distribution.

In most circumstances, the data (x) are usually vectors of feature values or predictor variables with n levels (x_n). As the dimensionality of x increases (number of predictor variables increase), the amount of data within each bin of the histogram of related variables shrinks, and it becomes difficult to estimate the posterior probability without more training data (Marsland, 2009). For example, long strings of continuous detections in series may only occur when the power of a detection is fairly high. Therefore, a simplifying assumption, the Naïve Bayes classifier, was employed.

C.2.1 Naïve Bayes Classifier

The Naïve Bayes classifier assumes that the elements (j) of the feature vector x (predictor variables) are conditionally independent of each other given the classification (Marsland, 2009). Therefore, the probability of getting a particular string of feature values of predictor variables is equal to the product of multiplying all of the individual probabilities (Marsland, 2009). The likelihood is given with:

$$P(x_1, \dots, x_n|\theta_i) = \prod_{j=1}^{n} P(x_j|\theta_i) \qquad \text{Equation 3}$$

Where n is equal to the number of features or predictor variables in x and θ_i is the hypothesis (either true or false positive). The classifier rule for Naïve Bayes is to select the detection class θ_i for which the following computation is maximized:

$$argmax\left\{ P(\theta_i|x_n) \propto P(\theta_i) * \prod_{j=1}^{n} P\left(x_j\middle|\theta_i\right) \right\} \qquad \text{Equation 4}$$

The detection class θ_j with the maximum posterior probability classifies every line of data belonging to a study tag into one of two classes: true or false positive. This is known as the maximum a posteriori or MAP hypothesis (Marsland, 2009).

The Naïve Bayes classifier was nothing more than a database application designed to keep track of which feature gives evidence to which class (Richert & Pedro-Coelho, 2013). However, there were circumstances where a particular feature variable level did not occur for a given detection class in the feature dataset (e.g., false positive detection with very high power and many consecutive hits in series), meaning that the likelihood for that feature given a detection class is zero. When multiplied together, the posterior probability was zero and uninformative. Therefore, the Naïve Bayes classifier used add-one smoothing, which simply adds 1 to all histogram counts (Richert & Pedro-Coelho, 2013). The underlying assumption here is that even if the feature value was not seen in the training dataset for a particular detection class, the resultant likelihood probability would be close to zero allowing for an informative posterior.

The training dataset consists of known true and false positive detections. By placing study tags at strategic locations throughout the study area for the duration of the study, these beacon tags give the algorithm information on what a known true positive detection looks like. On the other hand, known false positive detections are generated by the telemetry receivers themselves, and consist of detections coded toward tags that were not present in the list of tags released for the study.

Following the completion of the study, several predictor features were calculated for each received line of data. Predictor features include a detection history of pulses, the consecutive record hit length, hit ratio, miscode ratio, consecutive detection, detection in series, and power. The pulse detection history consists of a string of 1s and 0s that look forwards and backwards in time from the current detection in series, and identifies whether or not a pulse from that particular tag was detected. For example, if a particular tag had a 3-second burst rate, the algorithm will look forwards and backwards in time 3 seconds, query the entire dataset, and then return 1 if it was detected or 0 if it was not. The algorithm looks forwards and backwards for a user-defined set of detection intervals. Consecutive detection length and hit ratio are derived from this detection history. Consecutive detection length simply counts the number of detections in series, while hit ratio is the ratio of the count of heard detections to the length of the detection history string (Table C.2-1).

Note from Table C.2-1 that both detection history events are considerably different, but they have the same hit ratios. The hit ratio counts the number of correctly assigned detections to the total number of detections within a user-defined set of time. The hypothesis behind this predictor stipulates that a detection is more likely to be true when there are less miscoded detections. Consecutive detections and detections in series are binary in nature and quite similar, but the consecutive detection feature was stricter. For consecutive detection to return as true, either the previous or next detection must occur within the next pulse (i.e., 3-second interval). Detections in series allow the previous or next detection to occur at intervals greater than the first pulse; however, recaptures need to be in series. For example, if the pulse rate is 3 seconds and the next consecutive detection was missed, series hit would return true if the next recorded transmission occurred on the 6^{th} or 9^{th} second. In other words, the pulse rate must be a factor of the difference in time between the present detection and next detection for a series hit to return true. The last predictor, power, is hypothesized to be higher for true detections than false positives.

Prior to classification, FirstLight assessed the accuracy of the Naïve Bayes false positive detection algorithm with a k-fold cross validation procedure. The cross validation procedure randomly assigned folds (1,…,10) to each row of data. Then, the procedure iterates over each fold. The data assigned to the current fold are classified while the remaining rows served as the training data. Then, the classifications were compared against the known states, compiled into a cross validation table, and assessed with accuracy statistics. FirstLight assessed the accuracy of the classifier with the positive predictive value, negative predictive value, sensitivity, and specificity.

Table C.2-1. Example detection histories with their derived consecutive record length and hit ratio predictor feature levels.

Detections in series originating at the present detection (T_0)							Consecutive Record Length	Hit Ratio
T_{-3}	T_{-2}	T_{-1}	T_0	T_1	T_2	T_3		
0	1	0	1	0	1	0	1	3/7
0	0	1	1	1	0	0	3	3/7

C.3 Overlap Reduction

The radio telemetry network for this assessment was complex due to the nature of the questions asked and small scale of movement in and around the tailrace. In order to assess the efficacy of the ultrasound array in deflecting movement away from the Cabot Station ladder entrance and into the bypassed reach, the study required an assessment of movement into and out of small discrete locations. Unfortunately, discretizing fish presence into a single location and time was difficult because of the amount of overlap between receiver detection zones. To reduce the amount of overlap, FirstLight utilized multiple antenna types, including using stripped coaxial cable, dipole antennas, and large aerial Yagi antennas where appropriate. The detection ranges on these antennas vary greatly, but it was assumed that the regions increase in size from stripped coaxial cable up to large aerial Yagis. An algorithm inspired by nested-Russian Dolls was developed to reduce overlap and discretize positions in time and space within the telemetry network. If a fish can be placed at a receiver with a limited detection zone (stripped coaxial cables or dipole), then it can be removed from the overlapping detection zone (Yagi) if it is also recaptured there.

Fish will often visit a limited range antenna for a certain amount of time, then leave that detection zone only to return sometime later. This behavior is commonly referred to as a "bout" in the ecological literature (Sibly, Nott, and Fletcher, 1990). FirstLight followed the method of Sibly, Nott and Fletcher (1990) to fit a three-process broken-stick model (piecewise-linear regression with two knots ($k = 2$)). We first calculated the lag between detections for each fish within each discrete detection zone. Then, we binned the lag time into 10-second intervals and counted the number of times a lag interval occurred within each bin. After log-transforming the counts, the three-process broken-stick model was fit using a brute-force procedure that tested every bout-length combination with an ordinary least squares regression. The best three-process model was the one that minimized the total residual error (sum of squares). The first bout process describes a continuous string of detections indicative of a fish being continuously present, the second bout process describes milling behavior at the edge of a detection zone where lags between detections may be 20 – 30 seconds or more, and the third bout process describes the lags between detections where a fish leaves one detection zone completely for another only to come back sometime later.

After deriving the bout criteria for each discrete telemetry location, presences were enumerated. We assumed that a fish left a detection zone at the start of the third process. Therefore, the second knot location in the piecewise linear process model (a.k.a. broken-stick model) described this lag-time. If the lag between detections is equal to or greater than this duration, a fish has left the telemetry location only to return much later. In other words, the fish experiences a new presence. We iterated over every detection, for every fish, at every receiver, applied this logic to each lag time, and then enumerated and described presences at each location with start and end time statistics.

After describing presences at each receiver (time of entrance, time of exit) it is possible to reduce the overlap between receivers that traditionally plague statistical assessments of movement. If we envision overlapping detection zones as a series of nested-Russian Dolls, we can develop a hierarchical data structure that describes these relationships. If a fish is present in a nested antenna while also present in the overlapping antenna, we can remove coincident detections in the overlapping antenna and reduce bias in our statistical models. This hierarchical data structure is known as a directed graph, where nodes are detection zones and the edges describe the hierarchical relationships among them. For this assessment, edges were directed from a larger detection zone towards a smaller. Edges identify the successive neighbors (smaller detection zones) of each parent node (larger detection zone).

Movement within the tailrace was very complex and overlapping detection zones added to the complexity. Each node on the telemetry network consisted of one or more telemetry receivers (Table C.3-1). We described the hierarchical relationships between nested receivers with the directed graph depicted in Figure C.3-1. Here, the edges between nodes indicate successors, or nodes with successively smaller detection zones. In cases where aerial Yagi antennas overlap, removal was conservative and favored those receivers closer to the tailrace. In other words, if statistics are biased after overlap removal, they will favor delay within the tailrace.

The Russian Doll algorithm iterated over each detection at each node in Figure C.3-1. Then, the algorithm iterated over each presence at each successor node and asked a simple question: Was the fish detected at the child node while it was also detected at the parent node? If the answer is yes, then the detection at the parent node overlaps the detection at the child node. The algorithm is nothing more than an iterative search over a directed graph that applies a simple Boolean logic statement. However, it is very powerful in its ability to simplify movement and place fish in discrete spatial locations at discrete points in time. Following false positive and overlap removal, we created detection histories for a Cormack-Jolly-Seber survival model and processed strings of detections into counting-format style for analysis with time-to-event modeling.

Table C.3-1: Node to telemetry receiver relationship

Node	Telemetry Antennas
S01	T02
S02	T01
S03	T03O
S04	T03L
S05	T07
S06	T04, T05, T06
S08	T08
S09	T09
S10	T10
S11	T11
S12	T13
S13	T12

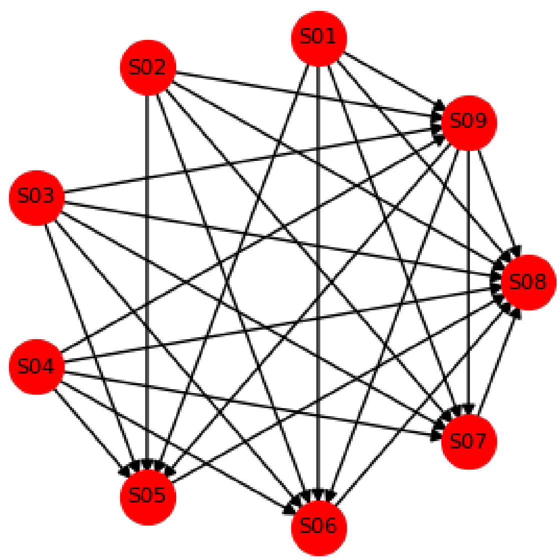

Figure C.3-1: The hierarchal relationships used to reduce overlap between Cabot Station tailrace antennas. Note edges show which nodes are successors (i.e., have successively smaller detection zones).

C.4 Cormack-Jolly-Seber Open Population Mark-Recapture Model

Mark-recapture survival analysis is typically used to assess passage effectiveness of fish ladders (Beeman and Perry, 2012). Use of the term "survival" is standard for mark-recapture analysis, which is predominantly used to assess the actual survival of marked animals over time. Survival in this context simply means successful passage, it should not convey mortality. Given that the temporal and spatial horizon is very short for those stretches studied with mark-recapture techniques (on the order of hours to less than 1,000 ft), mortality was not tested using a mark-recapture framework. Therefore, to reduce confusion, we will refer to the estimate as arrival. To estimate arrival parameters in the field under natural or anthropogenic conditions, one must follow individually marked animals through time (Lebreton et al., 1992). However, it is rarely possible to follow all individuals of an initial sample over time (Lebreton et al.,

1992) as is evident by varying recapture rates at each telemetry receiver location. Open population mark-recapture models allow for change (emigration and mortality) during the course of a study (Armstrup, McDonald, and Manly, 2005). The Cormack-Jolly-Seber (CJS) model is based solely on recaptures of marked animals and provides estimates of arrival and capture probabilities only (Armstrup, McDonald, and Manly, 2005). The CJS model has the following assumptions:

- Every marked animal present in the population at time (t) has the same probability of recapture (p_t).
- Every marked animal in the population immediately after time (t) has the same probability of surviving to time $(t + 1)$.
- Marks are not lost or missed.
- All samples are instantaneous, relative to the interval between occasion (t) and $(t + 1)$.
- Each release is made immediately after the sample (Cooch and White, 2006).

An animal that has not been observed for some time may have survived and escaped recapture by chance or for biological reasons its recapture might occur if the study were to continue (Lebreton et al., 1992). With this binary state of nature in mind, the presence and absence of animals at each location along a telemetry network is encoded with a string of 1s or 0s denoting presence and absence respectively. To properly assess arrival with variability in recapture, more parameters are required.

Under the assumption of independence of fates and identity of individuals, the observed detection history strings are observations of a multinomial probability distribution (Lebreton et al., 1992). The method of maximum likelihood estimation was used to estimate the parameters in the model (Lebreton et al., 1992). The statistical likelihood is the product of the probability of observing a particular detection history given release over those capture histories actually observed (Lebreton et al., 1992). More than one animal may have the same recapture history; therefore, the number observed in each recapture history appears as an exponent in its corresponding probability likelihood statement (Lebreton et al., 1992). MARK uses the profile likelihood estimation of variance to construct the confidence intervals (Cooch & White, 2006). Consequently, the shape of the log-likelihood function estimated by the maximum likelihood procedure provides information on the precision of the estimators (Lebreton et al., 1992). Profile likelihood intervals have better coverage with small samples and because the distribution of estimators is often very non-normal and the parameter space has boundaries (e.g., 0 and 1) (Lebreton et al., 1992).

The following lists the steps of the procedure for model creation and selection, which relied on methods from Lebreton et al. (1992) and Cooch and White (2006):

1. Build a global model compatible with the biology of the species studied and with the design of the study.
2. Assess model fit using appropriate goodness-of-fit (GOF) measures.
3. Select a more parsimonious model using Akaikes Information Criteria (AIC) to limit number of formal tests.
4. Test for the most important biological questions by comparing this model with neighboring ones using likelihood ratio tests.
5. Obtain maximum likelihood estimates of model parameters with estimates of precision.

The first step was to build a saturated model, which is loosely defined as the model where the number of parameters equals the number of data points or data structures (Cooch and White, 2006). The saturated model estimated a survival (ϕ) between each facility location and recapture (p) probability at each facility relocation (Figure C.4-1). It is not possible to differentiate between the final survival (ϕ_5) and recapture station (p_4) because it is not known if an animal died or was simply not recaptured at the final telemetry station. Following the creation of the saturated model, GOF testing was performed.

GOF procedures tested the assumptions underlying the models that the data are being fit to. GOF is a necessary first step to ensure that the most general model adequately fits the data (Cooch and White, 2006). To accommodate for lack of fit, we needed a measure of how much extra binomial noise (variation) is in the data, which is known as the variance inflation factor or $\hat{c}$ (Cooch and White, 2006). The internal MARK program RELEASE assessed GOF for CJS model and consists of two important tests, Test 2 and 3. Test 2 deals with those animals known to be alive between time t and $t + 1$ and tests the assumption that all marked animals should be equally detectable at location $t + 1$ independent of whether or not they were captured at occasion t. Test 3 analyzes the assumption that all marked animals alive at t have the same probability of surviving to $t + 1$. If the resultant χ^2tests are significant, the assumptions are violated. Further, if the overall GOF test proves significant, it is necessary to assume the assumptions are violated. If the assumptions were violated, the Median-$\hat{c}$ procedure within MARK estimated the variance inflation factor and the models were adjusted accordingly. After adjustment or non-significant GOF, a series of reduced models were created: reduced survival and individual recapture ($\phi.p(t)$), individual survival and reduced recapture($\phi(t)p.$), reduced time and reduced recapture($\phi.p.$).

Following model creation, model selection starts with comparing AIC values and then computing likelihood ratio tests. Model selection is important as parsimony is desired. Therefore, models relating sample data and population parameters should contain enough parameters to account for all of the significant variation (Lebreton et al., 1992). An important tradeoff exists between the number of parameters in the model and sampling variance (Lebreton et al., 1992). The goal in model selection is to identify a biologically meaningful model that explains the variability in the data but excludes unnecessary parameters. The AIC is a measure of the relative quality of statistical models for a given set of data and provides a means for model selection. The lower the AIC, the more parsimonious the model (best fit with fewest parameters). However, the AIC value should not be the deciding factor, especially when hypothesis testing is available with other techniques. The likelihood ratio test compares a restricted model nested within the full model. If the likelihood ratio test is significant, there is evidence to suggest for variance in survival between stations. Once the final model was chosen, MARK provided estimates of critical survival (ϕ) and recapture (p) ratios.

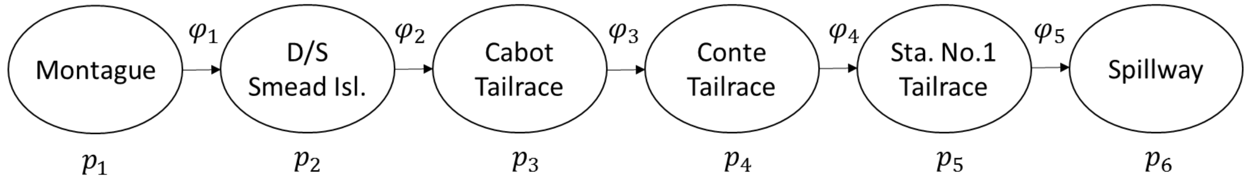

Figure C.4-1. Graphical schematic of the CJS model to assess the arrival rate of fish at the Turners Falls spillway having been recaptured at Montague. Survival probabilities (φ_i) are assessed between stations while recapture rates (p_i) are measured at a station.

C.5 Time-to-Event Analysis

A multi-state model is used to understand situations where a tagged animal transitions from one state to the next (Therneau, Crowson, & Atkinson, 2016). A standard survival curve (Kaplan-Meier) can be thought of as a simple multi-state model with two states (alive and dead) and one transition between those two states (Therneau, Crowson, & Atkinson, 2016). For the purpose of this assessment, these two states are staging and passing. Competing risks generalize the standard survival analysis of a single endpoint (as described above) into an investigation of multiple first event types (Beyersmann, Allignol, & Schumacher, 2011). Competing risks are the simplest multi-state model, where events are envisioned as transitions between states (Beyersmann, Allignol, & Schumacher, 2011). For competing risks, there is a common initial state for all models (Beyersmann, Allignol, & Schumacher, 2011). For example, with the assessment of time to move either upstream or downstream of the ultrasound array, the common initial state is within the array. When fish move upstream or downstream of the array, they enter an absorbing state. The baseline hazard is measured with the Nelson-Aalen cause specific cumulative incidence function. One can think of the hazard as the probability of experiencing an event (passage) within the next time unit conditional on still being in the initial state (Beyersmann, Allignol, & Schumacher, 2011). The Nelson-Aalen ($\hat{A}(t)$ is computed with (Beyersmann, Allignol, & Schumacher, 2011):

$$\hat{A}(t) = \sum_{k=1}^{K} \frac{number\ of\ individuals\ observed\ to\ transition\ into\ state\ i\ at\ t_k}{number\ of\ individuals\ at\ risk\ just\ prior\ to\ t_k}$$

Where t is a time of interest, K is the number of event times for fish entering state i, and k is an event (duration an animal took to transition from the array into a passing state). This formula is simple, it counts the number of individuals to experience the event of interest (i.e., movement upstream from within the array) at t_k divided by the number of individuals still in the array just prior to t_k. The sum term simply adds the probability across all discrete event times K. Therefore, the end probability is the probability of an animal traversing from the array into an absorbing state i. If we lose track of an animal, it is not censored at its last event time, rather it enters an unknown state. By attributing each tagged animal to a state at all times, we are ensured our final probabilities match empirical expectations. In other words, if 50 out of 100 animals transitioned upstream of the array, and 25 of 100 animals transitioned downstream, and we lost track of 25 animals, the Nelson-Aalen cumulative incidence estimators will result in 50% transitioning upstream of the array, 25% transitioning downstream of the array, and 25% within a state-unknown at the final event time. Animals are only censored if they are still being tracked within the array until the end of study. If we happen to lose track of a fish before the end of the study, they enter an unknown state. After computing the Nelson-Aalen estimators for each route of passage (competing event) and plotting the survival function (Kaplan-Meier) for those fish still remaining in the tailrace, we generated the probability of being in a state (across all times) while summing to 1.0.

Following the computation of cause-specific Nelson-Aalen estimators, an assessment of delay was carried out with Cox Proportional Hazards regression analysis for each separate event. Therneau, Crowson, & Atkinson (2016) state that a common mistake with competing risks is to use the Kaplan-Meier separately on each event type while treating other event types as censored. When this occurs, the probability of transitioning into the absorbing state of interest is positively biased, and the reason why competing risk curves may sum to less than 1.0. When analyzed in the frameowrk proposed by Therneau, Crowson, and Atkinson (2016), each separate Cox model ignores the other absorbing events and assesses the cause-specific transition. Here, rates depend only on the set of subjects who are at risk (fish in staging state) at a given moment. The Cox models for a competing risk assessment were fit in a procedure analogous to multiple regression modeling, where individual time-dependent covariates were added in an iterative fashion constructing ever more complex models. Model quality was assessed with the omnibus likelihood ratio test statistic, the null hypothesis of which states that the model is not better than chance. If this statistic is rejected at the $\alpha = 0.05$ level, then the model is considered to be better than chance, and we observe the estimated hazard ratio associated with the covariate of interest and its significance. If the covariate is significant at the $\alpha = 0.05$ level, then we conclude that the estimated hazard ratio is significant, and interpret the results. When the hazard ratio is greater than 1, a unit increase in the covariate (i.e., flow) would increase the instantaneous risk (or hazard) of the event occurring and delay is reduced. If for example, the model described attraction towards a ladder with a time varying covariate of flow and the hazard ratio greater than 1.0, then the risk of the event occurring (passage towards the ladder) increases with a unit increase in flow as compared to baseline. One would conclude that the population appears to experience less delay as flow is increased. If the hazard ratio is less than 1.0, then the instantaneous risk decreases, and the proportion of fish that have passed into the structure at time (t) decreases, thus delay is incurred. The "best" model minimized AIC scores and/or had a significant omnibus statistic ($p < 0.05$) and informative hazard estimate ($HR \neq 1.0$).

FirstLight diagnosed the fit of the CoxPH models by testing for the proportional hazard assumption using the R software Survminer. If the p-value of Schoenfeld Individual test was less than 0.05, the proportional hazards assumption was not met. If the test statistic comes back significant, a model was built where the covariate of interest interacts with time.

C.6 Treatment of Time-Series Data

At each event time, Cox Proportional Hazard (CoxPH) regression compares the current covariate values of a subject who had an event, to the current values of all others who were at risk at that time (Therneau, Crowson, & Atkinson, 2017). The event in question being movement from one location to another, and the number at risk being the number of fish remaining at the original location when the movement in question occurs. One of the drawbacks of CoxPH is that it regresses on the value of the covariate of interest immediately before an event occurs, and we are forced to assume that this was the value that affected movement. However, a fish that has been in the Cabot Station tailrace for a few hours, or in the river for a few weeks, has likely experienced a range of flows and conditions that will also affect movement. This information is lost if we only regress on the level of the covariate in the instant before an animal moves. Therefore, FirstLight also derived a number of statistics that incorporated greater amounts of information from time series data (flow, temperature, etc.) with moving window averages.

A rolling or moving average analyzes time series data by creating a series of averages at different subsets of the full timeseries. Rolling averages simply look behind the current time stamped measurement for a certain length of time. FirstLight chose window lengths that were biologically meaningful for migrating shad (1 hour, 2 hours, 5 hours and 24 hours). FirstLight also calculated the rolling variance, or volatility at these same window lengths. Volatility is a key variable, it either describes the short term or long-term variance (depending on window length) in flow. If volatility is high, the river is unsettled and is indicative of changing flows due to a rain storm or operations. Changing river conditions in the short term may cue fish to migrate, while long term variability may inhibit movement. We also calculated the cumulative average and variance, which described the average flow conditions experienced by a migrating shad while present at a location before moving. These variables were incorporated into the CoxPH models just like other time dependent covariates and provided new insight into reasoning behind shad movement in the Connecticut River.

FirstLight also developed metrics that incorporated the change in flow over a fish's presence. After enumerating bouts, FirstLight matched the start and end times of a presence with their nearest 15-minute flow reading and calculated the change in flow over a presence (dQ), the absolute change in flow over a presence ($|dQ|$), and the rate of change in flow over a presence (dQ/dt). These flow variables, along with instantaneous gage readings, cumulative averages and variances over presences, and rolling averages and volatilities were used to assess the effect of flow and flow variability on the movement of American Shad within the Connecticut River.

APPENDIX D – DATA REDUCTION

APPENDIX D DATA REDUCTION

TABLE OF CONTENTS

LIST OF TABLES

LIST OF FIGURES

D DATA REDUCTION INTRODUCTION

Data analysis was made complicated by the presence of false positives and receivers with overlapping detection zones. The following sections describe the results of FirstLight's efforts to identify and remove false positive detections, validate training data, and to remove overlapping detections with an algorithm inspired by nested Russian Dolls.

D.1 False positive reduction algorithm results

FirstLight's false positive reduction algorithm trained data with known classifications using four beacon tags placed at strategic locations throughout the 2018 study area (Figure D.1-1). These beacon tags provided the algorithm with information on what known true detections looks like, while detections from tags not in our study tag list provided information on what known false positive detections looked like. The resulting training data consisted of 735,910 detections, with 691,362 known classifications at eight Orion receivers, and 44,548 known classifications at five Lotek SRX 800 receivers. The breakdown of the number of known true and false positive detections by receiver is provided in Table D.1-1 and the breakdown of known classifications at Lotek receivers in Table D.1-2.

FirstLight also classified Orion detections from receivers at Holyoke in an attempt to identify fall back fish and those fish making a successful emigration out of the system. Table D.1-1 contains the number of detections classified as false positive and true positive across all Orion receivers. Note that upon examination, a majority of false positive detections at the Cabot tailrace area antennas (T04, T05, T06, T08, T09) and Holyoke antennas (T02Hol, T03Hol and T08Hol) were mortalities. Also noteworthy is the number of true positive detections at the entrance to the bypass reach (T09). This receiver had the single most detections out of any other receiver in the study suggesting that a majority of the fish are recaptured in the entrance to the bypass. However, relatively few true positive detections were recorded at the spillway (T12, and T13 on Table D.1-1) suggesting that a majority of fish may enter the bypass reach, but are not successful in their migration attempts.

When aggregated and displayed with histograms, the training data collected at Orion and Lotek receivers provided information on known true and false positive detection classes. An examination of histograms across known classes of detections showed excellent discriminatory powers. Known true positive detections had a much higher hit ratio (Figure D.1-1) and consecutive hit length (Figure D.1-2) than known false positive detections, suggesting that true positive detections will have detections histories primarily consisting of 1s. Known true positive detections had a slightly higher power reading than known false positive detections (Figure D.1-3). Known true positive detections also had a much lower rate of change in lag between detections (Figure D.1-4), suggesting that true positive detections will show a steady pattern of tag pulses indicative of a metronome.

Following the training of Orion receivers, Kleinschmidt also trained the Lotek SRX800 receivers. The prior probability that a detection at a Lotek SRX800 receiver as false positive was higher than Orion's at 13.8%. Due to frequency shifting of Lotek SRX800 receivers, hit ratio (Figure D.1-5) and consecutive record length (Figure D.1-6) were not as high for known true positive detections, and consequently did not provide as good as a discriminatory predictor for Lotek receivers. However, signal power (Figure D.1-7) and lag rate (Figure D.1-8) did.

Table D.1-1: The number of known true positive detections from beacon tags and the number of known false positive detections from frequency and codes not in the study tag list at all Orion receivers

Receiver	Number of Known False Positive Detections	Number of Known True Detections (beacon tag hits)
T01	15	923
T03O	39	96,147
T04	1,365	122,544
T05	1,879	183,174
T06	613	0
T08	0	125
T09	5,755	278,624
T12	1	158

Table D.1-2: The number of known true positive detections from beacon tags and the number of known false positive detections from frequency and codes not in the study tag list at all Lotek receivers

Receiver	Number of Known False Positive Detections	Number of Known True Detections (beacon tag hits)
T02	990	285
T03L	4,043	36,585
T07	870	1,317
T10	6	204
T13	228	20

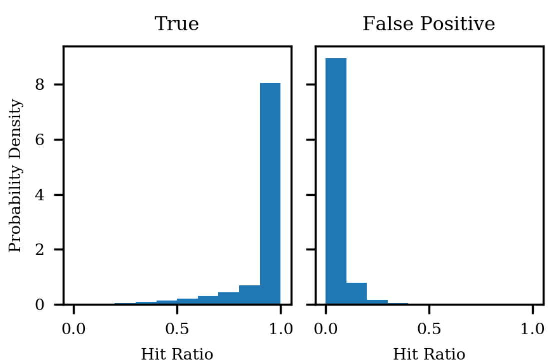

Figure D.1-1: Comparison of hit ratio histograms between detections with known classifications at Orion receivers

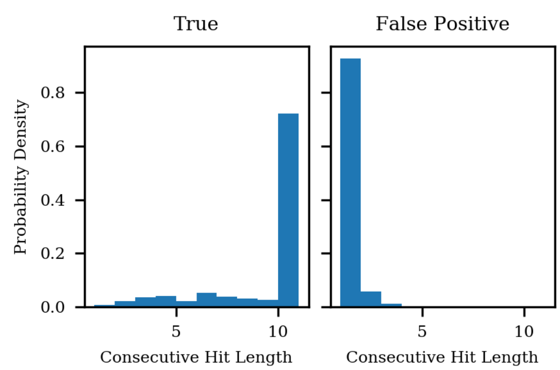

Figure D.1-2: Comparison of the consecutive hit length between detections with known classifications at Orion receivers

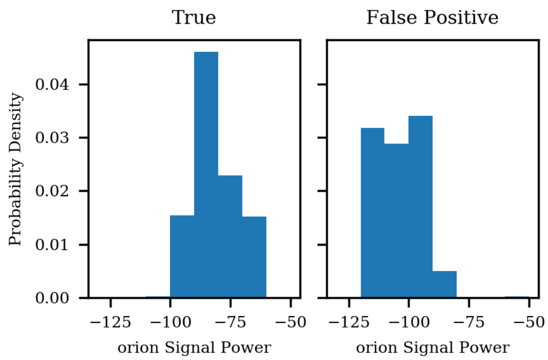

Figure D.1-3: Comparison of signal power between detections within known classifications at Orion receivers.

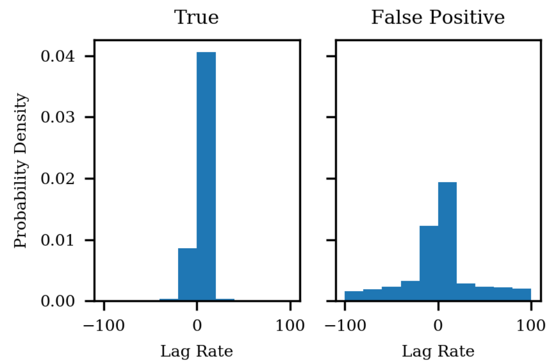

Figure D.1-4: Comparison of signal power between detections with known classifications at Orion receivers

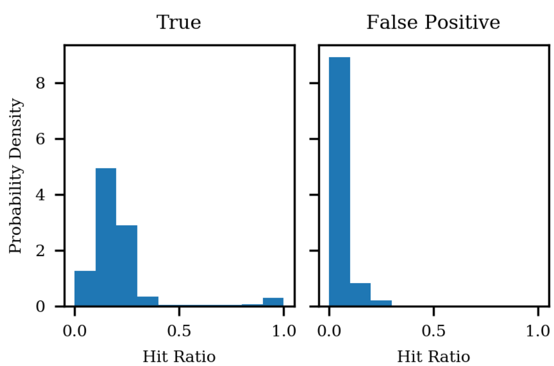

Figure D.1-5: Comparison of hit ratio between detections with known classifications at Lotek SRX800 receivers.

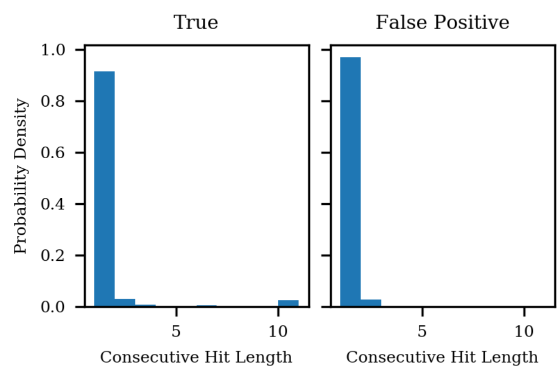

Figure D.1-6: Comparison of consecutive hit length between detections with known classifications at Lotek receivers.

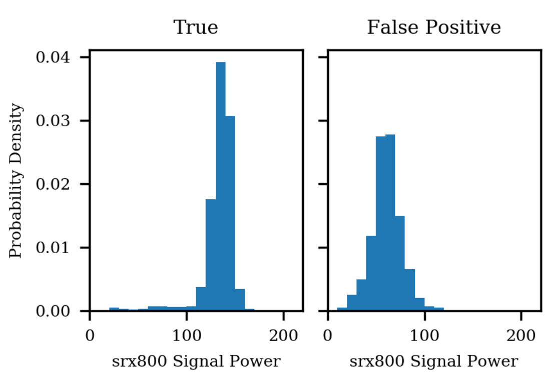

Figure D.1-7: Comparison of signal power between detections with known classifications at Lotek receivers.

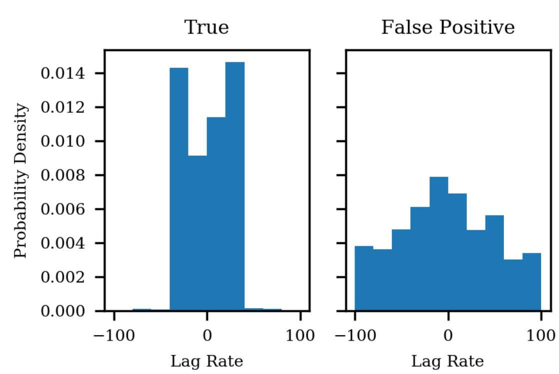

Figure D.1-8: Comparison of lag rate between detections with known classifications at Lotek receivers.

D.2 K-fold Cross Validation

Prior to classification, FirstLight assessed the accuracy of the Naïve Bayes false positive detection algorithm with a k-fold cross validation procedure using consecutive record length, hit ratio, power, and lag rate as predictor variables. The cross-validation results for Lotek SRX 800 receivers (Table D.2-1) showed few false negatives; however, it still allowed in some false positives. The positive predictive value and negative predictive value were very high at 95.3% and 99.8%, respectively. These statistics calculate the probability that a record classified as true or false was correct. FirstLight also conducted a k-fold cross validation procedure on the Orion receivers using consecutive hit length, hit ratio, power, and lag rate as predictors. The cross-validation table displayed a moderate number of misclassifications (Table D.2-2).

The sensitivity of the SRX 800 classifier was very high at 99.9% suggesting that known true positive detections were nearly always classified as true. The specificity of Lotek SRX 800 receivers was lower at only 70%, suggesting that false positive detections are being incorrectly classified as true. Given these results, and the low hit ratios associated with frequency switching receivers, a hard hit-ratio filter of 0.30 was applied to Lotek data.

The relative proportion of misclassified data to correctly classified data for Orion receivers was much smaller than Lotek receivers. The positive predictive value was very high again (99.9%); however, the negative predictive value was a little lower for Orions than it was for Loteks at 89%. This suggests that the algorithm will produce more false negatives for Orion receivers than Loteks making it stricter. For Orions's, the negative predictive value was lower, but the specificity was much higher at 91%. While the specificity was higher, we still felt a hard filter of 0.30 applied to hit ratios was warranted.

Table D.2-1: Cross validation results for Lotek SRX 800 receivers

	Classified False	Classified True
Known False	3,876	1,699
Known True	8	34,510

Table D.2-2: Cross validation results for Orion receivers

	Classified False	Classified True
Known False	7,918	778
Known True	982	612,548

D.3 False Positive Classification

Following data training and cross validation, FirstLight proceeded to false positive identification and removal. There were 5,608,301 detections from study tags at Orion receivers, and the probability that a detection from a study tag was classified as true was 71%. The algorithmic removal of false positive detections from Lotek receivers proved successful as well. In total, Lotek receivers generated 1,285,868 study tag detections, and the algorithm classified 91.7% as true positive detections.

An examination of the predictor variable histograms showed significant discrepancy between classified true and false positive detections. In other words, the false positive detection algorithm was able to correctly discriminate the two types of detection classes. Figure D.3-1 shows a comparison of hit ratios between detections classified as true and false positive. Overwhelmingly, those detections classified as false had lower hit ratios and lower consecutive hit lengths (Figure D.3-2). This suggests that detection histories from false positive detections are very sparse. Interestingly, there was not much difference between signal strength (Figure D.3-3). The histogram for lag rate shows minor differences between true and false detections. False positive detections appear to have a larger rate of change in lag between detections. In other words, signals from true positive detections were stable, while signals from false positive detections came in at lags that were large and random, or volatile.

The breakdown of the number of false positive and true positive detections for Orion and Lotek is found in Tables D.3-1and D.3-2. As with Orion receivers, false positive detections overwhelmingly had lower hit ratios (Figure D.3-4) and consecutive record lengths (Figure D.3-5). Interestingly, false positive detections had a higher signal power than true positive detections (Figure D.3-6). Figure D.3-7shows a comparison of lag rates between true and false positive detections. False positives exhibited large and random lags, and their histories did not appear as steady stream pulses. Following false positive removal, we proceeded to the overlap removal phase, which required the enumeration of bouts and bout criteria and an implementation of Kleinschmidt's Russian Doll algorithm.

Table D.3-1: Counts of the number of false positive and true detections by Orion receivers

Receiver	False Positive	True
T01	1,623	16,800
T02Hol	73,216	111,466
T03Hol	109,318	150,030
T03O	4,593	33,796
T04	415,764	429,472
T05	452,848	675,626
T06	48,816	26,638
T08	5,492	14,214
T09	280,000	1,851,811
T09Hol	89	334
T10Hol	26	1,421
T12	173	49

Table D.3-2: Count of the number of false positive and true detections by Lotek receivers

Receiver	Classified False	Classified True
T02	30,109	533,044
T03L	13,728	91,729
T07	49,116	332,625
T10	655	98,254
T11	176	6,300
T13	13,392	116,740

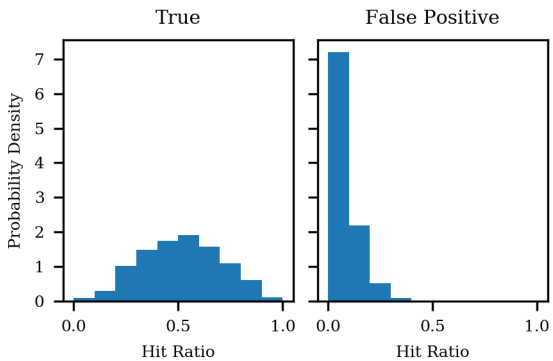

Figure D.3-1: Comparison of hit ratios between classified study tag detections at Orion receivers.

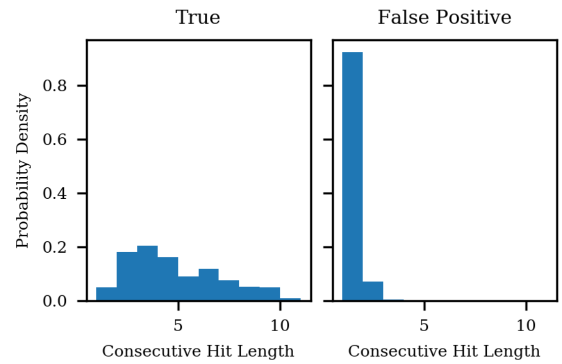

Figure D.3-2: Comparison of consecutive hit lengths between classified detections at Orion receivers.

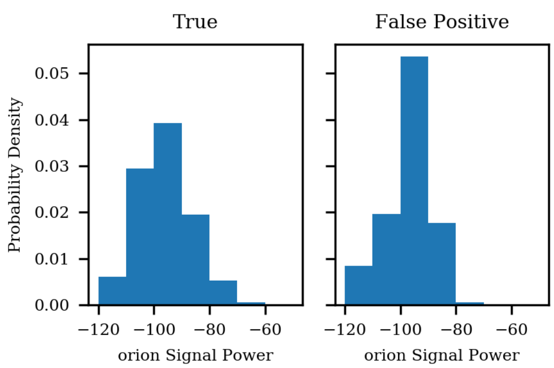

Figure D.3-3: Comparison of signal power between classified detections at Orion receivers.

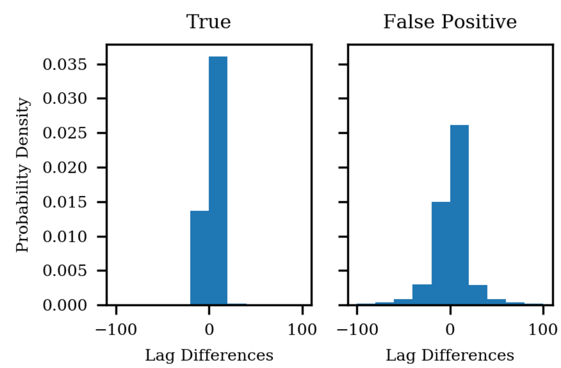

Figure D.3-4: Comparison of lag rate between classified detections at Orion receivers.

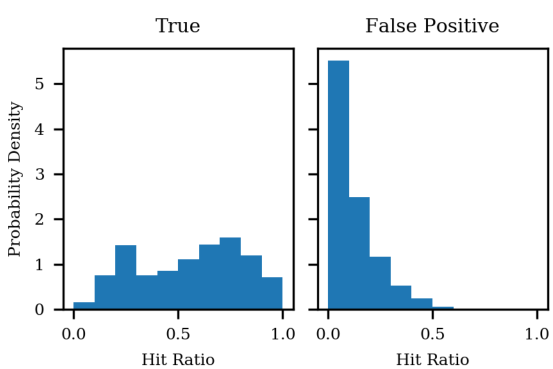

Figure D.3-5: Comparison of hit ratios across true and false positive detections at Lotek receivers.

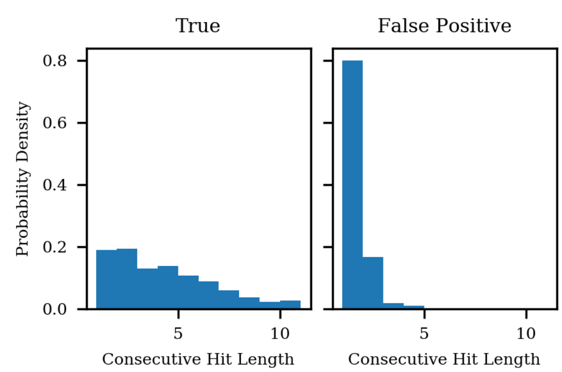

Figure D.3-6: Comparison of consecutive hit lengths across true and false positive detections at Lotek receivers.

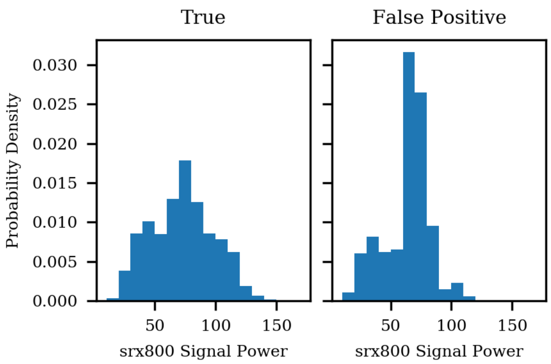

Figure D.3-7: Comparison of signal power across true and false positive detections at Lotek receivers.

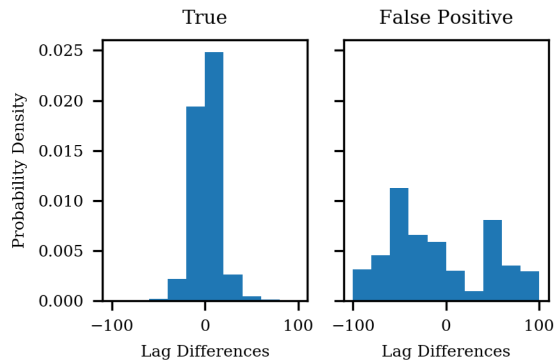

Figure D.3-8: Comparison of lag rates between true and false positive detections at Lotek receivers.

D.4 Overlap Removal

Due to the nature of questions asked, FirstLight's radio telemetry network was complex and exhibited significant overlap. Overlap removal consisted of two steps: deriving bout criteria and implementing a novel algorithm inspired by a nested-Russian Doll. Table D.4-1contains the bout length for each network node. Note that some of the longest residency times were within the Cabot Station tailrace area (Farfield to Nearfield).. The broken-stick model for each telemetry network node is provided in Figures D.4-1 – D.4-12. Following completion of bout criteria, FirstLight applied the Russian Doll algorithm to all true positive records with a hit ratio greater than 0.30. In total, there were 3,419,704 true positive detections with a hit ratio greater than 0.30. Of those records, 421,090 were removed because they were overlapping.

Table D.4-1: Bout length criteria for each telemetry node

Network Node	Reach Location	Bout Length (s)
S01	Montague	1490
S02	Deerfield River	90
S03	Smead Island West	160
S04	Smead Island East	460
S05	Cabot Farfield	820
S06	Cabot Tailrace	920
S07	Cabot Nearfield	630
S08	Cabot Ladder	380
S09	Bypass Entrance	810
S10	D/S Station No. 1	310
S11	U/S Station No. 1	140
S12	Spillway	810

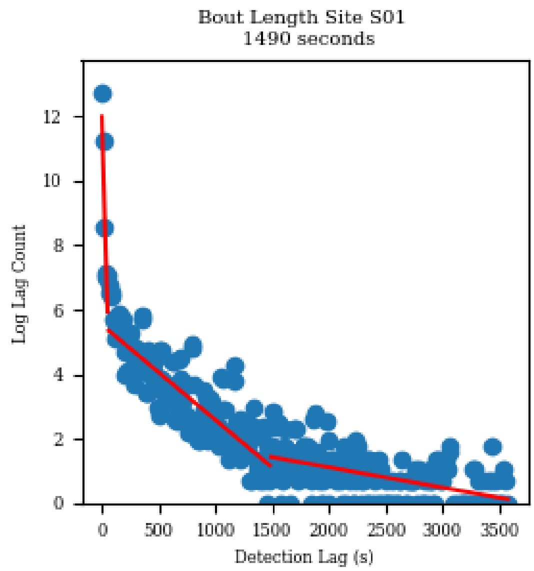

Figure D.4-1: Best fit broken-stick model for telemetry node S01 at Montague (T02). A lag of 1490 seconds or more indicates a new presence.

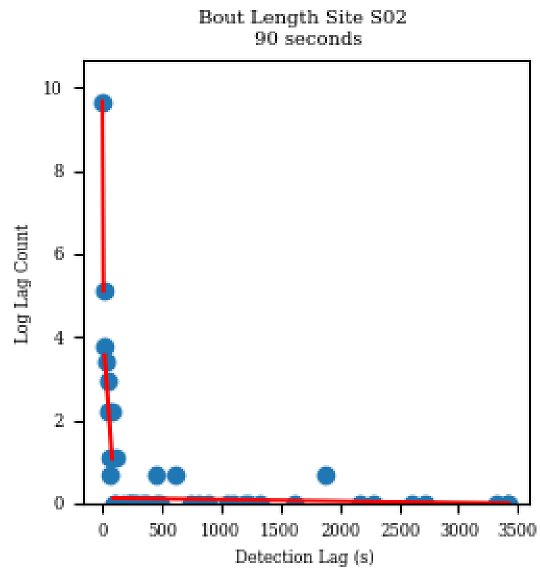

Figure D.4-2: Best fit broken-stick model for telemetry node S02 at Deerfield (T01). A lag of only 90 seconds or more indicates a new presence.

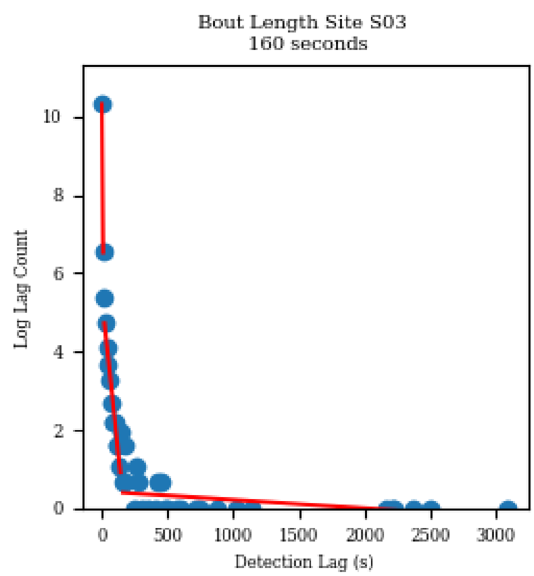

Figure D.4-3: Best fit broken-stick model for telemetry node S03 at Smead Island West (T03O). A lag of 160 seconds or more indicates a new presence.

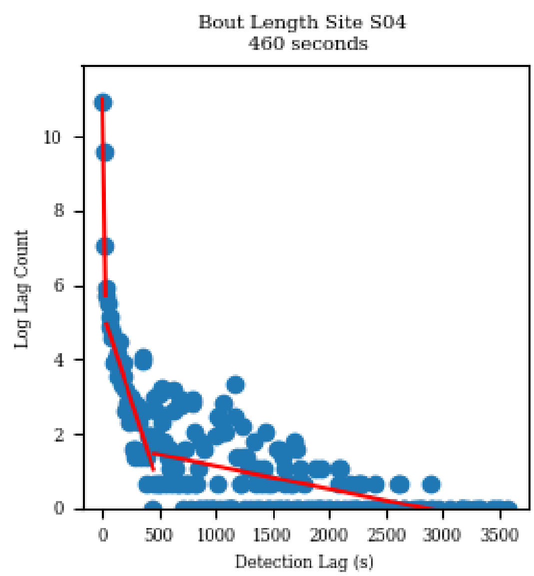

Figure D.4-4: Best fit broken-stick model for telemetry node S04 at Smead Island East (T03L). A lag of 460 seconds or more indicates a new presence.

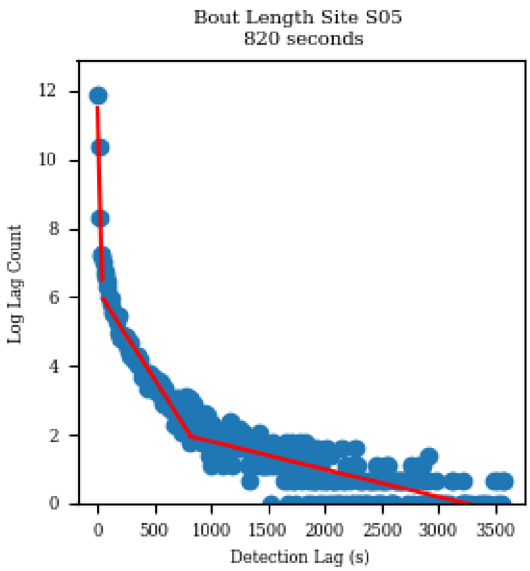

Figure D.4-5: Best fit broken-stick model for telemetry node S05 at Cabot Farfield (T07). A lag of 820 seconds or more indicates a new presence.

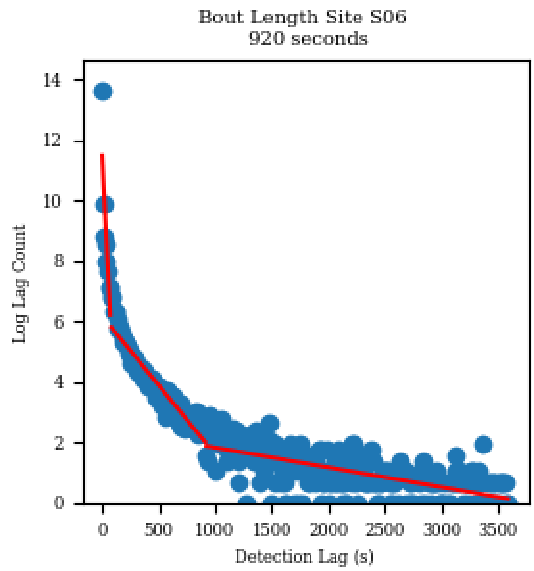

Figure D.4-6: Best fit broken-stick model for telemetry node S06 at Cabot Tailrace (T04, T05). A lag of 920 seconds or more indicates a new presence.

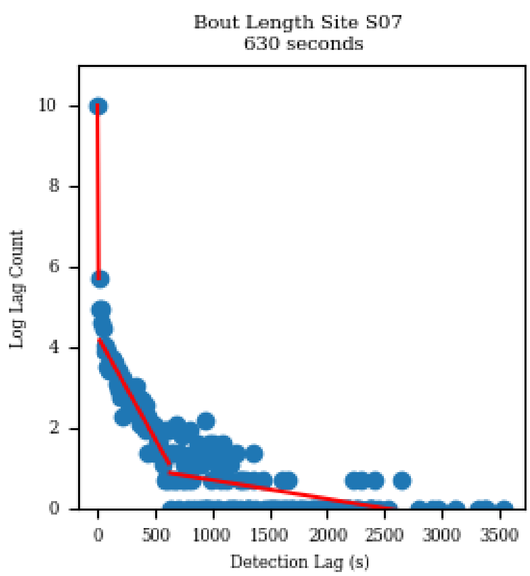

Figure D.4-7: Best fit broken-stick model for telemetry node S07 at Cabot Nearfield (T06). A lag of 630 seconds or more indicates a new presence.

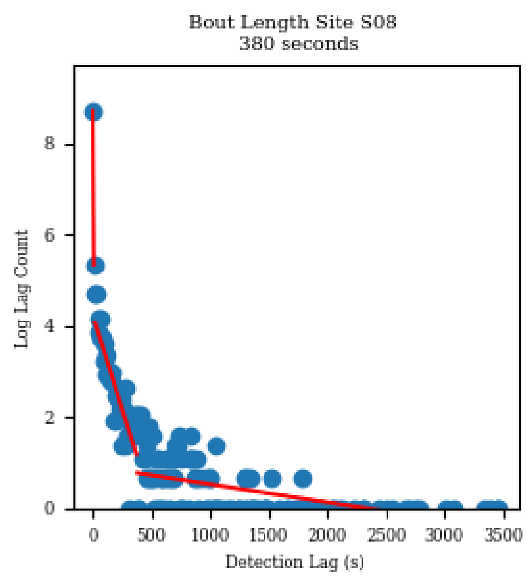

Figure D.4-8: Best fit broken-stick model for telemetry node S08 at Cabot Ladder (T07). A lag of 380 seconds or more indicates a new presence.

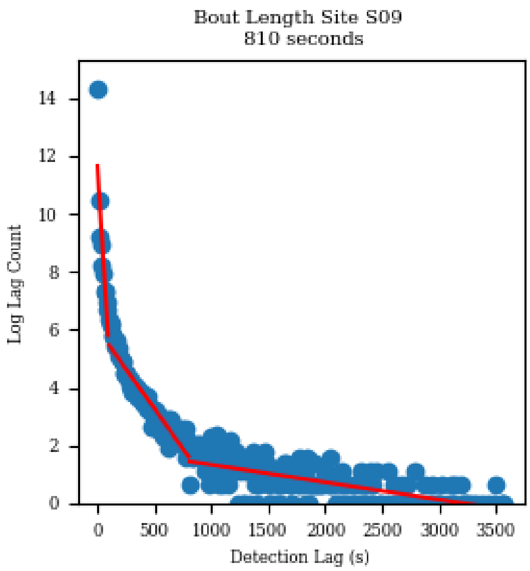

Figure D.4-9: Best fit broken-stick model for telemetry node S09 at the Conte Discharge/Bypass entrance (T09). A lag of 810 seconds or more indicates a new presence.

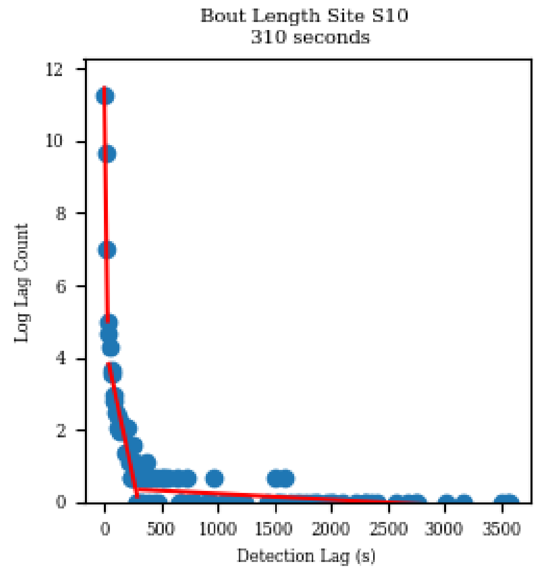

Figure D.4-10: Best fit broken-stick model for telemetry node S10 at D/S Sta. No.1 (T10). A lag of 310 seconds or more indicates a new presence.

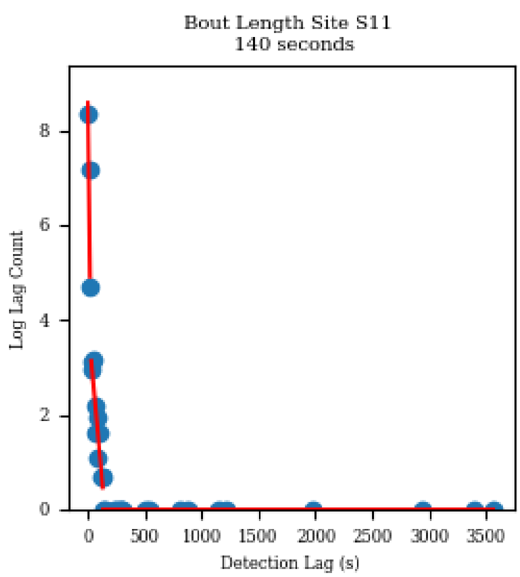

Figure D.4-11: Best fit broken-stick model for telemetry node S11 at U/S Sta. No.1 (T11). A lag of 140 seconds or more indicates a new presence.

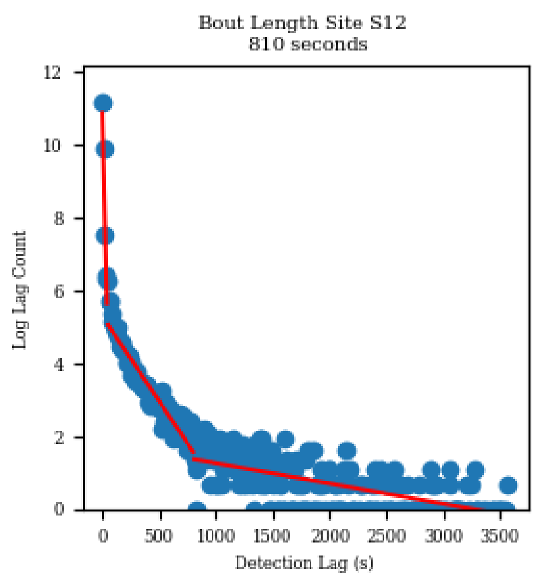

Figure D.4-12: Best fit broken-stick model for telemetry node S12 at Turners Falls Spillway (T13). A lag of 810 seconds or more indicates a new presence.

APPENDIX E – BYPASS MOVEMENT ANALYSIS

APPENDIX E BYPASS MOVEMENT

TABLE OF CONTENTS

LIST OF TABLES

LIST OF FIGURES

E. THREE YEARS OF BYPASS MONITORING, WHAT HAVE WE LEARNED?

Utilizing radio telemetry techniques, FirstLight tracked the movements of American Shad within the bypass reach in 2015, 2016 and 2018. In each year, approximately only 20 – 30% of the test fish that arrived at the Project continued to the Turners Falls Dam (TFD) spillway. The following analysis investigates potential reasons for these low arrival rates. In 2018, FirstLight identified a bottleneck between the entrance of the bypass reach at Conte discharge (i.e., the discharge from the USGS's S.O. Conte Anadromous Fish Research Laboratory) and the Station No. 1 tailrace, with only 43% of the test fish successfully migrating through this reach. Analysis of movement within the bypass reach was plagued with low samples sizes in 2015 and 2016, which prohibited a robust statistical assessment of movement in those years. To overcome these shortfalls, FirstLight aggregated telemetry data from each year into an overall bypass movement dataset.

E.1 Aggregate Bypass Movement

Fish arriving at the Conte discharge have two options: continue their upstream migration to the TFD spillway or return downstream to the Cabot Station tailrace area or anywhere else downstream. In 2015, 20 of 54 fish (38%) made 23 movements to the spillway area (Table E-1.1); in 2016, 11 of 28 (39%) fish made 11 movements to the spillway from the bypass reach (Table E-1.2); and in 2018, 30 of 85 (35%) fish made 38 movements towards the spillway (Table E-1.3). These results are comparable with the 2018 Cormack Jolly Seber (CJS) model, which concluded that there is a 35% chance that a fish recaptured at the entrance to the bypass reach will arrive at the TFD spillway. FirstLight aggregated recapture data from three years of research to improve statistical assessments of movement.

The Nelson-Aalen cumulative incidence plot (Figure E.1-1) shows around 35% of the movements from the Conte discharge were directed towards the spillway within 200 hours of arriving in the bypass reach. This estimate aligns with the CJS model, and analytical estimates obtained for 2015 (Table E.1-1), 2016 (Table E.1-2) and 2018 (Table E.1-3). No other fish transitioned from the lower bypass to the Turners Falls spillway faster than 2.25 hours. Transit times (Table E.1-4) shows the median travel time to the spillway area as 14.4 hours.

A series of Cox Proportional Hazards (CoxPH) regression models were fit to event times in the bypass reach to see how project operations affects movement within the bypass reach. The model that best described aggregated bypass movement (Conte discharge to TFD spillway in 2015, 2016 and 2018; Table E.1-5) incorporated the cumulative average bypass discharge while present (kcfs or thousand cubic feet per second), the absolute change in bypass flow ($|dQ|$), and an interaction effect with cumulative average bypass discharge and day of year (1 – 365). The model was significant (LR = 0.005). An examination of the bypass flow conditions on transition to the spillway show that a majority of fish move when flow is greater than or equal to 4,000 cfs (Figure E.1-2). As the cumulative average flow while present increases by 1,000 cfs over the baseline, fish are nearly 7 times more likely to migrate to the spillway. The hazard ratio associated with a change in bypass flow of 1,000 cfs was 0.72, suggesting that fish are less likely to migrate to the spillway if flow is changing. Figure E.1-3 depicts movement durations as a function of absolute change in flow. Note that more variable flow while fish are present leads to longer event times. Interestingly, the interaction effect between average flow and day of year showed a decreasing effect of discharge later in the season. The hazard rate associated with a higher than average discharge and another day later in the season (HR = 0.99) suggests that fish are less likely to migrate to the spillway. In other words, there is diminishing returns with higher flow later in the season.

Table E.1-1: State table describing bypass movement in 2015

	Conte Tailrace	Turners Falls Spillway	Downstream
Conte Tailrace	n = 54	n = 20 m = 23 min = 1 med = 1 max = 2	n = 18 m = 26 min = 1 med = 1 max = 3
Turners Falls Spillway	n = 4 m = 4 min = 1 med = 1 max = 1	n = 20	n = 0 m = 0 min = 0 med = 0 max = 0
Downstream	n = 13 m = 20 min = 1 med = 1 max = 3	n = 1 m = 1 min = 1 med = 1 max = 1	n = 18

Table E.1-2: State table describing bypass movement in 2016

	Conte Tailrace	Turners Falls Spillway	Downstream
Conte Tailrace	n = 28	n = 11 m = 11 min = 1 med = 1 max = 1	n = 24 m = 30 min = 1 med = 11 max = 3
Turners Falls Spillway	n = 8 m = 8 min = 1 med = 1 max = 1	n = 13	n = 0 m = 0 min = 0 med = 0 max = 0
Downstream	n = 28 m = 34 min = 1 med = 1 max = 3	n = 2 m = 2 min = 1 med = 1 max = 1	n = 58

Table E.1-3: State table describing bypass movement in 2018

	Conte Tailrace	Turners Falls Spillway	Downstream
Conte Tailrace	n = 85	n = 30 m = 38 min = 1 med = 1 max = 4	n = 66 m = 152 min = 1 med = 2 max = 9
Turners Falls Spillway	n = 8 m = 8 min = 1 med = 1 max = 1	n = 30	n = 14 m = 20 min = 1 med = 1 max = 4
Downstream	n = 49 m = 121 min = 1 med = 2 max = 9	n = 0 m = 0 min = 0 med = 0 max = 0	n = 70

Table E.1-4: Time until movement in Bypass Reach (hours) aggregated (2015, 2016, 2018)

Destination	Min	25^{th}	Median	75^{th}	Max
Spillway	2.3	6.4	14.4	25.4	97.13
Downstream	<1	<1	6.1	2.7.4	733.1

Table E.1-5: CoxPH regression for bypass to spillway movements (cumulative analysis of 2015, 2016, and 2018)

Model Number	Covariates	AIC	Robust LR Test	HR	SE	p	(+/-)	Proportional Hazard Assumption
1	Tag year: 2016	604.79	0.45	0.97	0.44	0.95	(0.41,2.31)	0.60
	Tag year: 2018			1.37	0.28	0.35	(0.70,2.68)	0.007
2	Day of Year (1:365)	590.52	0.02	0.02	0.02	0.002	(0.91,0.98)	0.46
3	Bypass flow (kcfs)	601.21	0.10	1.15	0.08	0.09	(0.98,1.36)	0.25
4	Cumulative average flow while present (kcfs)	603.30	0.24	1.09	0.07	0.24	(0.94,1.26)	0.59
5	Absolute change in Bypass flow (kcfs) while present ($\|dQ\|$)	595.83	0.003	0.67	0.11	<0.001	(0.53,0.84)	0.62
6	Rate of change in Bypass flow (kcfs per second) (dQ/dt)	604.27	0.47	0.55	0.76	0.44	(0.12,2.48)	0.95
7	1 hour rolling average Bypass flow (kcfs)	601.70	0.09	1.14	0.07	0.08	(0.98,1.31)	0.42
8	1 hour rolling Bypass flow (kcfs) volatility	477.13	0.57	1.66	0.92	0.42	(0.49,5.66)	0.69
9	2 hour rolling average Bypass flow (kcfs)	601.87	0.10	1.13	0.08	0.09	(0.98,1.31)	0.41
10	2 hour rolling Bypass flow (kcfs) volatility	603.90	0.09	0.46	0.82	0.34	(0.09,2.30	0.09
11	5 hour rolling average Bypass flow (kcfs)	602.26	0.13	1.12	0.07	0.12	(0.97,1.30)	0.42
12	5 hour rolling Bypass flow (kcfs) volatility	603.49	0.18	0.61	0.60	0.40	(0.19,1.95)	0.84
13	24 hour rolling average Bypass flow (kcfs)	599.58	0.02	1.20	0.07	0.02	(1.03,1.39)	0.44
14	24 hour rolling Bypass flow (kcfs) volatility	603.19	0.14	0.91	0.06	0.12	(0.80,1.03)	0.94
15	Bypass Flow Recommendation (1,000 – 2,000 cfs)	597.82	0.006	0.24	1.27	0.26	(0.02,2.84)	0.87
	Bypass Flow Recommendation (2,000 – 4,500 cfs)			0.14	1.20	0.10	(0.01,1.45)	0.95
	Bypass Flow Recommendation (> 4,500 cfs)			0.35	1.20	0.38	(0.03,3.67)	0.98
16	Bypass Flow (3,000 – 6,000 cfs)	600.00	0.03	2.23	0.34	0.02	(1.14,4.38)	0.39
	Bypass Flow (6,000 – 9,000 cfs)			2.13	0.38	0.05	(1.00,4.52)	0.50
17	Cumulative average flow while present (kcfs)	583.97	0.005	6.92	0.50	<0.001	(2.62,18.31)	0.62
	Absolute change in Bypass flow (kcfs) while present ($\|dQ\|$)			0.72	0.12	0.006	(0.57,0.91)	0.34
	Day of Year:Cumulative average flow while present (kcfs)			0.99	0.003	<0.001	(0.98,0.99)	0.43

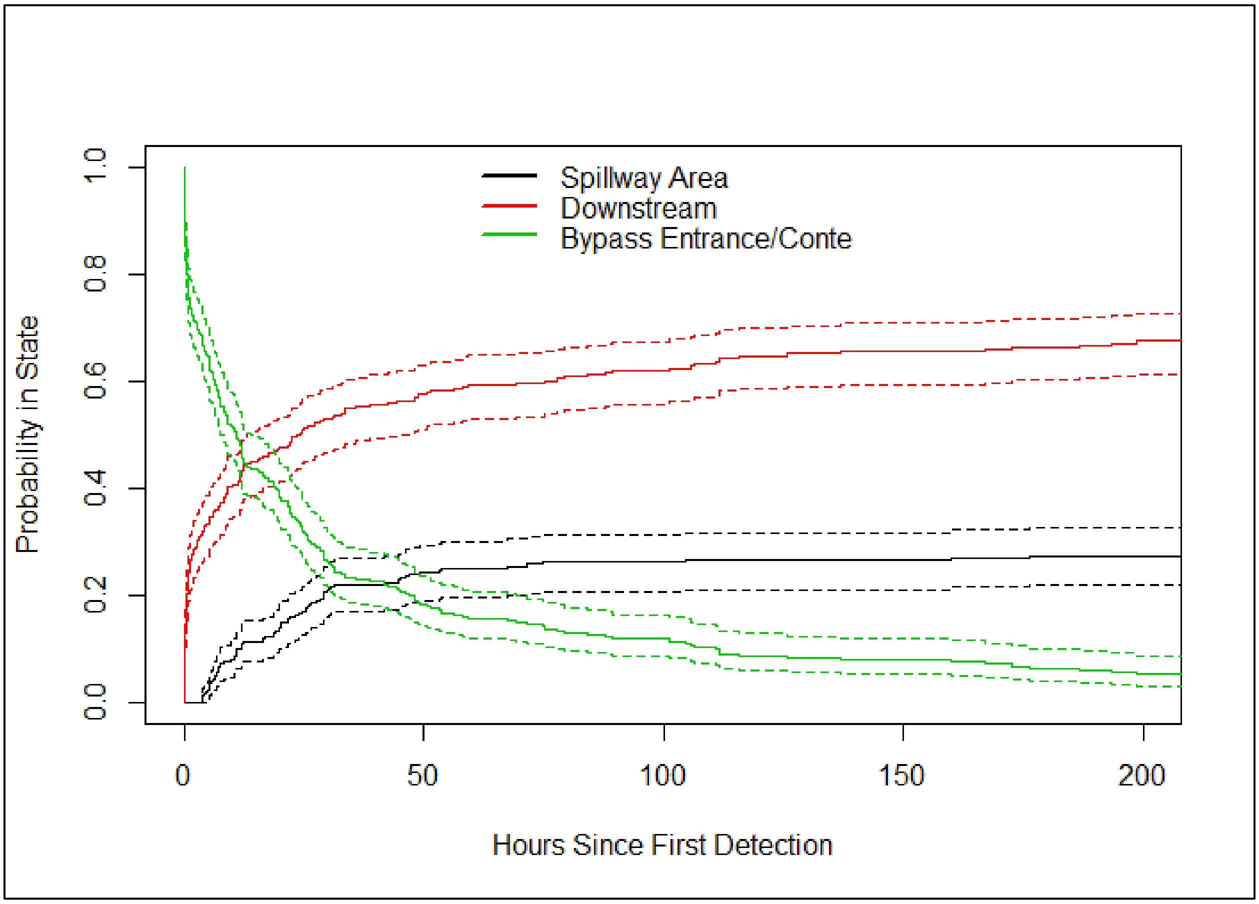

Figure E.1-1: Nelson-Aalen cumulative incidence plot of movement from the bypass reach. Fish can either move to the TFD spillway or return downstream.

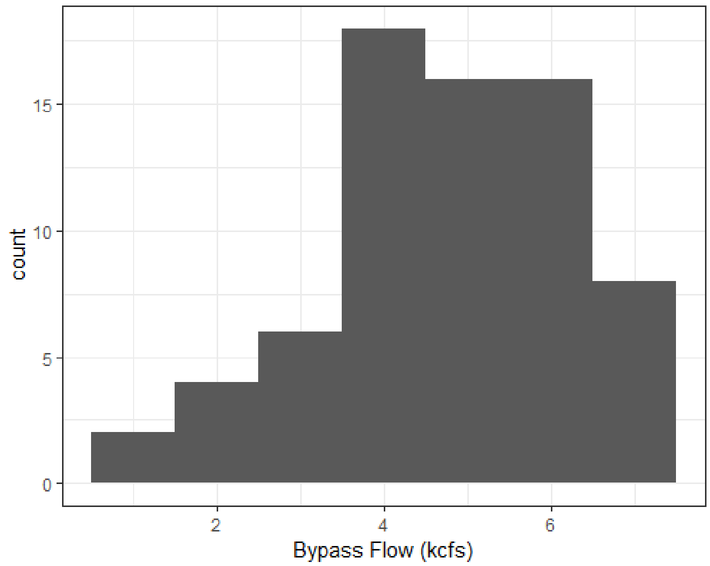

Figure E.1-2: Bypass flow conditions while fish transition into the area of the spillway

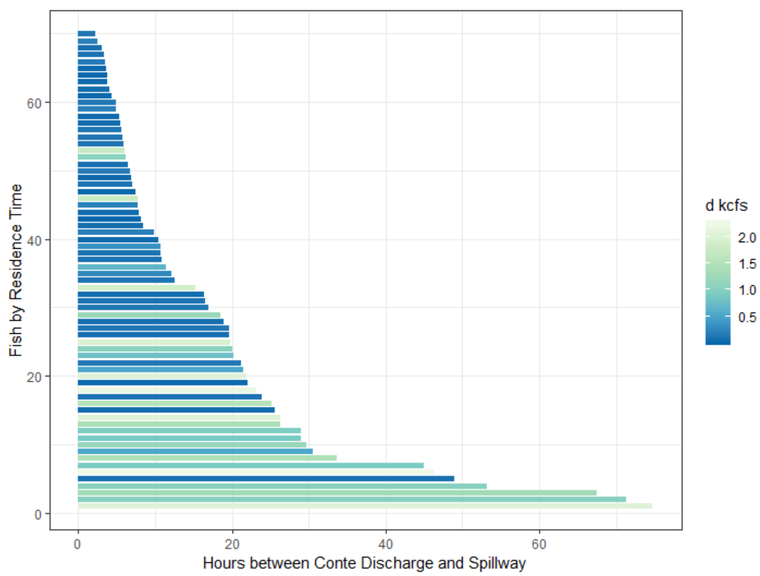

Figure E.1-3: Absolute change in bypass flow conditions while fish are present in relation to movement duration. Note longer durations are associated with variable bypass conditions.

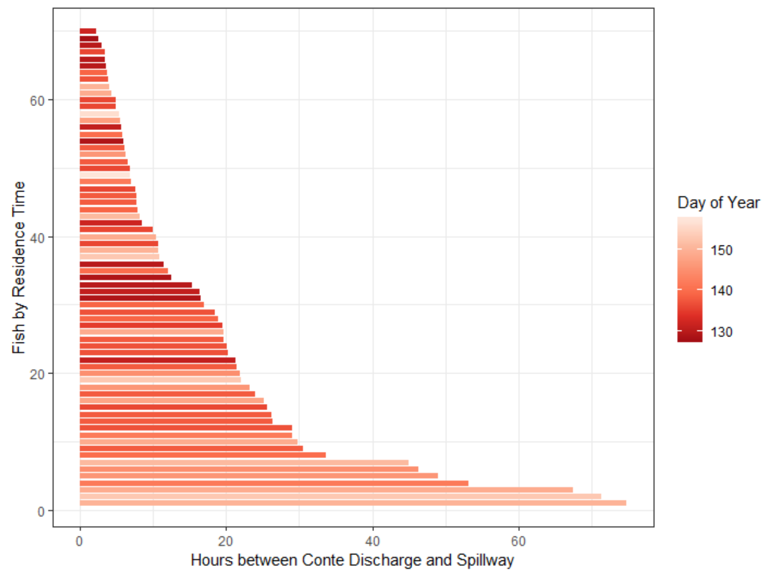

Figure E.1-4: The duration of movement by day of year (DOY). Note shorter durations were associated with transitions made earlier in the year while longer transitions occurred later in the year.

E.2 2018 Detailed Bypass Movement

In 2018, recapture at Station No. 1 was high enough to warrant a robust assessment of detailed movement within the bypass reach. We constructed a multi-state counting process dataset that described movement within the bypass reach where: State 1 was anything downstream of the bypass (including Cabot Station tailrace); State 2 was the entrance to the bypass reach at Conte discharge (T09); State 3 was recapture within the Station No. 1 tailrace (T10 and T11); and State 4 was recapture in the TFD spillway (T13). In total, 137 fish were recaptured downstream, 85 at the entrance to the bypass, 36 at Station No. 1, and 33 at the TFD spillway. Of the 85 fish to enter the bypass reach (with recapture at Conte discharge), only 36 were recaptured at Station No. 1 (36/85 = 42%). However, of the 36 fish at Station No. 1, 33 were recaptured at the spillway (33/36 = 92%), suggesting a bottleneck between the area of the Conte discharge and the Station No. 1 tailrace. These numbers were corroborated with a CJS live recapture model. Movement between states was enumerated with a state table (Table E.2-1). Movement into the bypass reach was high with 85 fish making 232 movements and 1 fish making as many as 9 movements into the bypass reach (Table E.2-1). However, once within the bypass reach, a majority of the fish returned downstream (68 fish made 173 movements back downstream). Of the 36 fish recaptured at the Station No. 1 discharge, 29 continued upstream and made 41 movements (Table E.2-1). However, once those fish were recaptured in the spillway, 23 returned back downstream. As with 2015, fish appear to have trouble finding the entrance to spillway ladder.

With greater rates of recapture at Station No. 1, we performed a robust assessment of movement within the bypass reach. Two competing risk models are presented: movement from Conte discharge, and movement from Station No. 1 tailrace. The median travel time from Conte discharge to the Station No.1 tailrace was 8.56 hours (Table E.2-1) while the median travel time from Station No.1 tailrace to the spillway was 5.62 hours (Table E.2-3). The Nelson-Aalen cumulative incidence plot for movement from Conte discharge shows a greater proportion of fish falling back downstream than arriving at Station No.1 tailrace (Figure E.2-1) while the same plot for movement from Station No.1 tailrace shows a greater proportion of movements from the tailrace arriving at the TF spillway than retreating downstream (Figure E.2-2). Figure E.2-2 shows approximately 60% of all movements from the Station No.1 result in fish arriving at the spillway. The CJS overall estimate of arrival from Station No.1 to the spillway was high at 96%, suggesting fish have multiple movement events from Station No.1, with back-and-forth movements in the upper bypass reach (Table E.2-1, rows 2, 3 and 4).

An examination of flow conditions while fish are present paints a dynamic picture of the bypass reach, with flow entering from both gaged and ungaged (modeled) locations. When fish are moving from the Conte discharge upstream towards the Station No.1 tailrace, they are experiencing combined flows from Station No.1 (discharge and leakage), Fall River, spillway ladder attraction, and spill at TFD (bascule gates 1 and 4). Figure E.2-3 depicts how flow conditions change as a fish moves to the Station No.1 tailrace. The color of the line represents the flow experienced and note that some fish experience more variable flow conditions than others, which may affect their movement rates. It appears that both the shortest and longest movement times coincided with lower Reach 2 discharges (Figure E.2-3). The Reach 2 time-series (Figure E.2-4) overlays the residence time on top of Reach 2 discharge. The line starts when a fish arrives at the Conte discharge and ends when it arrives at Station No. 1 tailrace. Note the contribution from Station No.1 is highlighted (red line). The difference between the Reach 2 flow and Station No.1 discharge is equal to the spill over TFD, spillway ladder attraction flow, Fall River flow, and leakage through Station No.1. Around May 21 an inflection occurred, where movement durations increased, and it appeared as though less fish experienced a movement event with time.

From Station No.1, a tagged fish can continue its migration to the TFD spillway, where they experience flow contributions from the Fall River, spill over TFD (bascule gates 1 and 4), and the spillway ladder attraction flow. Figure E.2-5 depicts the flow conditions experienced by a tagged fish while migrating between Station No. 1 and the TFD spillway. Note that the longest movement duration from Station No. 1 to the spillway is about half the longest duration from Conte to Station No. 1. The time series plot with overlaid transition histories (Figure E.2-6) shows the same inflection point at or around May 21 that is also present on Figure E.2-4, suggesting that migration events after this time occur less frequently and take longer to complete. If there is a vertical line drawn with vertices at the end points of the horizontal lines in Figure E.2-3 and Figure E.2-5, this approximates the profile of the Kaplan-Meier survival curves. For continuous variables, CoxPHs will regress on the value of the covariate in the instant before movement occurs. Thus, we experimented with moving and cumulative averages in 2018.

A series of CoxPH regression models were fit to Reach 2 flow to understand movement between the Conte discharge and Station No. 1 tailrace. While figures (Figures E.2-4 to Figure E.2-6) suggest that reach specific flow has an effect on movement rates within the bypass reach, the best model did not incorporate Reach 2 specific flow. Rather, the absolute change in flow while present and time of day in quarter day increments were the best predictors of movement within this reach. Fish were nearly 3 times more likely to move to the Station No. 1 tailrace during the late morning hours (0600 – 1200) than at any other time of day. Like the overall bypass movement model, fish prefer stable flows. As absolute change in flow increases by 1,000 cfs, fish are only 0.62 times as likely to move towards Station No. 1. For migration from Station No. 1 tailrace to the TFD spillway, no model was significant. The only marginally significant model (LR = 0.08) contained the median range 5-hour volatility. More volatile flow within the past 5 hours (nearly half the duration of the median transition time from the tailrace to spillway) increases the likelihood fish will transition.

Table E.2-1: State table describing movements between states within the bypass reach where n is the number of fish within and making a movement from a state; m is the total number of times fish made a specific movement; and min, med and max describe the expected number of movements a fish will make.

	Downstream	**Conte Discharge**	**Sta. No. 1**	**Spillway**
Downstream	n = 137	n = 85 m = 232 min = 1 med = 2 max = 9	n = 1 m = 1 min = 1 med = 1 max = 1	n = 0 m = 0 min = 0 med = 0 max = 0
Conte Discharge	n = 68 m = 173 min = 1 med = 2 max = 9	n = 85	n = 33 m = 47 min = 1 med = 1 max = 5	n = 5 m =6 min = 1 med = 1 max = 2
Station No. 1	n = 17 m = 23 min = 1 med = 1 max = 4	n = 9 m = 13 min = 1 med = 1 max = 5	n = 36	n = 29 m = 41 min = 1 med = 1 max = 6
Spillway	n = 2 m = 3 min = 1 med = 1.5 max = 2	n = 1 m = 1 min = 1 med = 1 max = 6	n = 23 m = 34 min = 1 med = 1 max = 1	n = 33

Table E.2-2: Time until movement from Conte discharge in decimal hours

Destination	0%	25%	50%	75%	100%
Station No. 1	0.005	2.74	8.56	17.55	118.26
Spillway	6.78	12.05	22.37	28.34	69.99
Downstream	0.008	0.34	1.93	1.95	468.69

Table E.2-3: Time until movement from Station No. 1 tailrace in decimal hours

Destination	0%	25%	50%	75%	100%
Spillway	0.17	3.55	5.62	12.79	59.82
Conte	0.05	2.57	23.81	34.54	757.22
Downstream	0.57	3.28	8.35	20.16	228.76

Table E.2-4: CoxPH regression for Conte Discharge to Station No. 1 (2018)

Model Number	Covariates	AIC	Robust LR Test	HR	SE	p	(+/-)	Proportional Hazard Assumption
1	Reach 2 Flow (kcfs)	284.10	0.40	0.89	0.13	0.36	(0.68,1.15)	0.40
2	Cumulative Avg Reach 2 flow while present	283.36	0.30	0.85	0.13	0.22	(0.65,1.10)	0.03
2a	Cumulative Avg Reach 2 flow while present	260.19	0.03	0.82	0.11	0.06	(0.66,1.01)	0.40
	duration			0.92	0.04	0.07	(0.85,1.01)	0.70
	Cumulative Avg Reach 2 flow while present:duration			1.01	0.007	0.18	(0.99,1.02)	0.71
3	Magnitude of change in Reach 2 flow while present (kcfs)	283.96	0.29	1.13	0.11	0.27	(0.91,1.42)	0.11
4	Percent change in Reach 2 flow while present (d%)	284.76	0.47	1.56	0.61	0.46	(0.47,5.18)	0.15
5	Rate of change in Reach 2 flow while present (dQ/dt)	282.96	0.32	0.12	1.29	0.10	(0.01,1.5)	0.17
6	Quarter Day: 0600 - 1200	280.35	0.02	2.85	0.49	0.03	(1.09,7.48)	0.73
	Quarter Day: 1200 - 1800			2.25	0.44	0.06	(0.95,5.33)	0.91
	Quarter Day: 1800 - 2400			0.86	0.49	0.78	(0.33,2.25)	0.55
7	1 hour rolling average Reach 2 flow (kcfs)	283.98	0.38	0.88	0.14	0.34	(0.67,1.15)	0.45
8	1 hour Reach 2 flow volatility (kcfs)	284.91	0.29	0.21	2.62	0.56	(0.001,36.41)	0.29
9	2 hour rolling average Reach 2 flow (kcfs)	283.93	0.37	0.88	0.11	0.34	(0.67,1.15)	0.44
10	2 hour Reach 2 flow volatility (kcfs)	285.02	0.57	2.05	1.15	0.47	(0.30,14.14)	0.57
11	5 hour rolling average Reach 2 flow (kcfs)	283.90	0.37	0.88	0.14	0.33	(0.67,1.14)	0.50
12	5 hour Reach 2 flow volatility (kcfs)	283.17	0.18	5.75	1.03	0.09	(0.76,43.59)	0.50
13	24 hour rolling average Reach 2 flow (kcfs)	284.61	0.52	0.91	0.14	0.49	(0.69,1.20)	0.16
14	24 hour Reach 2 flow volatility (kcfs)	285.34	0.89	0.96	0.33	0.89	(0.50,1.82)	0.82
15	Reach 2 Flow Bin: 3,000 - 6,000 cfs	284.15	0.45	0.51	0.75	0.37	(0.11,2.23)	0.94
	Reach 2 Flow Bin: 6,000 – 9,000 cfs			0.36	0.82	0.21	(0.07,1.80)	0.73

Table E.2-5: CoxPH regression for Station No. 1 to TFD Spillway (2018)

Model Number	Covariates	AIC	Robust LR Test	HR	SE	p	(+/-)	Proportional Hazard Assumption
1	Reach 1 Flow (kcfs)	126.17	0.89	0.97	0.21	0.89	(0.64,1.46)	0.20
2	Cumulative Avg Reach 1 flow while transitioning	125.98	0.56	0.90	0.18	0.56	(0.63,1.29)	0.35
3	Magnitude of change in Reach 1 flow while present (kcfs)	126.01	0.58	0.88	0.23	0.58	(0.57,1.38)	0.54
4	Percent change in Reach 1 flow while present (d%)	125.90	0.51	0.55	0.90	0.51	(0.09,3.24)	0.52
5	Rate of change in Reach 1 flow while present (dQ/dt)	123.69	0.09	33.12	1.84	0.06	(0.90,1219)	0.47
6	1 hour rolling average Reach 1 flow (kcfs)	125.79	0.45	0.85	0.25	0.45	(0.57,1.28)	0.15
7	1 hour Reach 1 flow volatility (kcfs)	126.04	0.65	1.67	1.04	0.62	(0.22,12.86)	0.79
8	2 hour rolling average Reach 1 flow (kcfs)	125.73	0.42	0.84	0.21	0.42	(0.55,1.28)	0.14
9	2 hour Reach 1 flow volatility (kcfs)	124.85	0.08	3.71	0.92	0.15	(0.62,22.32)	0.95
10	5 hour rolling average Reach 1 flow (kcfs)	125.46	0.33	0.79	0.23	0.32	(0.50,1.25)	0.11
11	5 hour Reach 1 flow volatility (kcfs)	123.85	0.08	5.3	1.06	0.04	(1.05,26.77)	0.06
11a	5 hour Reach 1 flow volatility (kcfs)	115.30	0.14	2.53	0.98	0.34	(0.37,17.29)	0.07
	Duration			0.96	0.01	<0.001	(0.94,0.98)	0.37
	5 hour Reach 1 flow volatility (kcfs):Duration			1.10	0.04	0.007	(1.03,1.18)	0.31
12	24 hour rolling average Reach 1 flow (kcfs)	125.99	0.62	0.87	0.27	0.62	(0.51,1.49)	0.26
13	24 hour Reach 1 flow volatility (kcfs)	126.11	0.70	1.27	0.64	0.70	(0.37,4.44)	0.34
14	Reach 1 Flow Bin: 3,000:6,000 cfs	127.96	0.87	0.64	1.06	0.67	(0.08,5.18)	0.95
	Reach 1 Flow Bin: 6,000: 9000 cfs			0.55	1.16	0.61	(0.06,5.37)	0.63

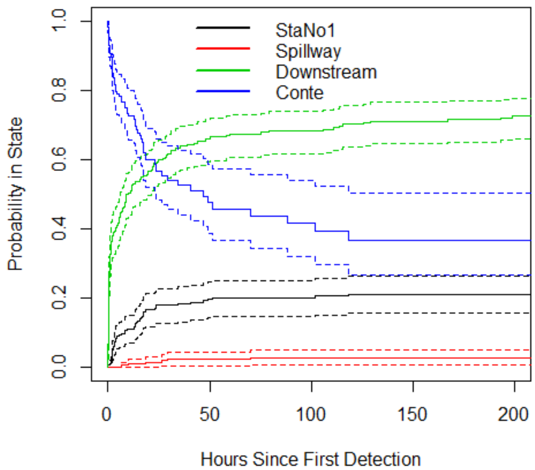

Figure E.2-1: Nelson-Aalen cumulative incidence plot showing probability in state after a fish was first detected at Conte discharge.

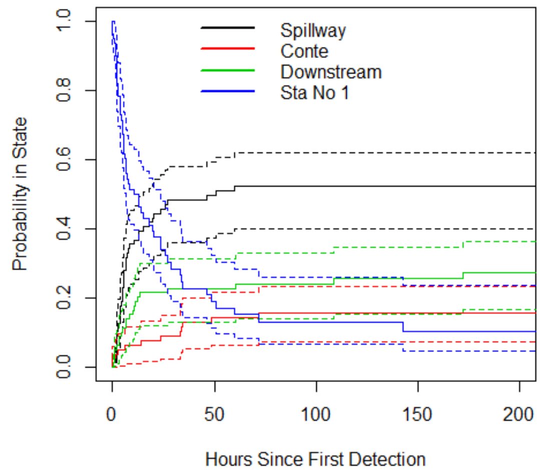

Figure E.2-2: Nelson-Aalen cumulative incidence plot showing probability in state after a fish was first detected at the Station No. 1 tailrace.

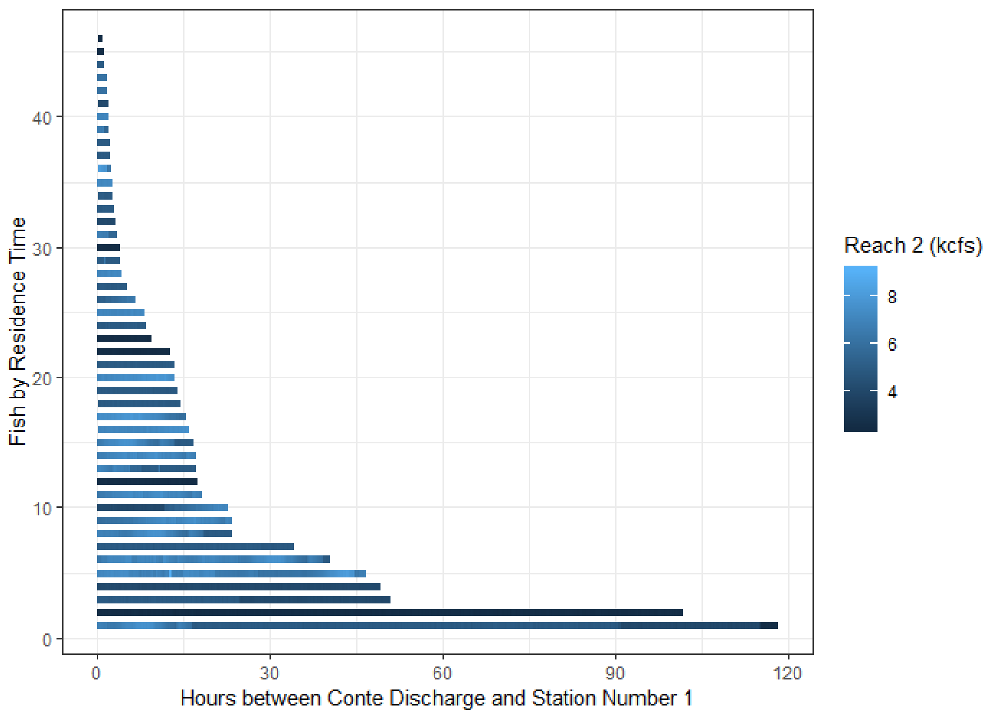

Figure E.2-3: Reach 2 flow conditions within movement from Conte to Station No. 1 ranked by residence time

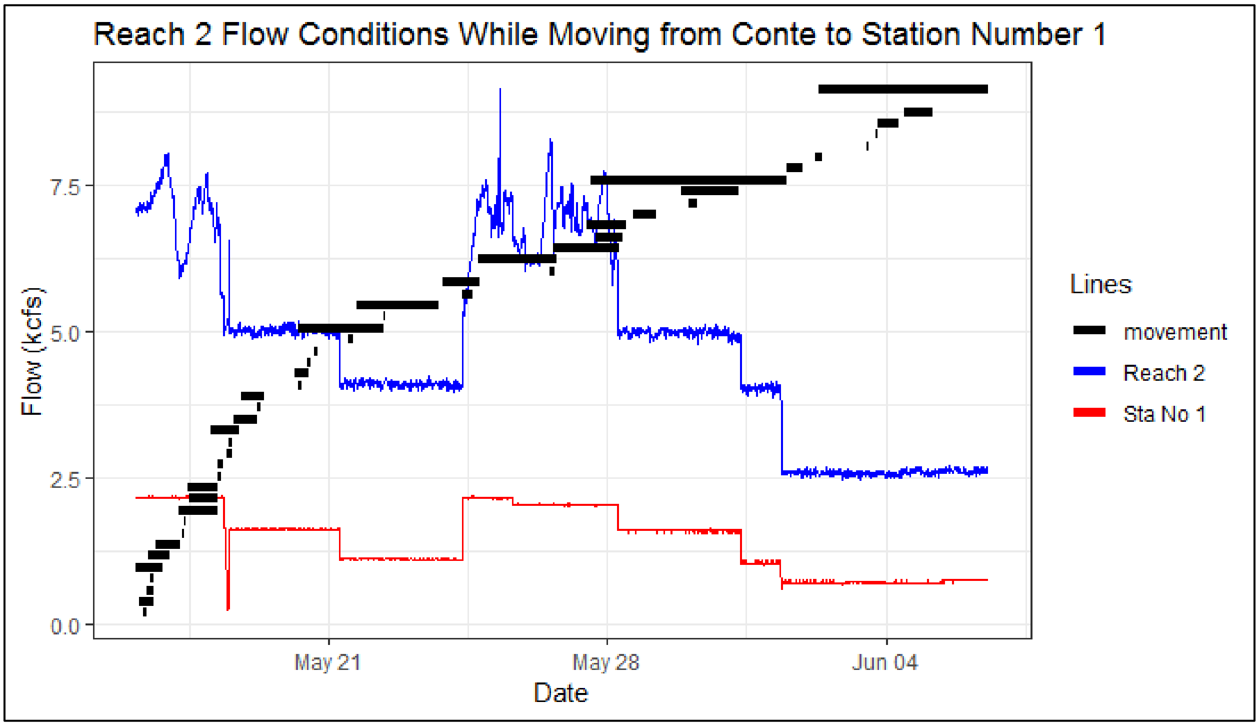

Figure E.2-4: Reach 2 flow time series with fish exposure overlaid. Length of line represents duration of movement from Conte discharge to Station No. 1 tailrace. Note the Station No. 1 discharge component of the Reach 2 flow total is highlighted. Significant spill events occurred in May.

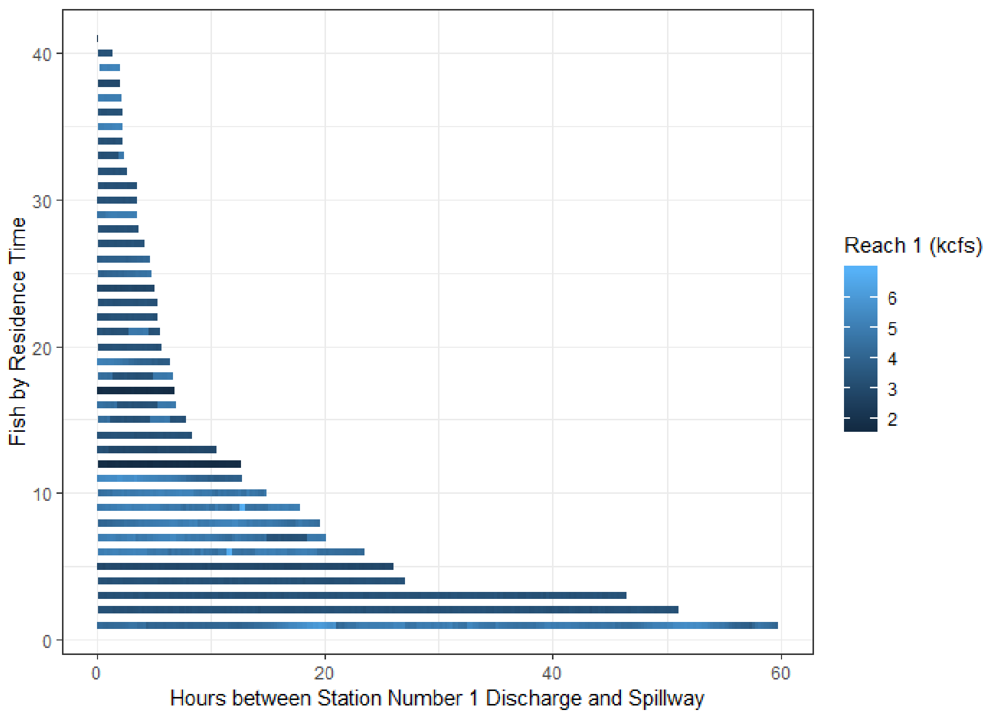

Figure E.2-5: Reach 1 flow conditions experienced while moving from Station No. 1 to the TFD spillway.

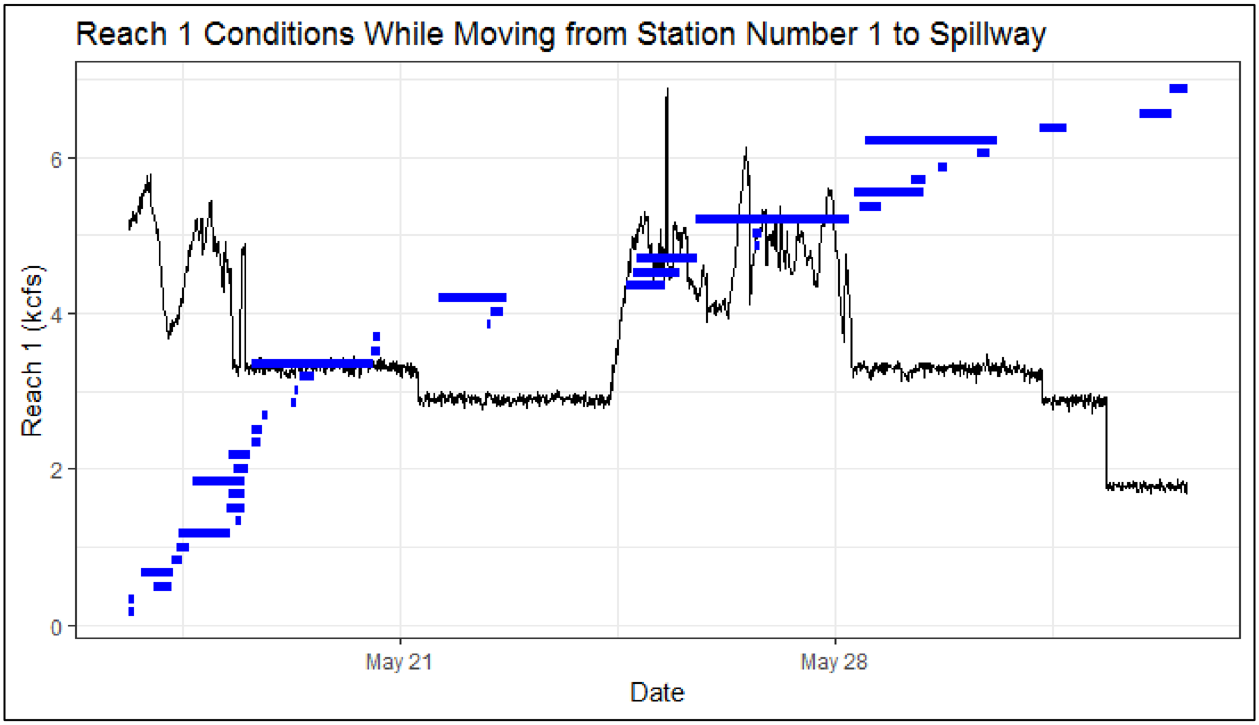

Figure E.2-6: Reach 1 flow time series with fish exposure overlaid. Length of line represents duration of movement from the Station No. 1 discharge to the TFD spillway.

E.3 Rawson Island Velocity

An important discovery during the 2018 telemetry study was the bottleneck that exists between the Conte discharge and the Station No. 1 tailrace. Between these two telemetry stations lies the Rawson Island complex, a series of braided channels with complex hydraulics. These channels may create localized high velocity zones that inhibit migration. These zones, otherwise known as velocity barriers, may exceed the maximum sustainable swim speeds of migratory fish and limit their distribution (Castro-Santos, 2006)[1]. Could the velocity through these channels be high enough to limit the upstream extent of migrating shad?

FirstLight developed a two-dimensional (2-D) River2D hydraulic model of the Rawson Island complex for a range of bypass releases and Cabot Station operations scenarios (Figures E.3-1– Figure E.3-7). Generally, when Cabot Station discharge was 0 cfs, velocities at the southern end of the Rawson Island complex were higher. Areas of high velocity exist in the Right Channel and over Rock Dam at every scenario. Passage via the right channel would expose migrating shad to a high velocity region for approximately 700 feet, while passage via the Rock Dam is shorter but may represent a physical barrier due to the height of the cascade. The middle channel appears watered at bypass flows of 4,000 cfs with high velocity riffles starting to form at 7,000 cfs.

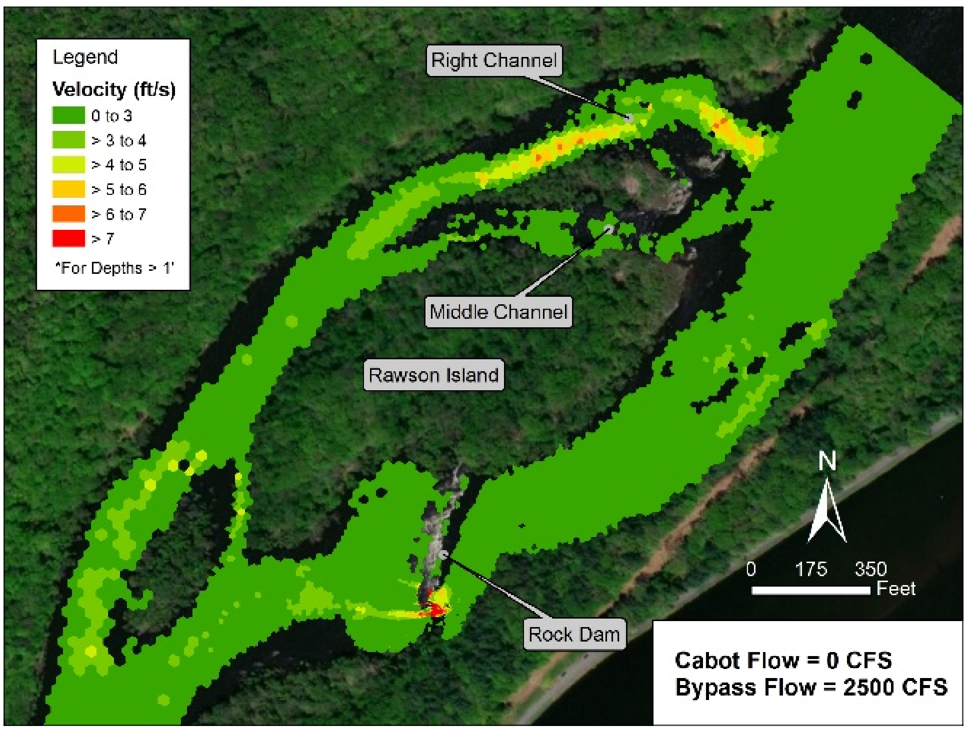

Figure E.3-1: Rawson Island velocity with Cabot at 0 cfs and a bypass flow of 2,500 cfs.

[1] Castro-Santos, T. (2006). Modeling the effect of varying swim speeds on fish passage through velocity barriers. *Transactions of the American Fisheries Society, 135*, 1230-1237.

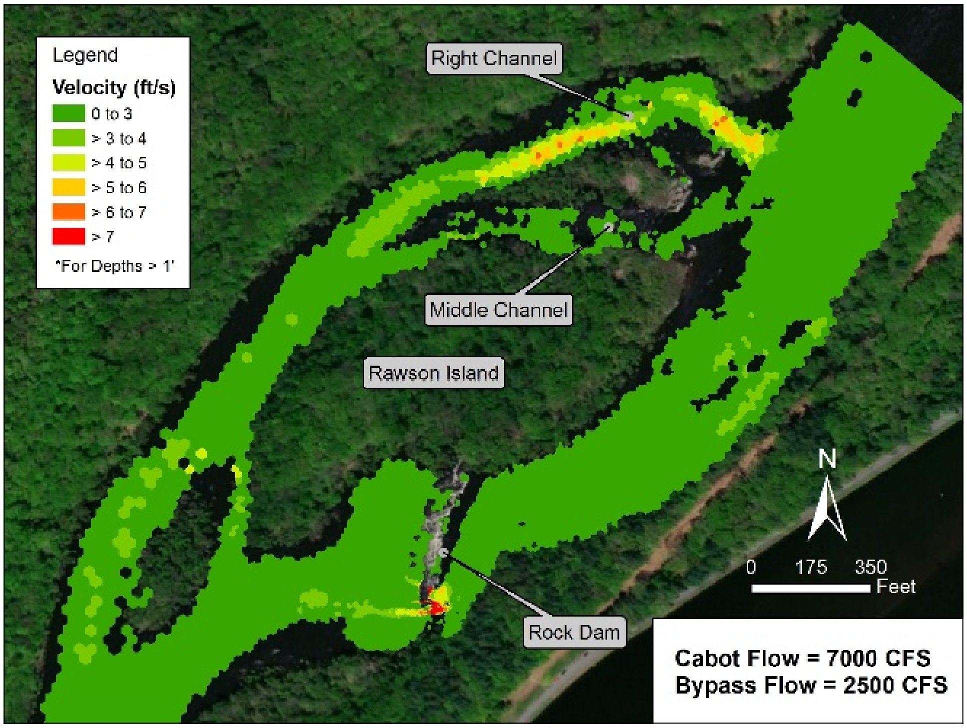

Figure E.3-2: Rawson Island velocity with Cabot Station at 7,000 cfs and a bypass flow of 2,500 cfs.

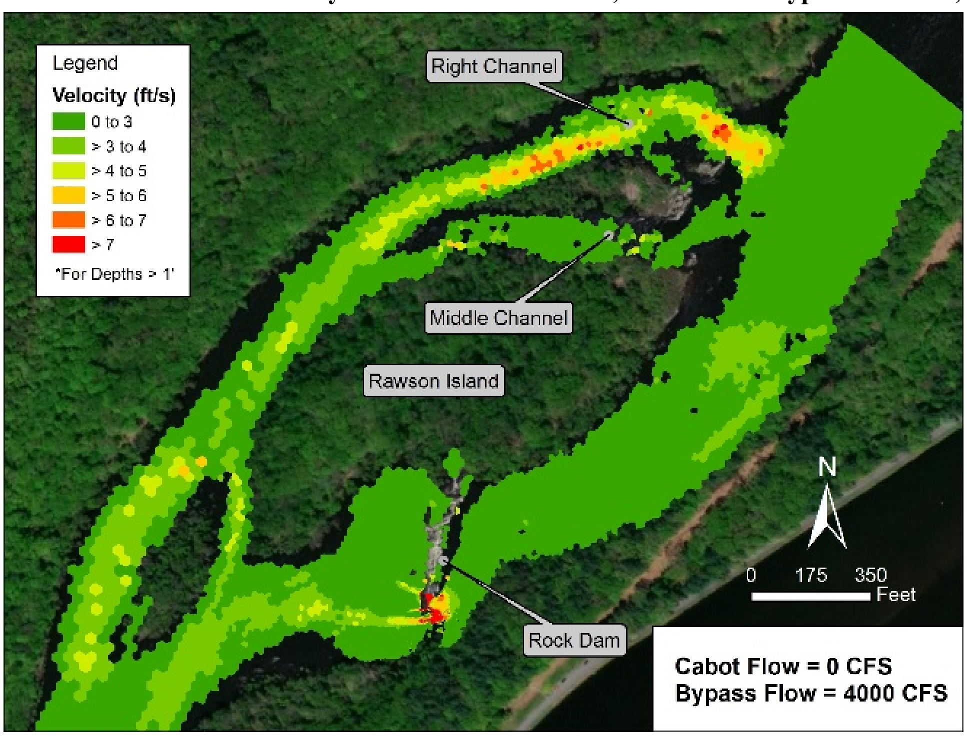

Figure E.3-3: Rawson Island velocity with Cabot Station at 0 cfs and a bypass flow of 4,000 cfs

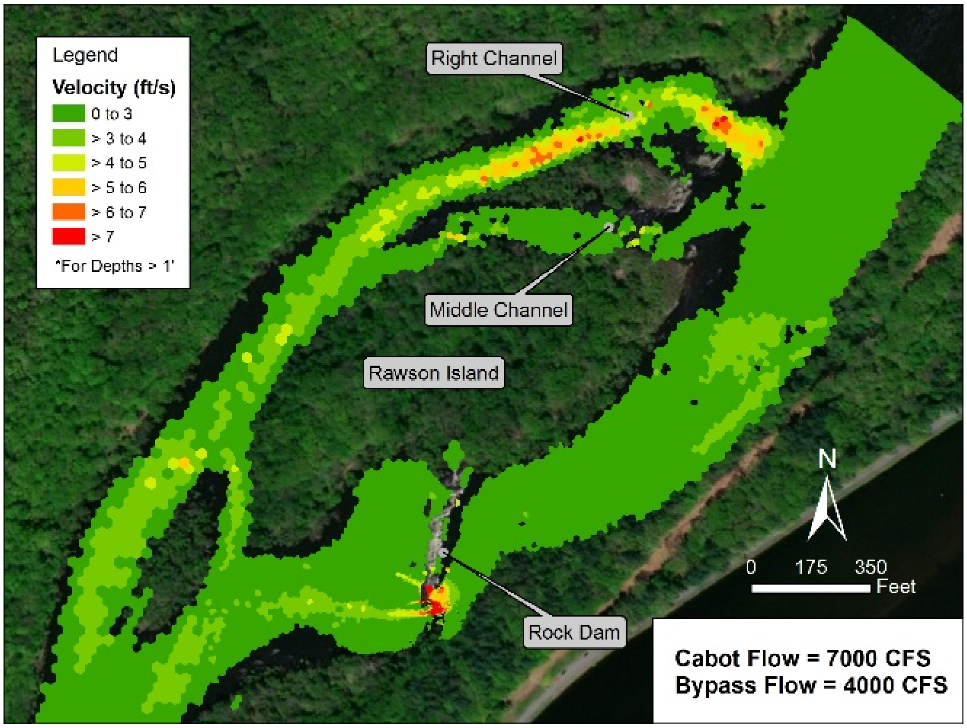

Figure E.3-4: Rawson Island velocity with Cabot Station at 7,000 cfs and a bypass flow of 4,000 cfs

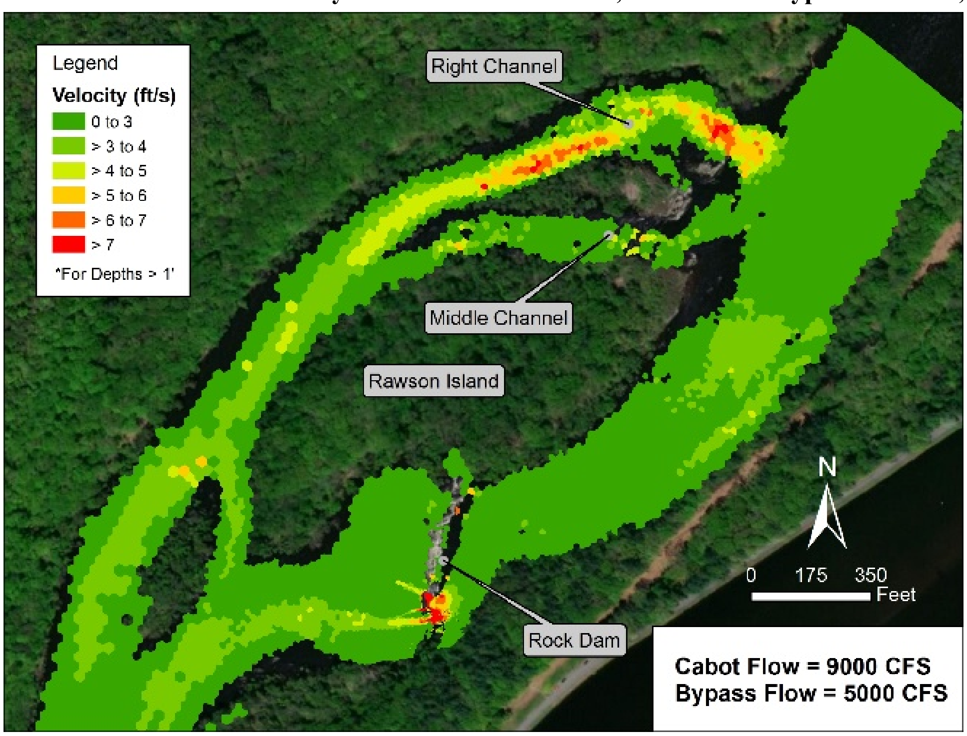

Figure E.3-5: Rawson Island velocity with Cabot Station at 9,000 cfs and a bypass flow of 5,000 cfs

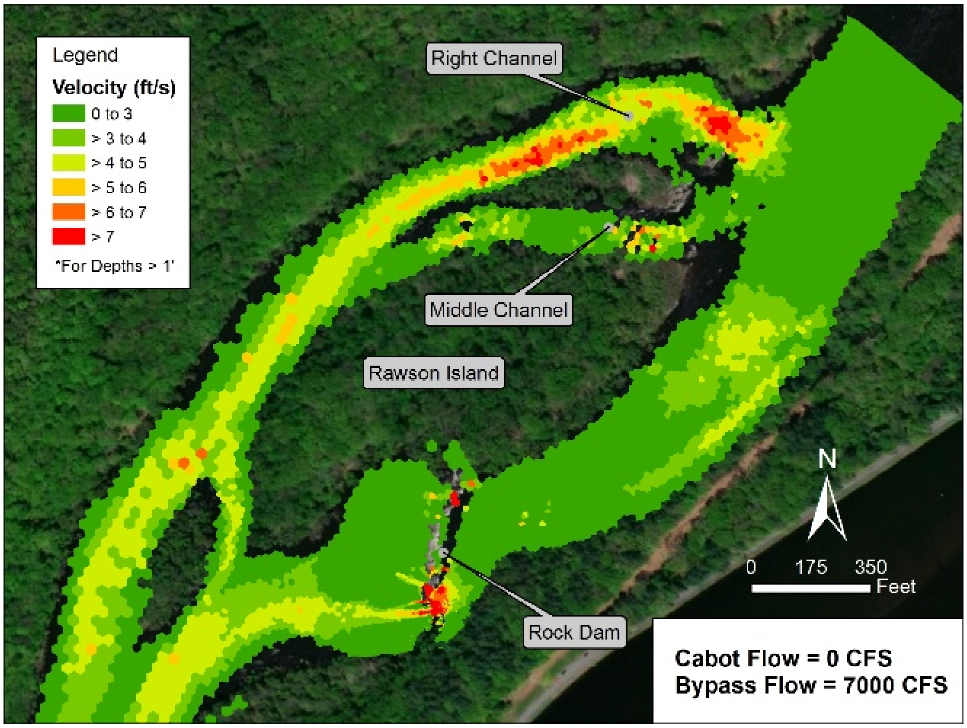

Figure E.3-6: Rawson Island velocity with Cabot Station at 0 cfs and a bypass flow of 7,000 cfs

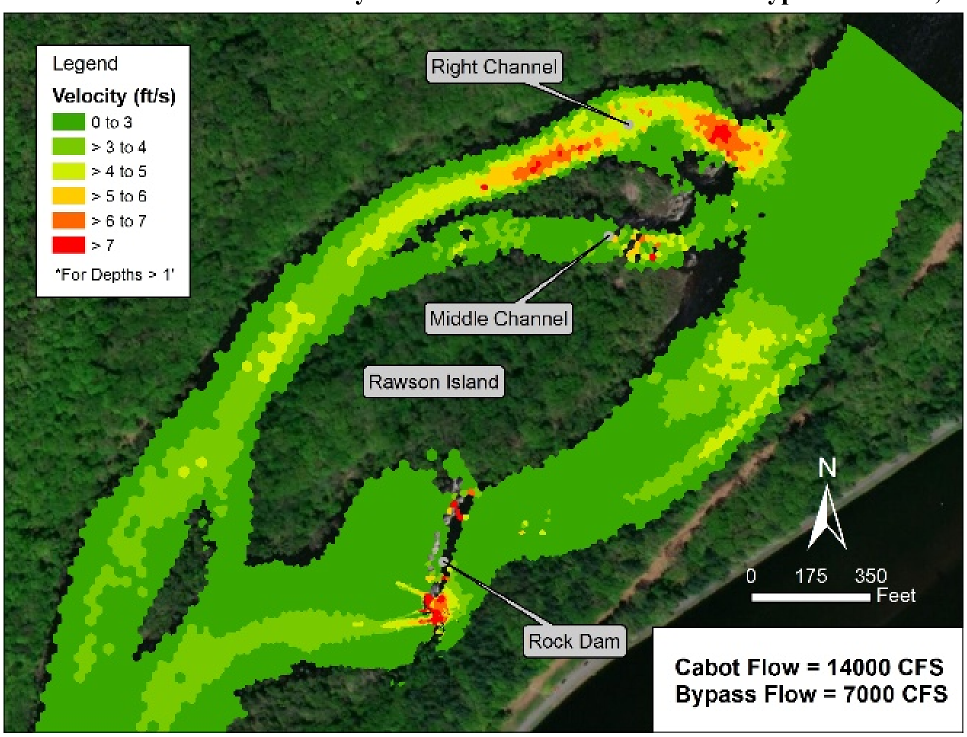

Figure E.3-7: Rawson Island velocity with Cabot Station at 14,000 cfs and a bypass flow of 7,000 cfs

APPENDIX F – DETECTION HISTORY APPENDIX

F. CJS DETECTION HISTORIES

The following table contains the detection histories of the 135 fish that arrived at Montague and were used in the spillway-arrival open-population mark-recapture model.

Table F-1: Recapture histories of all fished used in the TFD spillway CJS arrival model

FreqCode	Montague	D/S Tailrace	Tailrace	Bypass	Station No. 1	Spillway
150.500 100	1	1	1	0	0	0
150.500 101	1	1	1	1	1	1
150.500 103	1	1	1	1	0	0
150.500 109	1	1	1	0	0	0
150.500 110	1	0	0	0	0	0
150.500 111	1	1	1	0	0	0
150.500 113	1	1	1	0	0	0
150.500 114	1	0	0	0	0	0
150.500 115	1	1	1	1	0	0
150.500 117	1	1	1	0	0	0
150.500 118	1	1	1	1	0	0
150.500 119	1	1	1	0	0	0
150.500 120	1	1	1	1	0	1
150.500 122	1	1	1	1	1	1
150.500 123	1	1	1	1	0	0
150.500 124	1	1	1	1	0	0
150.500 128	1	1	1	0	0	0
150.500 130	1	0	0	0	0	0
150.500 131	1	1	1	1	0	0
150.500 132	1	1	1	0	0	0
150.500 134	1	1	1	0	0	0
150.500 135	1	1	1	0	0	0
150.500 136	1	1	1	1	0	0
150.500 137	1	0	1	1	1	1
150.500 138	1	1	1	0	0	0
150.500 140	1	1	1	1	1	1
150.500 146	1	0	0	0	0	0
150.500 147	1	1	1	1	0	0
150.500 151	1	1	1	1	1	1
150.500 152	1	1	1	1	1	1
150.500 153	1	1	1	1	1	1
150.500 154	1	1	1	0	0	0
150.500 155	1	1	1	1	1	1

FreqCode	Montague	D/S Tailrace	Tailrace	Bypass	Station No. 1	Spillway
150.500 156	1	1	1	1	1	1
150.500 160	1	1	1	1	0	0
150.500 161	1	1	1	1	1	1
150.500 164	1	0	0	0	0	0
150.500 165	1	1	1	1	0	0
150.500 166	1	1	1	1	1	1
150.500 168	1	1	1	1	1	1
150.500 170	1	1	1	1	0	0
150.500 171	1	0	0	0	0	0
150.500 172	1	1	1	0	0	0
150.500 173	1	1	1	0	0	0
150.500 175	1	1	1	0	0	0
150.500 176	1	0	0	0	0	0
150.500 178	1	1	1	1	1	0
150.500 180	1	1	1	0	0	0
150.500 181	1	1	1	1	0	0
150.500 182	1	0	0	0	0	0
150.500 183	1	1	1	1	0	0
150.500 185	1	1	1	1	1	1
150.500 186	1	1	1	0	0	0
150.500 188	1	1	1	0	0	0
150.500 190	1	1	1	1	0	0
150.500 192	1	1	1	1	0	0
150.500 197	1	1	0	0	0	0
150.500 199	1	1	1	1	1	1
150.500 200	1	1	1	0	0	0
150.500 201	1	1	1	0	0	0
150.500 204	1	1	1	1	1	1
150.500 205	1	1	1	0	0	0
150.500 206	1	1	1	1	0	0
150.500 207	1	1	1	1	0	0
150.500 74	1	0	0	0	0	0
150.500 75	1	0	1	1	0	0
150.500 76	1	1	1	1	0	0
150.500 77	1	1	1	1	0	0
150.500 78	1	1	1	1	0	0
150.500 80	1	0	0	0	0	0
150.500 81	1	1	1	1	1	0
150.500 84	1	1	1	0	0	0
150.500 85	1	1	1	1	0	0

FreqCode	Montague	D/S Tailrace	Tailrace	Bypass	Station No. 1	Spillway
150.500 88	1	1	1	1	0	0
150.500 89	1	1	1	1	0	0
150.500 90	1	1	1	1	0	0
150.500 92	1	1	1	1	0	0
150.500 94	1	1	1	1	1	1
150.500 97	1	1	1	0	0	0
150.500 98	1	1	1	1	1	1
150.560 100	1	1	1	1	0	0
150.560 102	1	0	0	0	0	0
150.560 103	1	1	1	0	0	0
150.560 105	1	1	1	0	0	0
150.560 106	1	0	1	0	0	0
150.560 109	1	0	0	0	0	0
150.560 111	1	1	1	1	1	1
150.560 114	1	1	1	1	0	0
150.560 117	1	0	0	0	0	0
150.560 126	1	1	1	0	0	0
150.560 127	1	1	1	1	1	1
150.560 130	1	1	1	1	0	0
150.560 132	1	1	1	1	0	0
150.560 136	1	0	0	0	0	0
150.560 20	1	1	1	0	0	0
150.560 21	1	1	1	1	1	1
150.560 24	1	1	1	1	1	1
150.560 25	1	1	1	1	0	0
150.560 27	1	0	0	0	0	0
150.560 29	1	1	1	1	0	0
150.560 32	1	1	1	1	1	1
150.560 33	1	1	1	1	1	1
150.560 34	1	1	1	1	1	1
150.560 35	1	1	1	1	0	0
150.560 36	1	1	1	1	0	0
150.560 38	1	1	1	1	1	1
150.560 39	1	1	1	1	0	0
150.560 40	1	1	1	1	1	1
150.560 41	1	1	1	1	0	0
150.560 44	1	1	1	1	0	0
150.560 47	1	1	1	0	0	0
150.560 51	1	1	1	0	0	0
150.560 53	1	0	1	1	1	0

FreqCode	Montague	D/S Tailrace	Tailrace	Bypass	Station No. 1	Spillway
150.560 54	1	1	1	1	0	0
150.560 55	1	0	1	1	0	0
150.560 59	1	1	1	0	0	0
150.560 61	1	1	1	1	0	0
150.560 62	1	1	1	1	1	1
150.560 65	1	1	1	0	0	0
150.560 67	1	1	1	1	0	0
150.560 69	1	1	1	1	0	0
150.560 71	1	1	1	0	0	0
150.560 73	1	1	1	1	1	1
150.560 74	1	1	0	0	0	0
150.560 78	1	1	1	1	0	0
150.560 80	1	0	0	0	0	0
150.560 82	1	0	1	1	0	0
150.560 83	1	1	1	1	1	1
150.560 84	1	1	1	1	1	1
150.560 85	1	1	1	1	1	0
150.560 86	1	0	0	0	0	0
150.560 92	1	0	1	1	1	1
150.560 94	1	1	1	1	0	0
150.560 95	1	1	1	1	0	0
150.560 98	1	1	1	1	0	0

APPENDIX G – FALLBACK APPENDIX

APPENDIX G FALLBACK

TABLE OF CONTENTS

LIST OF TABLES

LIST OF FIGURES

G. ASSESSMENT OF FALLBACK FISH

Fallback has been defined as the immediate downstream directed movement of an upstream migrating anadromous fish following tagging (Frank 2009). From the perspective of a study, a fish that falls back represents lost data, as any behavior we could have observed is swept downstream. Therefore, the scientific community should take any action necessary to reduce the rate at which fall back occurs in future studies. After three years of study (two with valid data for analysis), we have observed enough fall back where it is possible to develop statistical models that predict whether or not a fish will fall back based upon a suite of explanatory variables. This model should serve as a guideline for future studies to reduce the rate at which fish fall back after tagging and improve their statistical power, and should be updated as more data becomes available.

In 2015, a fish fell back if it did not arrive at any upstream telemetry stations, with the first occurring at the Red Cliff Canoe Club within the Holyoke Impoundment. In this case, absence of any upstream movement was indicative of a fish abandoning migration after tagging. In 2018, Kleinschmidt Associates was monitoring the movement of Shortnose Sturgeon at the Holyoke Project, and we had Orion receivers placed around the project that could identify shad passing through. A fish fell back if it was recaptured at any of the Orion stations without subsequent movement upstream. Fish from 2016 were not utilized because neither Holyoke Dam, nor the stretch of river between the Holyoke impoundment and Montague Wastewater were monitored.

G.1 Methods

A logistic-regression assessed the factors that influenced fall back within a generalized linear model (GLM) framework using a logit link function. A series of logistic models were created to predict the rate at which fish fall back based on a set of predictor variables including; sex, length, percent fat, descaling, discharge, and water temperature. Understanding the potential predictors of fall back fish will benefit future tagging studies by providing valuable insights to help maximize the performance of tagged fish.

The model building strategy was iterative, with nested models assessed with an analysis of variance (ANOVA). The null hypothesis of which stated that the explanatory power gained by a more complex model did not significantly increase. Rejection of the null hypothesis would warrant the more complex model. All fish were tagged and released at Holyoke Fish Lift in Holyoke, Massachusetts. A total of 1258 tagged shad were used for this analysis.

Throughout two years of telemetry studies, several metrics were collected during the tagging process that increased handling time. In 2015, 601 fish were measured for fat content (% bodyfat) using a Fish Fat Meter (Assurant Innovations, MFM 1092). The Fish Fat Meter is a non-invasive handheld device that takes three measurements of fat content in meat along the dorsal musculature of the adult American shad. The meter provides an instantaneous reading of the fat content as a percentage of body mass. The handling and tagging procedure also required an assessment of descaling, which involved checking both sides of the fish to subjectively determine the percentage of scales missing. Throughout the years of studies, a total of 911 shad were assessed for descaling. These metrics, along with other variables including water temperature, river discharge at Montague, sex, and length, allowed FirstLight to identify the factors that contributed most to adverse tagging effects. Both years of tagging data were aggregated and merged with R. Fallback was treated as a binary variable that takes the value of 1 if a fish fell back or 0 if it successfully migrated to the project.

G.2 Results

Table G.2-1 displays the total number of fish used in the analysis (n=1,258), the number of fish that successfully migrated to the Project (n=773, 61%), and the number of fish that fell back (n=485, 39%). There were 590 female shad used in this analysis and 668 males. In total, 365 females and 408 males successfully migrated upstream to the Project. There were 225 females and 260 males that fell back (Table G.2-2).

A series of tables and histograms highlighted the apparent effect our covariates have on the likelihood that a fish will fall back, and they later assisted us with model creation. Contingency tables were assessed with a chi-square test of independence, where the null hypothesis states that the count of fish falling back is independent of our predictor variables.

Table G.2-3 counts the number of fish that fell back or successfully arrived at the project as a function of whether or not they exhibited de-scaling. Fish with more descaling may have been in the river longer or be less healthy then fish without descaling. There were 771 fish that displayed no descaling and 389 of those fish successfully migrated to the Project while 382 fell back downstream. Only 140 fish that displayed descaling were tagged, and 37 arrived at the Project while 103 fell back downstream (Table G.2-3). The test was significant, the count of fish falling back depends on whether or not a fish exhibited descaling.

Table G.2-4 counts the number of fish that fell back or successfully arrived at the project as a function of whether or not they were tested with the fat meter. Of the 657 fish not tested with the fat meter, 474 successfully made it to the Project, while 183 fell back. In contrast, of the 601 fish that were tested with the fat meter, only 299 successfully made it to the Project while 302 fell back (Table G.2-4). The chi-square test of independence was significant, assessing fish for their fat content effects the likelihood that a fish will arrive at the project.

Figure G.2-1 contains the Montague discharge flows experienced by fish at the time of release. In general, both fall back and successful fish experienced flows between 5,000 and 20,000 cfs at the time of release, and it appears that the majority of successful fish were released when river flows (Montague Gage) were around 10,000 cfs. While not as strong as an association, the count of fall back fish appeared to peak around 17,000 cfs. Figure G.2-2 shows density plots of the percent fat readings from successful males and females and fallback fish. In both cases, successful females and males had a slightly higher percent fat content than males and females that fell back.

Not all fish were assessed for body fat percentage and descaling. However, the logistic regression requires observations with complete cases. Of the 1,258 fish released in 2015 and 2016, only 512 had complete cases. A second series of logistic regressions were also created to include all fish, these models incorporated two new binary variables; (1) whether or not fish were assessed for fat or (2) whether or not a fish was assessed for descaling. The estimates are expressed as a logit (log odds). To convert the logit to probability use: $\exp(logit)\,/(1+\exp(logit))$. The covariate estimate should be understood as the change in baseline odds (intercept). For continuous variables, we interpret the covariate as the change in log odds per unit increase in the independent variable.

Table G.2-5 contains the results from the first series of logistic regression models, which only tested those fish with complete cases. The best model in terms of AIC was model 7, which incorporated water temperature at release (C), whether or not a fish exhibited de-scaling, and percent body fat. The slope associated with each covariate was significant as was the intercept. The baseline log odds that a fish without descaling will fall back at 0 C and 0% body fat is 4.54 or 99%. The log odds associated with a change in 1 degree C was -0.22. At 15 C, the change in log odds -3.3. The log odds associated with a change in percent body fat is also negative (Table G.2-6), meaning fish with more fat have a reduced probability of falling back. Finally, the presence of descaling was also significant. The log odds of a fish with some amount of descaling present and falling back is 1.23 or 77%. From this model, we are able to determine that fish are more likely to fall back if they have lower percent body fat, exhibit any kind of descaling, or were released in colder waters. Table G.2-6 contains the output of the second series of logistic regression models. The best model in terms of AIC included whether or not the fish was tested for fat. The baseline log odds ratio of a fish falling back (intercept) was -0.48 or 38%. The change in log odds associated with testing a fish for body fat percentage was 0.96, which corresponds to an increase in the probability of falling back by 24% from 38% to 62%.

Table G.2-1: Total number of fish that successfully made it to the Project and those considered fallback fish

Fish	Number
Successful Migrant	773
Fallback Fish	485
Total	**1,258**

Table G.2-2: The number of females and males that successfully made it to the Project or that fell back. The X^2 was not significant, sex has no effect on fish falling back ($X^2 = 0.05$, $p = 0.82$).

Fish	Females	Males	Total
Successful Migrant	365	408	**773**
Fallback Fish	225	260	**485**
Total	**590**	**668**	**1258**

Table G.2-3: The number of fish that displayed descaling or otherwise appeared healthy that either successfully made it to the Project or fell back. Note only 911 fish out of the 1,258 were assessed for descaling. The X^2 test of independence was significant ($X^2 = 26.515$, $p < 0.001$), descaling appears to effect fallback.

Fish	No Descaling	Descaling	Total
Successful Migrant	389	37	**426**
Fallback Fish	382	103	**485**
Total	**771**	**140**	**911**

Table G.2-4: The number of fish that were tested with the fat meter that successfully made it to the Project or that fell back. The X^2 test of independence was significant ($X^2 = 26.515$, $p < 0.001$), assessing with a fat meter appears to effect fallback.

Fish	Not Assessed with Fat Meter	Assessed with Fat Meter	Total
Successful Migrant	474	299	773
Fallback Fish	183	302	485
Total	**657**	**601**	**1,258**

Table G.2-5: Logistic regression output for the 512 fish with complete cases.

Model Number	AIC	Parameter	Estimate (logit)	Standard Error	P value
1	682.12	Intercept	0.22	0.10	0.02
		Descaling Present (yes)	1.06	0.29	<0.001
2	696.92	Intercept	0.41	0.13	0.002
		Sex (M)	-0.09	0.18	0.62
3	688.49	Intercept	0.78	0.17	<0.001
		Percent Fat (%)	-0.06	0.02	0.003
4	677.83	Intercept	3.89	0.88	<0.001
		Water Temp (C)	-0.20	0.05	<0.001
5	661.00	Intercept	4.14	0.90	<0.001
		Water Temp (C)	-0.22	0.04	<0.001
		Descaling Present (yes)	1.19	0.30	<0.001
6	672.3	Intercept	4.22	0.89	<0.001
		Water Temp (C)	-0.19	0.05	<0.001
		Percent Fat (%)	-0.06	0.02	0.006
7	654.78	Intercept	4.54	0.93	<0.001
		Water Temp (C)	-0.22	0.05	<0.001
		Descaling Present (yes)	1.23	0.30	<0.001
		Percent Fat (%)	-0.06	0.02	0.004

Table G.2-6: Logistic regression output for the 1,258 fish released in 2015 and 2016.

Model Number	AIC	Parameter	Estimate	Standard Error	P value
1	1614.47	Intercept	-0.48	0.08	<0.001
		Fat Content Assessed	0.96	0.09	<0.001
2	1681.36	Intercept	-0.48	0.08	<0.001
		Sex (M)	0.03	0.11	0.78
3	1677.82	Intercept	-0.81	0.19	<0.001
		Montague (kcfs)	0.03	0.01	0.06
4	1263.09	Intercept	-18.57	350.15	0.96
		Assessed for Descaling	18.70	350.15	0.96

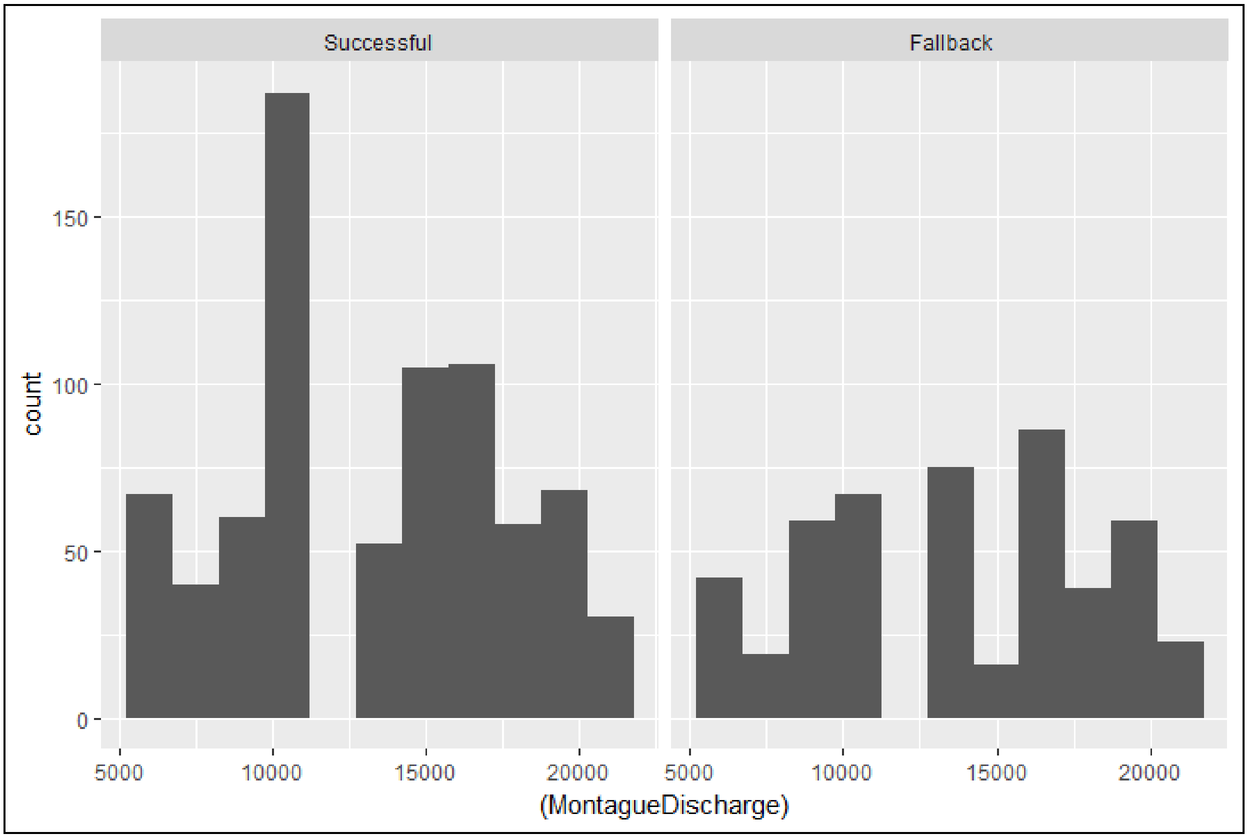

Figure G.2-1: Flow histograms for fallback and successful fish (2015 and 2016)

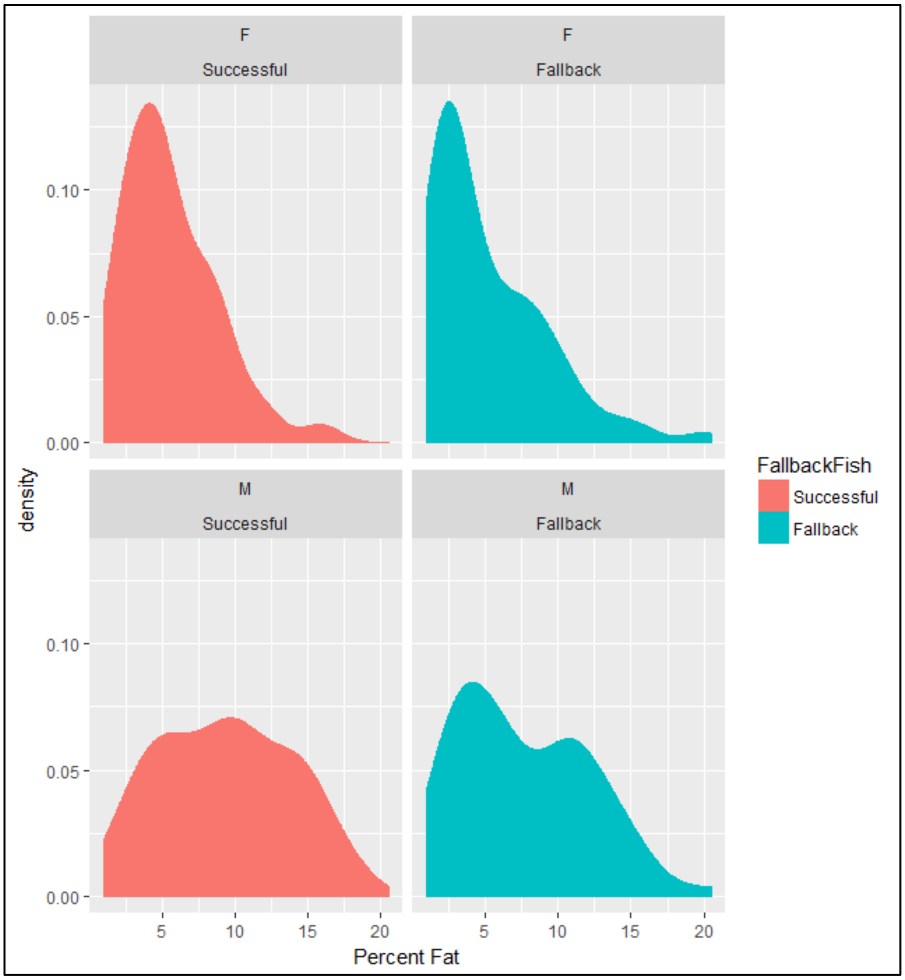

Figure G.2-2: Density plots of displaying percent fat for successful and fallback fish, males and females

G.3 Discussion

Efforts for the 2018 study included tagging 250 American Shad, which were captured and released at the Holyoke fish lift in the early portion of the 2018 migratory season (May 14 through May 18, 2018). The 2015 and 2016 telemetry studies have proven that tagging the earliest arrivals at Holyoke results in more motivated and biologically fit upstream migrants as compared to tagging later in the season. Of the 250 shad tagged, 137 (~55%) arrived at the Project. Fish that did not make it to the Project were considered fallback fish. An in-depth analysis of fish that fell back in 2015 and 2016 found that the most significant factors influencing fallback are the use of the fat meter and Montague discharge. When the fat meter was not used during the tagging process (n = 657), the ratio of fish successfully making it to the Project verses falling back was approximately 2.5:1 (n=474 successful fish, n=183 fallback). Conversely, when the fat meter was used during the tagging process, that ratio became approximately 1:1(n=299 successful fish, n=302 fallback). This analysis indicates that increased handling time of fish for fat measurements, adversely affects the performance of tagged shad moving upstream from Holyoke to the Project. In future studies, performance of tagged fish may benefit if efforts are focused solely on immediate tagging and release of the fish, rather than taking additional morphometric measurements, such as the percentage of fat, length, sex, and presence of descaling.